H_2^- Anions in Solid Hydrogen

Takayuki KUMADA

Dissertation in Physics

Osaka University
Graduate School of Science
Toyonaka, Osaka

November 1998

Contents

Chapter 1

Introduction

Hydrogen molecules form the simplest and most fundamental molecular solids. Because of the simplicity and fundamentality, it seems that the hydrogen solids do not show interesting phenomena. However, they have a number of characteristic properties reflecting quantum effects due to their light mass and small intermolecular interactions. Thus, together with helium solids, hydrogen solids are categorized as quantum solids and their properties have been studied in the field of low temperature physics [1–3].

Ionic species trapped in hydrogen solids also show various quantum properties. Since the ionic species have much higher cohesive and zero-point energies compared with the intermolecular interaction among hydrogen molecules, the surrounding hydrogen molecules are remarkably affected by the ionic species. It has been reported that excess electrons trapped in superfluid helium, well known quantum liquid, push back surrounding helium atoms to form electron bubbles with radius of 15 ~ 20 Å [4]. The electron bubbles are formed to minimize much higher zero-point vibration energy of the excess electrons compared with the van der Walls interaction energy among helium atoms. It is expected that the ionic species trapped in hydrogen solids also show such anomalous physical properties.

The ionic species in hydrogen solids are produced by radiolysis. The ionic species together with radiation effects in hydrogen solids have received much attention not only in the field of low temperature physics but also in low temperature chemistry, astronomy, and fusion system development.

Reactive species such as ions and radicals have very short lifetime in gas and liquid phases, because they suddenly meet and react with other reactive species. The lifetime, however, can be elongated by isolating in inert molecular solid matrix [5]. This technique called matrix isolation method has been extensively used to study properties of the reactive species and their related chemical reactions. In 1980s, Miyazaki et al. [6] applied hydrogen solids as the isolating matrix and found that D atoms produced in a γ-ray

irradiated HD solid react with their surrounding HD molecules as: $D + DH \rightarrow D_2 + H$ via quantum mechanical tunneling. The tunneling reaction can be also observed only in the solid phase, because the D atoms suddenly migrate and recombine with other D or H atoms in the gas and liquid phases. They preferably used the hydrogen solid on the study of the tunneling reactions. The lighter species tunnels much more rapidly [7]. Thus, hydrogen atoms play a very important role in low temperature chemical reactions, because almost all chemical reactions occur via the quantum mechanical tunneling at low temperatures. Therefore, the study of chemical reactions of hydrogen atoms, molecules, and ions in hydrogen solids have been spreading together with improvement of experimental techniques [8,9] and must be increasingly interesting in future.

It has been considered that molecules in space are produced via ion-molecule collision reactions. Because of low temperature, kinetic energies for the reactions are given only by the long-range attractive interaction between the ions and molecules [10]. It is expected that hydrogen ions, such as H_3^+, play the most important role on the chemical reactions in space, because concentration of H atom in space is much higher than that of any other atomic species [11]. Properties of the hydrogen ions, however, have not been sufficiently understood. Thus, they have also been studied in laboratories. The hydrogen ions produced in irradiated hydrogen solids will be one of the most available system for studying their properties and for the establishment of astronomy [12].

Deuterium-tritium mixture solids, D-T, may be used as a nuclear fuel for fusion [2]. Since tritium is radioactive species with half-lifetime of 12.33 years, its radiation effects on the fuel and fusion system are not negligible. In 1980s, Souers et al. [2,13] studied the radiation effects on the D-T mixture solids and found various radiation effects. In the present day, proton-beam [14] or γ-ray [15] irradiated H_2, HD, and D_2 solids are used instead of T-mixture for the precise study of the radiation effects because of difficulty in handling of T. These researches may play an important role on the development of the fusion system in future.

1. 1. Historical Background

The ionic species produced in irradiated hydrogen solids has been studied for about 20 years. Souers et al. [13] firstly observed Stark shifted infrared absorption peaks of hydrogen molecules in HT, DT, and T_2 mixture solids in 1980. They have assigned these new peaks as the hydrogen molecules nearby ionic species, such as H_3^+ and electron bubbles, produced by the radioactivity of T atoms. Brooks et al. [14] have extended these researches using proton beam radiolysis instead of the radioactivity of T and found several absorption peaks, which suggest the existence of electron bubbles, small polaron holes, interference effects, and ion clustering (cf. Fig. 1-1). However, these assignments have some uncertainties because of the reasons as follows. First, the authors obtained the radiuses of the ionic species by the Stark shift of their surrounding hydrogen molecules and then assigned the ionic species only due to the radiuses. Moreover, the radiuses obtained is unreliable especially at smaller ones less than about 3 Å, because the calculations are based on charge-induce dipole and charge-quadruple interactions. The point charge model is not accurate at smaller in distance. Second, the peak which assigns H^- anions has not been observed, although it must be observed. Third, such signals have not been reproduced by Oka et al., although their infrared absorption system has much better resolution [12,15]. The study of ionic species in these systems has not well progressed due to these unresolved uncertainties.

In 1990s, Oka et al. [12,15] have extended these researches using high-resolution infrared and Raman spectroscopy and found new Raman peaks due to Condon effects shown in Fig. 1-2. These data indicated that the ionic species are produced by the radiolysis; however, they have not assign the ionic species.

ESR study of the ionic species in irradiated hydrogen solids had not been reported except for a very small peak which can be assigned as electron bubbles in D_2-T_2 mixture solid (cf. Fig. 1-3) [16]. It had been considered that the ESR spectroscopy is not useful for the study of the ionic species because of low resolution. However, Miyazaki [17] has recently found that ESR resolution of radical species trapped in the para-H_2 (p-H_2) solid is much better than in normal-H_2 (n-H_2) solid (see below). Using this high resolution ESR spectroscopy, new ionic species of H_2^- anions are firstly observed, which is the main topic

in this paper.

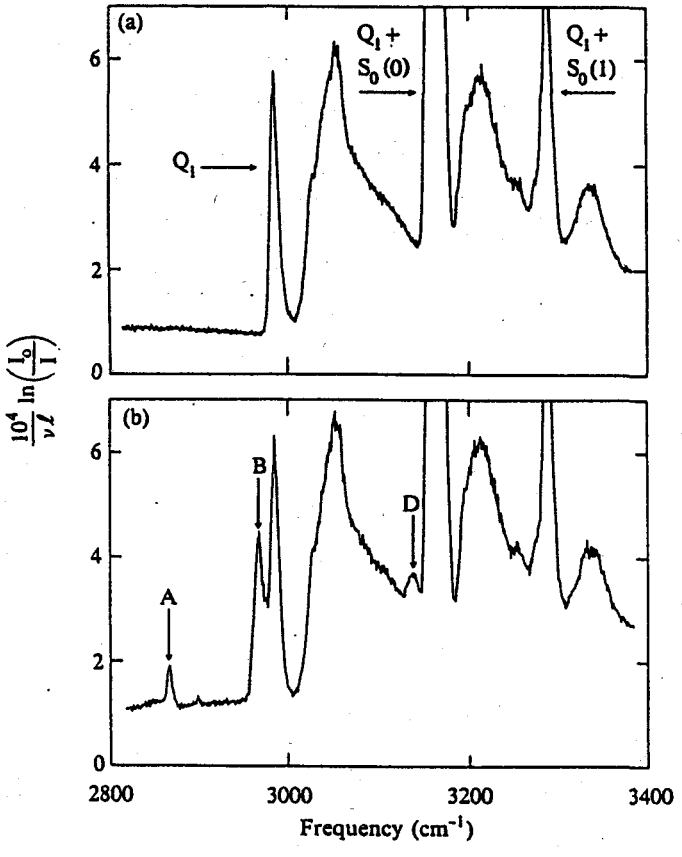

Fig. 1-1 Infrared absorption spectra of the fundamental vibrational band of solid D_2 at 4.2 K:* (a) before proton-beam irradiation, (b) after the irradiation. Peaks depicted by A, B, and D are the Stark shifted ones of D_2 molecules nearby ionic species [14].

* Vibration-rotation transitions are specified by the following convention: The capital letters Q, S, U, W, Y..... represent $\Delta J = 0, 2, 4, 6, 8$....., respectively. Their subscripts show the vibrational quantum number v in the upper state, and the number in parentheses represent the rotational quantum number J in the lowest state. Thus, $Q_1(0)$, $S_0(0)$, $S_0(1)$ denote ($v = 1 \leftarrow 0$, $J = 0 \leftarrow 0$), ($v = 0 \leftarrow 0$, $J = 2 \leftarrow 0$), ($v = 0 \leftarrow 0$, $J = 3 \leftarrow 1$), respectively.

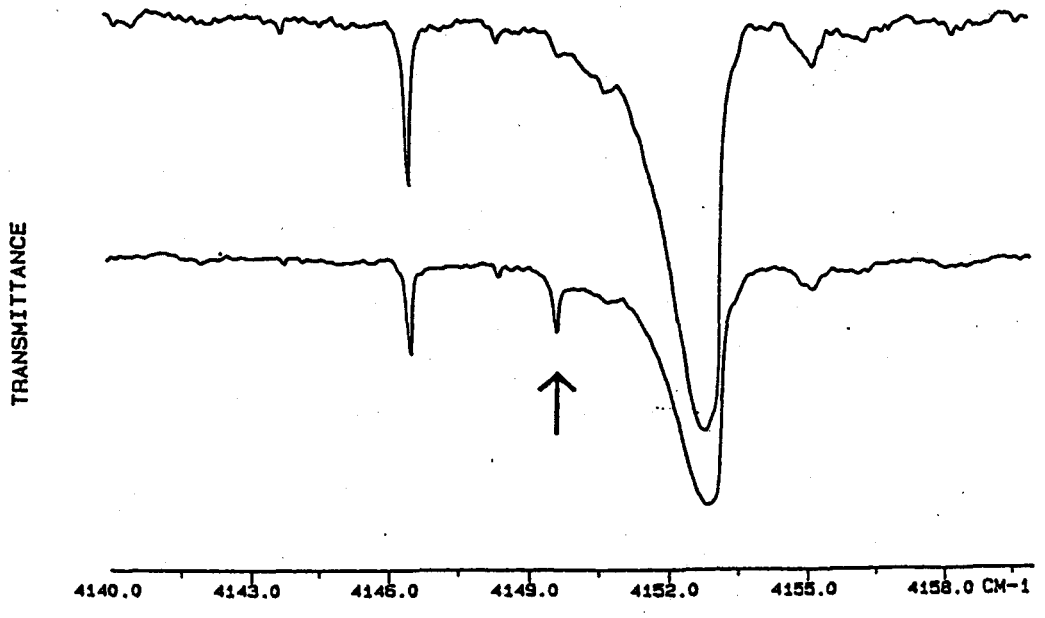

Fig. 1-2 FTIR spectrum of p-H_2 solid before (upper trace) and after γ-ray irradiation. Arrow shows the charge induced spectrum [15].

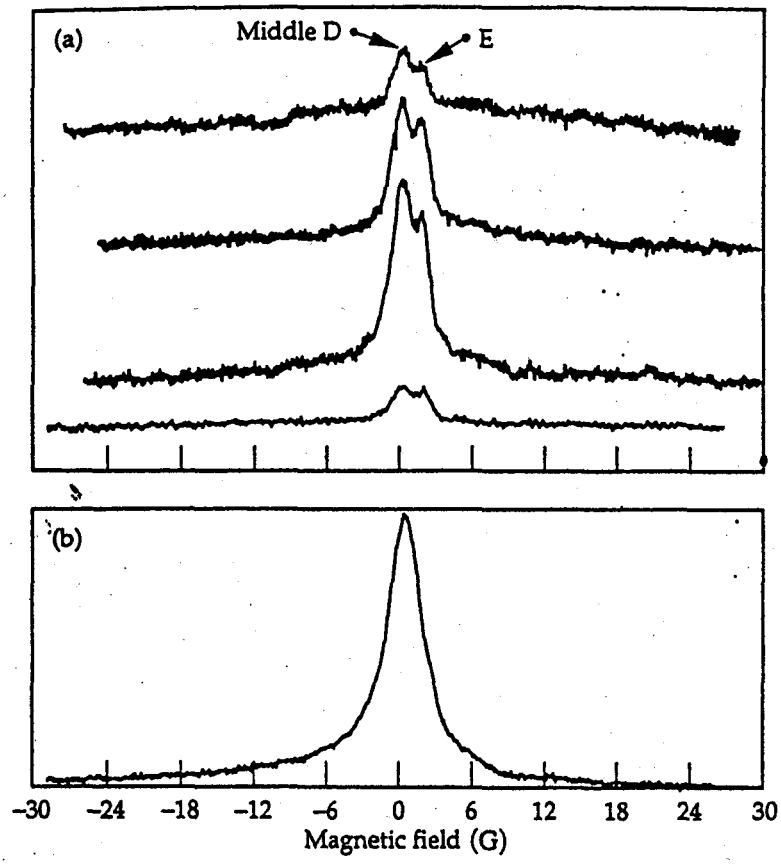

Fig. 1-3 ESR signal of the middle line of the D atom hyperfine triplet in D_2-T_2 (2 mol %) solid showing the presence of a new narrow signal, E, just to the high field side of the D line at 1.4 K [16]. (a) From top to bottom, the E and middle D atom line shape at 4, 30, and 54 min after cooling to 1.4 K, and 26 min after a "heat spike" [18]. Yields of D atoms and other radical species which assigns E increase with the increase in time as far as no heat spike is observed. (b) The middle D signal at 1.4 K when no heat spikes are observed for ~ 500 min. The yields of D increase with the increase in time whereas those of E saturate. This selectivity shows that the overlapped peaks are due to two other species. The authors speculated that the new narrow signal depicted by E is assigned as electron bubbles.

1. 2. Properties of Hydrogen Molecules and Solids

In this paragraph, properties of hydrogen molecules and solids are introduced. Because of small mass and small intermolecular interaction among hydrogen molecules, the hydrogen solids show characteristic properties reflecting their quantum effects.

1. 2. 1. Properties of hydrogen molecules and their variation

The hydrogen atoms forms hydrogen molecules with the bonding energy of 4.2 eV, the simplest of all molecular species. Fig. 1-4 shows the contours of equal in density of the hydrogen molecules in the ground electronic state [3]. The proton-proton separation is 0.74 Å. At the distance corresponding to nearest-neighbor separation in the hydrogen solid, the density is $\sim 3 \times 10^{-4}$, where the ratio of the minor to the major axis of the distribution is ~0.94. Thus, for low densities, the molecule must be visualized as being almost spherical rather than dumbbell shaped.

H atoms have isotopic species, D (^{2}H) and T (^{3}H). Generally, hydrogen is composed of H atoms at 99.915 mol % and their isotopic species of D atoms at 0.015 mol %, whereas T atoms are contained with the concentration of only 10^{-16} mol % [2]. The T atoms are radioactive species with the half lifetime of 12.33 years. The T atoms disintegrate by the nuclear reaction: $T \rightarrow {}^3He + \beta^- (18.6\ keV) + \bar{\nu}$ [2]. Generally, isotopes have mainly been used just as a marker, tracer, or prove, because the isotope effects on physical and chemical properties are negligible. However, in the case of the hydrogen isotopes, the isotope effects on these properties are not negligible in various aspects because of the reasons as follows. First, mass ratio among hydrogen isotopes are large (e.g. $m_T / m_H = 3$, $m_D / m_H = 2$). Second, because of their light mass, properties of hydrogens are dominated by quantum effects, such as zero-point motion, which are effectively depend on their mass. Therefore, the isotope effects of hydrogens are examined to study quantum effects on the properties of hydrogen molecules, solids, and ions.

Homonuclear diatomic molecule H_2 (D_2, T_2) is separated into two species: ortho and para. As shown in Fig. 1-5, ortho-H_2 (o-H_2) molecule has nuclear quantum spin number $I = 1$ and the rotational quantum number J = odd, whereas para-H_2 has $I = 0$ and J = even

[1~3,19]. This separation is originated from the reason as follows. Since proton is a fermion, total molecular wave function must be antisymmetric with respect to permutation of the protons. The wave function of the molecule can be written as a product of electric, vibrational, rotational, and nuclear spin wave functions. The electronic and vibrational wave functions are manifestly symmetric, whereas the easily accessible rotational and nuclear spin wave functions are either symmetric or antisymmetric. Thus, the allowed combinations for an antisymmetric total wave functions require consideration of only the latter two which are given in Table 1-1 [3]. As same as H_2, the homonuclear species of D_2 and T_2 also have such a distinction; whereas, the heteronuclear species such as HD do not have. It should be noted that, the ortho-para conversion of H_2 (D_2, T_2) do not occur without paramagnetic catalysts [1,3,20]. Therefore, H_2 (D_2 and T_2) are distinctly separated into ortho and para species which have different rotational and nuclear spin states.

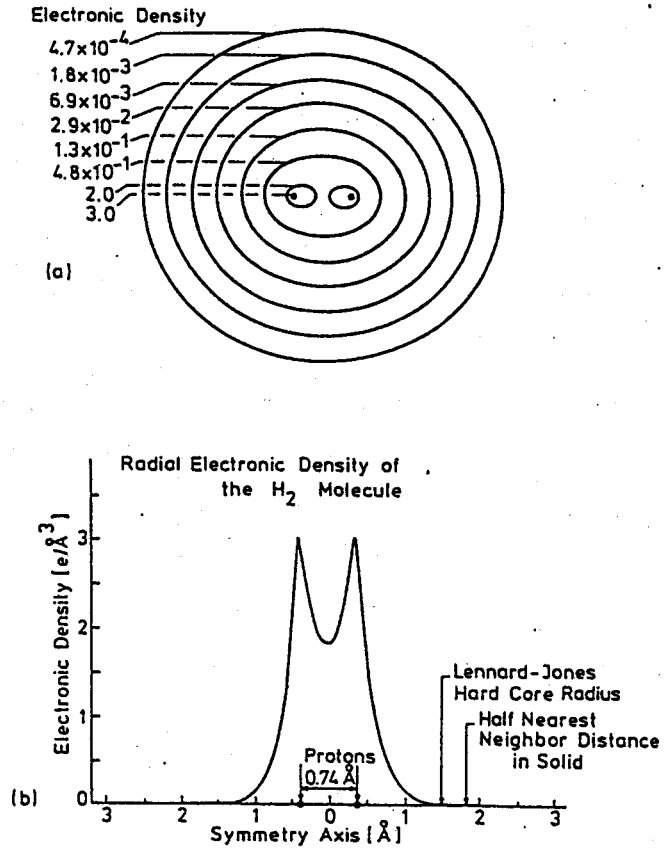

Fig. 1-4 The electronic charge density of the hydrogen molecule [3]. (a) Contours of equal density. (b) Density along the symmetry axis.

Molecule and spin of nucleon		I_{mol}	J	$\Psi(I_{mol})\Psi(J)$	Nuclear weight g_I	Designation
Hydrogen	State	0	Even			para
Tritium	Symmetry	AS	S	AS	1	
$I_N=\frac{1}{2}$	State	1	Odd			ortho
	Symmetry	S	AS	AS	3	
Deuterium	State	1	Odd			para
$I_N=1$	Symmetry	AS	AS	S	3	
	State	0, 2	Even			ortho
	Symmetry	S	S	S	6	

Table 1-1 Allowed combinations of nuclear-spin and rotational states for hydrogen, deuterium, and tritium, and the ortho-para designations [3]. Antisymmetric is depicted by *AS* and symmetric by *S*. I_{mol} is the total molecular nuclear spin and J is the rotational

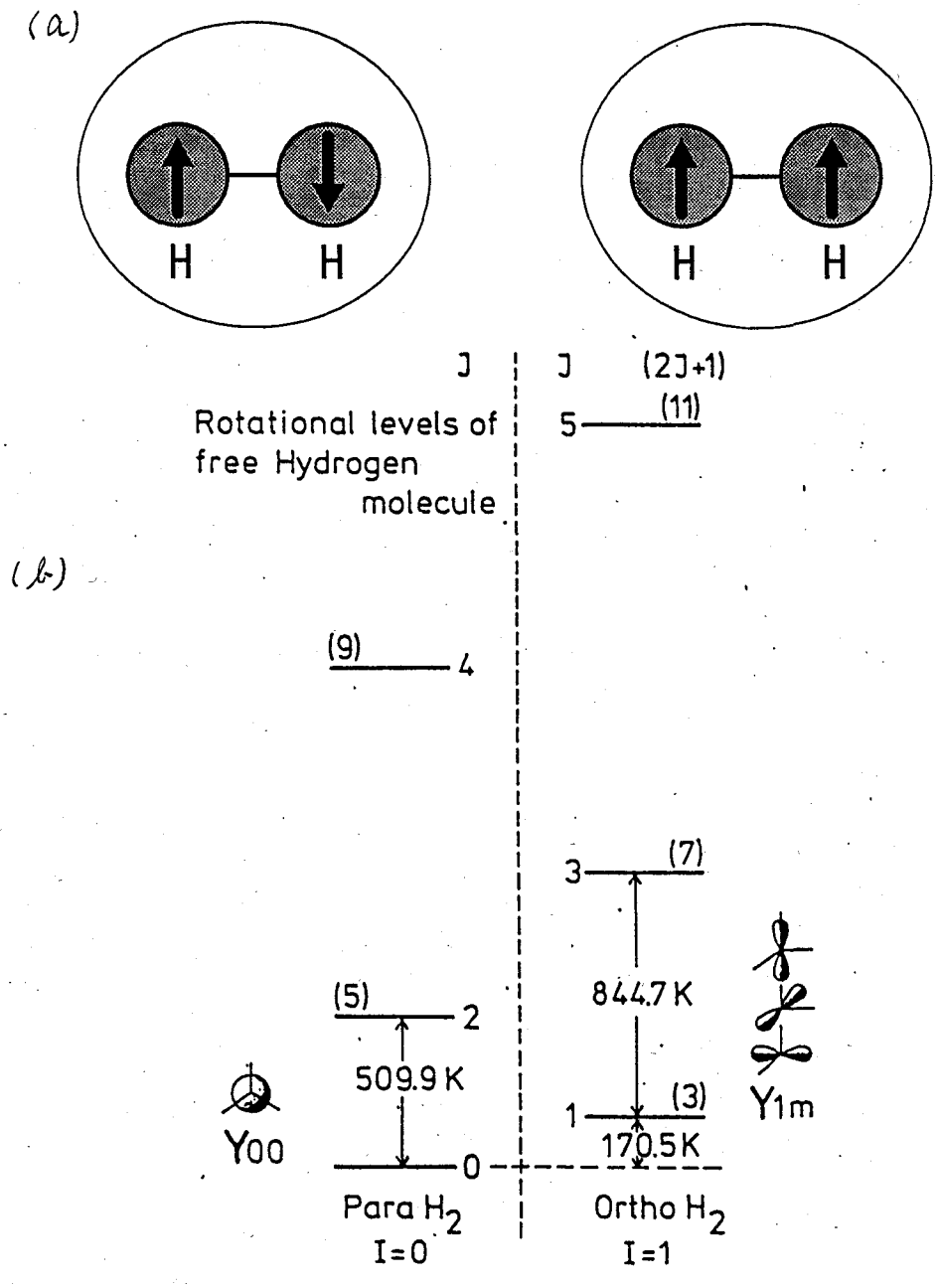

Fig. 1-5 (a) Models and (b) molecular rotational energy levels for an isolated H_2 molecules [3]. The rotational energy levels E_{rot} are obtained by: $E_{rot} = 85.25\ J\ (J + 1)$ K. The angular distribution of the two lowest rotational states are also indicated (Y_{10} and $Y_{11} \pm Y_{1-1}$ are actually shown). I is the total nuclear spin composed of two nuclear spins of proton $I_N = 1/2$ (arrows) aligned in antiparallel ($I = 0$) or in parallel ($I = 1$). Numbers in parenthesis are the m degeneracy, where m is the z-component of the rotational quantum number.

1. 2. 2. Properties of hydrogen solids [1–3,12]

Hydrogen molecules are condensed to form the molecular hydrogen solid with the hexagonal closed packed structure (hcp). Properties of the hydrogen solid are shown in Table 1-2 together with those of rare gas solids. The hydrogen solid is the solid which has the lowest melting temperature (14 K) in all solids at the normal condition on earth. Because of small mass and intermolecular interaction (~ 35 K), the hydrogen solids show various quantum effects characteristic of the quantum solid. The quantum mechanical zero-point energy is comparable to the binding energy and the root-mean-square deviation of a particle from its lattice site goes up to about 18 % of the nearest-neighbor distance (3.78 Å) [12]. Because of this large zero-point motion, the lattice constant is 0.22 Å larger than the equilibrium distance for the isotropic pair potential of H_2. Thus, the nearest neighbor distance of a hydrogen solid becomes larger than that of most other simple solids.* Fig. 1-6 shows solid molar volume of p-H_2, n-H_2, and o-D_2 [2]. The molar volume which is proportional to the cube of the nearest neighbor distance of p-H_2 solid is larger than that of n-H_2 and ortho-D_2 (o-D_2) solids. The difference between H_2 and D_2 is due to the difference in amplitude of zero-point vibration of these molecules in the solid, whereas that between p-H_2 and n-H_2 is ascribed to the quadruple-quadruple interactions between o-H_2 molecules contained in n-H_2. Such quantum properties are reflected on the molar volume. Another striking property of the hydrogen solids is that hydrogen molecules trapped have almost free vibrational and rotational quantum states, because of the larger intermolecular distance, small binding energy, and high symmetry of D_{3h} structure of the solid. This property shows that the effects of intermolecular interaction as a small perturbation on the properties of the free molecule.

Nearest neighbor distances of He (hcp), Ne (fcc), and Ar (fcc) crystals are 3.50, 3.20, and 3.83 Å, respectively. Note also that the intermolecular distance in the H solid is 0.22 Å greater than the equilibrium distance for the isotropic pair potential of H_2 and 0.44 Å shorter than the H_2-H_2 distance in a gaseous hydrogen dimer $(H_2)_2$.

	p-H_2	^{3}He	^{4}He	Ne	Ar
Triple point temperature (K)	13.8	-	-	24.5561	83.8058
Triple point pressure (kPa)	7.03	-	-	50	68.95
Boiling temperature at 1 atm (K)	20.28	3.20	4.2221	27.07	87.293
Density (cc / mol)	23.06	24.31	20.97	13.39	27.09
Crystal structure *	hcp	bcc	hcp / bcc	fcc / hcp	fcc / hcp
Nearest neighbor distance (Å)	3.78	3.73	3.6	3.156	3.755
Lennard-Jones parameter ε (K) **	37	10.2	10.2	35.6	119.3
σ (Å)	2.92	2.56	2.56	2.74	3.45
Minimum energy point of Lennard-Jones potential (Å)	3.28	2.87	2.87	3.07	3.87
Quantum parameter (λ^2) ***	0.076	0.241	0.182	0.0049	0.0027
Debye temperature (K)	100	18.4	34	66	84
Amplitude of zero-point vibration (Å)	0.68	1.18	1.03	0.29	0.18
Ratio of amplitude of zero-point vibration to nearest neighbor distance (%)	18	32	29	9	5

Table 1-2 Properties of hydrogen and rage gas solids [21]

* Crystal structure depends on pressure and temperature.

** Lennard-Jones potential shows interatomic (intermolecular) interactions depicted by $\phi(R) = 4\ \varepsilon\{(\sigma / R)^{12} - (\sigma / R)^6\}$. σ is the distance where $\phi(\sigma) = 0$, showing approximate core radius of atoms or molecules.

*** Quantum parameter λ is defined as $\lambda = \hbar / \sigma\sqrt{m\varepsilon}$, where m is mass of the atom or molecule. λ is approximately proportional to the amplitude of zero-point vibration.

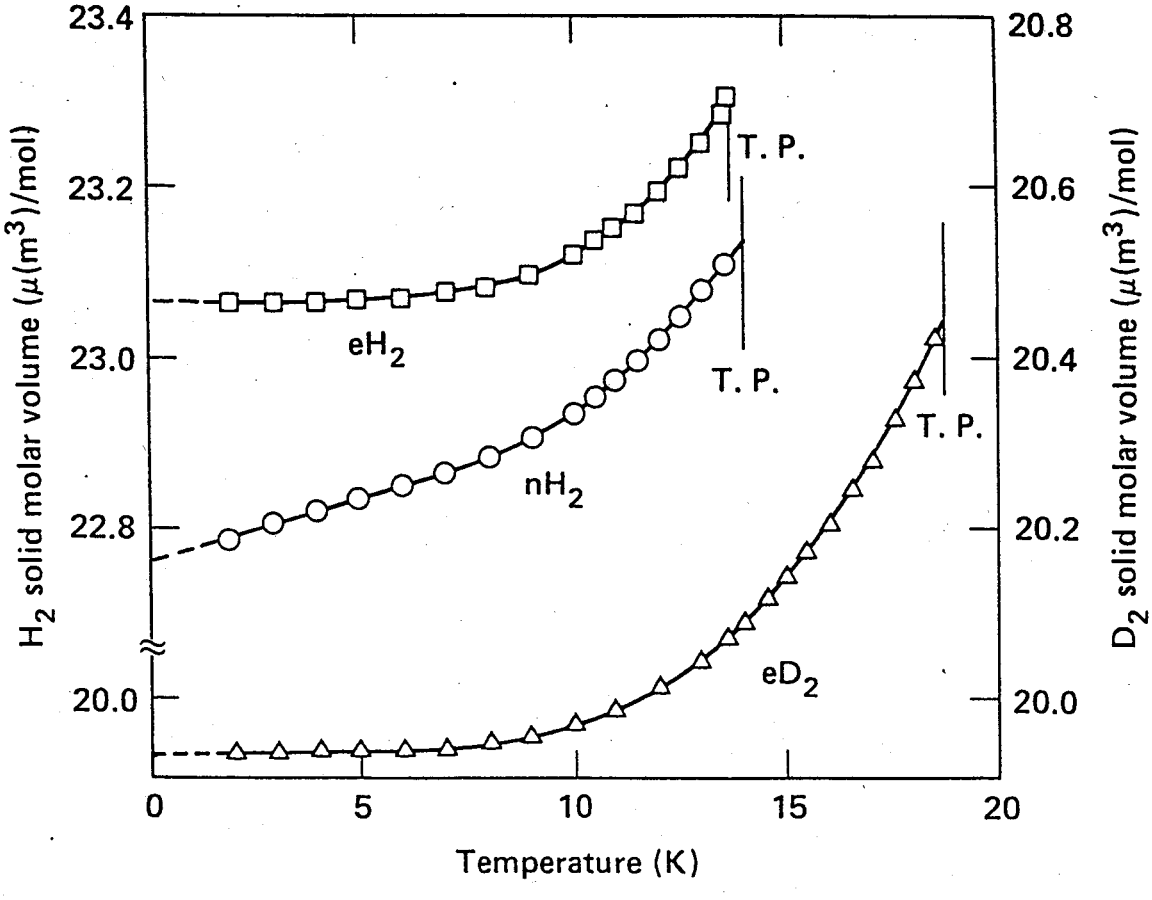

Fig. 1-6 Molar volumes of p-H_2, n-H_2, and o-D_2 solids. T.P. indicates the triple points [2].

1. 2. 3. Properties of p-H_2 solid and its advantage for high-resolution ESR spectroscopy

P-H_2 solids are composed almost exclusively of $I = J = 0$ H_2. Since probability distribution of the protons and electrons in the $J = 0$ rotational levels is spherically symmetric, the p-H_2 solid forms a highly-coherent crystal. Recently, Oka et al. [12] have found that infrared absorption and Raman spectra of molecular species trapped in the p-H_2 solid have very narrow linewidth due to the coherence, and reported precise properties of the solid. The technique has been applied to the study of radiation effects [15], tunneling reaction [8], non-linear optics [22] in the solid. In addition, the p-H_2 solid is useful for the study of quantum tunneling diffusion of particles in solids. Meyer et al. [23] and Sullivan et al. [24] have found that o-H_2 and HD molecules in the p-H_2 solid diffuses via quantum tunneling at low temperatures, respectively. These phenomena are ascribed to the high-coherence of the p-H_2 solid. As discussed in Chapters 4 and 5, the quantum tunneling diffusions are also reported in this thesis. These properties are attributed to the spherical symmetry ($J = 0$) of the p-H_2 molecule accompanied with high-coherence of the solid.

The most available property of the p-H_2 solid on the ESR measurement is rather absence of nuclear spins ($I = 0$) in the p-H_2 solid than the spherical symmetry [25]. Generally, ESR linewidth of sharp signal is broadened by distribution of internal magnetic field originated from nuclear spins of surroundings, that is, superhyperfine interaction [26]. Fig. 1-7 shows ESR spectra of ethyl radical in (a) n-H_2 and in (b) p-H_2. The resolution of the ESR spectrum in (b) is much better than in (a), because the linewidth in (a) is broadened due to the superhyperfine interaction with surrounding nuclear spins in o-H_2 molecules ($I = 1$) contained in the n-H_2 solid. On the other hand, the effects of the superhyperfine interaction on the linewidth is negligible in (b), because p-H_2 has no nuclear spins. It can be seen that the p-H_2 solid is useful for the ESR study of radical species trapped in hydrogen solids.

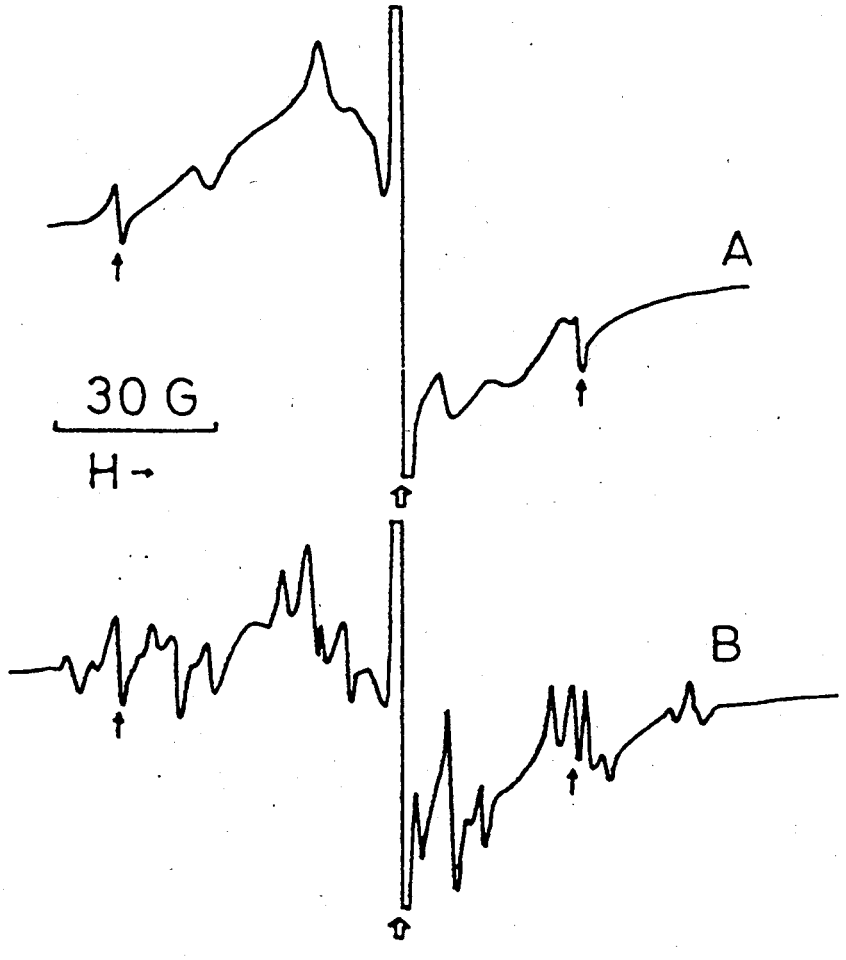

Fig. 1-7 ESR spectra of ethyl radicals (CH_3CH_2·) in (a) n-H_2 and (b) p-H_2 solid at 4.2 K [25]. The ethyl radicals are produced by the photolysis of ethyl-iodide (CH_3CH_2I). Broad signals overlapped are those of ethyl radicals produced in undissolved ethyl-iodide cluster.

1. 3. ESR Study of Ionic Species in P-H_2 Solid and Observation of H_2^- anions

The ionic species are generated by the radiolysis of hydrogen solids; however, it had not been well understood what species are produced by the radiolysis. I studied the ionic species produced in X(γ)-ray irradiated p-H_2 solid using the high-resolution ESR spectroscopy and found new quartet signals assigned as H_2^- anions for the first time.

1. 3. 1. Radiation effects

The ionic species are produced by radiolysis of the p-H_2 solid. High-energy X-ray (less than 50 keV) and γ-ray (1.17 and 1.33 MeV) ionize H_2 to form H_2^+ and electron initially by Compton scattering. The scattered electrons, having energies of a fraction of keV or MeV, initiate cascades of ionization which is rather the main process for the radiolysis. Thus, the radiation effects do not depend on those irradiation sources and energy of the incident beams. Precise processes of ionization in hydrogen solid have not been understood, although they have been inferred from those observed in gas phase (cf. Table 2-1). I discuss the product ions by the radiolysis of the hydrogen solids at the time after irradiation with ignoring fast process of ionization process during the irradiation in this thesis.

Such intense ionization would leave the ordinary dielectric materials as rubble of radiation damage, but the extraordinary self-repairing nature of hydrogen solids keep the crystal still ordered and transparent to radiation [12]. Details in the dissociation and ionization processes are reviewed in Ref. [2] and mentioned in Chapter 2.

1. 3. 2. Observation of H_2^- anions in X(γ)-ray irradiated p-H_2 solid

The new technique of high-resolution ESR spectroscopy was applied to the precise study of ionic species produced in X(γ)-ray irradiated p-H_2 solid. I succeeded in observing very small quartet signals which have not been observed in n-H_2 and assigned

them as H_2^- anions. This is the first direct and clear observations of ionic species produced in irradiated hydrogen solids and of stable species of H_2^- anions in hydrogen solids. I also studied decay behaviors of the H_2^- anions in the p-H_2 solid. The new finding shows irradiation effects in solid hydrogen, the trapping state of anionic species in quantum solid, and motions of the H_2^- anions at the time after irradiation.

References

[1] J. V. Kranendonk, Solid Hydrogen (Plenum, New-York, 1983).

[2] P. C. Souers, Hydrogen Properties for Fusion Energy (University of California Press, Berkeley, 1986), and references therein.

[3] I. F. Silvera, Rev. Mod. Phys. 52 (1980) 393.

[4] bubble

[5] Y. Tabata, Y. Ito and S. Tagawa, Handbook of Radiation Chemistry (CRC Press, 1991).

[6] T. Miyazaki, K-P. Lee, K. Fueki and A. Takeuchi, J. Phys. Chem. 88 (1984) 4959.

[7] V. A. Benderskii, D. E. Makarov and C. A. Wight, Chemical Dynamics at Low Temperatures (John Wiley & Sons, New York, 1994).

[8] T. Momose, H. Hoshina, N. Sonoshi, H. Katsuki, T. Wakabayashi, and T. Shida, J. Chem. Phys. 108 (1998) 1; T. Momose and T. Shida, Bull. Chem. Soc. Jpn. 71 (1998) 1.

[9] F. Vigliotti, M. Chergui, M. Dickgiessr, and N. Schwentner, Faraday Discuss. 108 (1997) 139.

[10] H. Suzuki, Toward Interstellar Chemistry (University of Tokyo, Tokyo, 1989).

[11] T. Oka, Rev. Mod. Phys. 45 (1992) 1141.

[12] T. Oka, Annu. Rev. Phys. Chem. 44 (1993) 299; T. Oka, Fiz. Niz. Temp. 22 (1996) 134.

[13] P. C. Souers, E. M. Fearon, P. E. Roberts, R. J. Tsugawa, J. D. Poll and J. L. Hunt, Phys. Lett. A 77 (1980) 277; P. C. Souers, E. M. Fearon, R. L. Stark, R. T. Tsugawa, J. D. Poll, and J. L. Hunt, Can. J. Phys. 59, 1408 (1981).

[14] R. L. Brooks, S. K. Bose, J. L. Hunt, Jack R. MacDonald and J. D. Poll, Phys. Rev. B 32 (1985) 2478; R. L. Brooks, J. L. Hunt, Jack R. MacDonald, J. D. Poll and J. C. Waddington, Can. J. Phys. 63 (1985) 937.

[15] T. Momose, K. E. Kerr, D. P. Weliky, C. M. Gabrys, R. M. Dickson and T. Oka, J. Chem. Phys. 100 (1994) 7840.

[16] G. W. Collins, P. C. Souers, F. Magnotta, E. R. Mapoles and, J. R. Gains, Phys. Rev. B 53 (1996) 8143.

[17] T. Miyazaki, H. Morikita, K. Fueki and T. Hiraku, Chem. Phys. Letters 182 (1991) 35; T. Miyazaki and H. Morikita, Bull. Chem. Soc. Jpn. 66 (1993) 2409.

[18] G.W. Collins, E. M. Fearon, J. L. Maienschein, E. R. Mapoles, R. T. Tsugawa, P. C. Souers, and J. R. Gains, Phys. Rev. Lett. 65 (1990) 444.

[19] G. S. Russibrooke, Introduction to Statistical Mechanics (Clarendon Press, Oxford, 1951)

[20] Motizuki and T. Nagamiya, J. Phys. Soc. Jpn. 11 (1956) 93; K. Motizuki and T. Nagamiya, J. Phys. Soc. Jpn. 11 (1956) 654.

[21] T. Momose and T. Oka, Ouyou Butsuri, 65 (1996) 902.

[22] M. Suzuki, M. Katsuragawa, R. S. D. Sihombing, J. Z. Li, and K. Hakuta, J. Low. Temp. Phys. 111 (1997) 463.

[23] H. Meyer, Can. J. Phys. 65 (1987) 1453.

[24] M. Rall, D. Zhou, Erika G. Kisvarsanyi, and N. S. Sullivan, Phys. Rev. B 45 (1992) 2800; D. Zhou, C. M. Edwards, and N. S. Sullivan, Phys. Rev. Lett. 62 (1989) 1528; E. F. DeRose, E. A. Gislason, N. H. Sabelli, K. M. Sluis, J. Chem. Phys. 88 (1988) 4878.

[25] T. Miyazaki, K. Yamamoto, and J. Arai, Chem. Phys. Lett. 219 (1994) 405.

[26] A. Abragam, The principle of Nuclear Magnetism (Oxford Press, 1961).

Chapter 2

ESR Study of X(γ)-ray Irradiated Solid Hydrogen

2. 1. Experimental Procedures

Experiments in this study have been done in laboratories at Japan Atomic Energy Research Institute (JAERI) and at Nagoya University, but experimental procedures are similar except for irradiation source, X- or γ-ray. Details of the experimental procedures are described below.

2. 1. 1. Sample Preparation

Para-hydrogen (p-H_2) is obtained by converting normal-hydrogen (n-H_2) with the aid of a catalyst ferric hydride (FeO(OH)) at low temperatures [1]. The schematic diagram of the conversion system is shown in Fig. 2-1. The normal gas with the purity higher than 99.99999 mol % is introduced in the Pyrex-glass vacuum line after evacuation higher than 10^{-5} torr. The gas is condensed in the Cryocooler (Nagase & Co. Ltd. Model UV204SC) where the powdered FeO(OH) is immersed in the condensed liquid hydrogen and the ortho-para conversion is achieved at 14 K after about 5 hours. The remaining ortho-hydrogen (o-H_2) is 1~4 mol %. The obtained p-H_2 is then transferred into the sample cells by evaporation the product in the Cryocooler by heating up to 22 K.

The purity of the sample was measured using gas chromatography [1] or Raman spectroscopy. A gas chromatogram of the n-H_2 and catalyzed H_2 samples and a Raman spectrum of the catalyzed H_2 sample are shown in Figs. 2-2 and 2-3, respectively. These

results indicate that almost all o-H_2 in the n-H_2 sample were converted into p-H_2 by the catalysis and that the purity of the p-H_2 was between 96~99 mol %. "pure p-H_2" in this paper denotes p-H_2 containing HD at natural abundance (0.03 mol %) and o-H_2 at 1~4 mol %. In some cases, HD, D_2, or o-H_2 were added to gaseous pure p-H_2.

Two types of sample cells used are illustrated in Fig. 2-4. The most parts of the cells are made of Pyrex glass, but the bottom tips of the cells are made of high-purity quartz glass to minimize color centers produced by X(γ)-ray radiolysis. The p-H_2 gas in the cell is solidified at the bottom tip of the cell by cooling the tip with cold helium gas or liquid. The solid p-H_2 sample is polycrystalline and transparent.

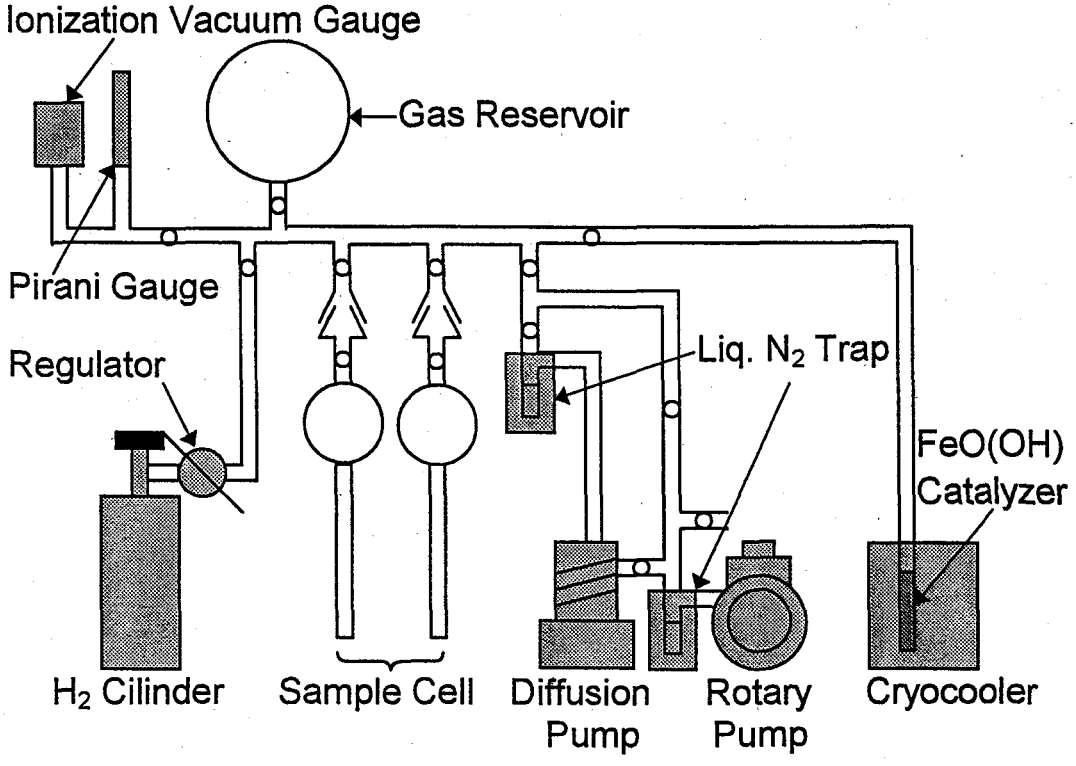

Fig. 2-1 Schematic diagram of the vacuum line.

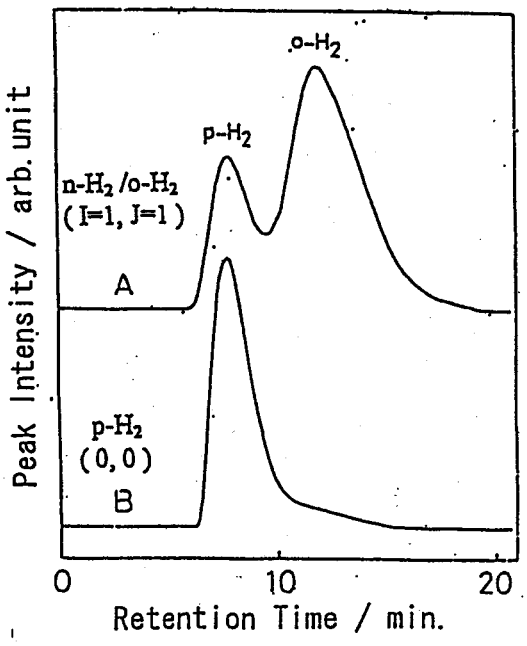

Fig. 2-2 Gas chromatogram of the n-H_2 and catalyzed H_2 sample.

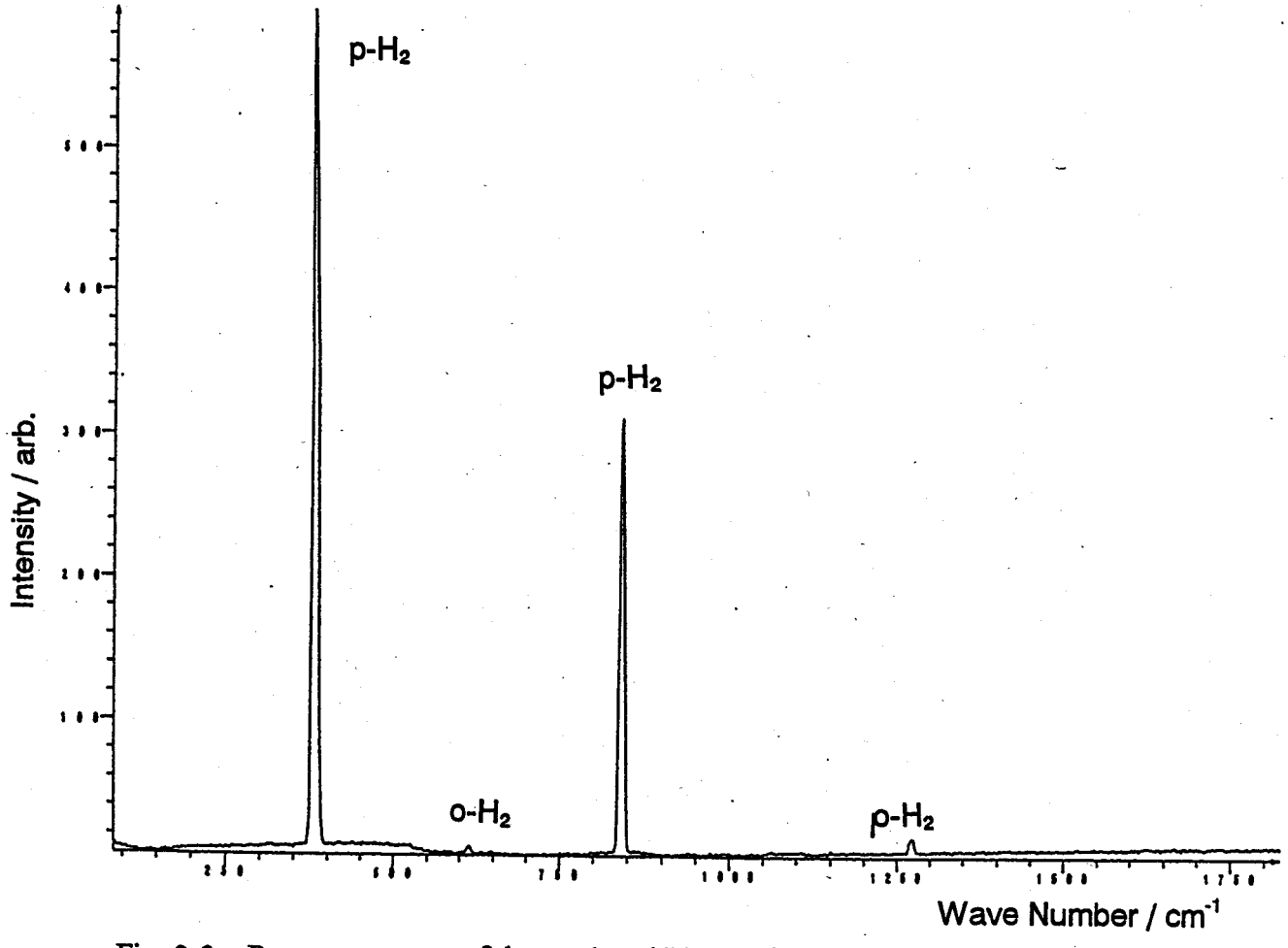

Fig. 2-3 Raman spectrum of the catalyzed H_2 sample.

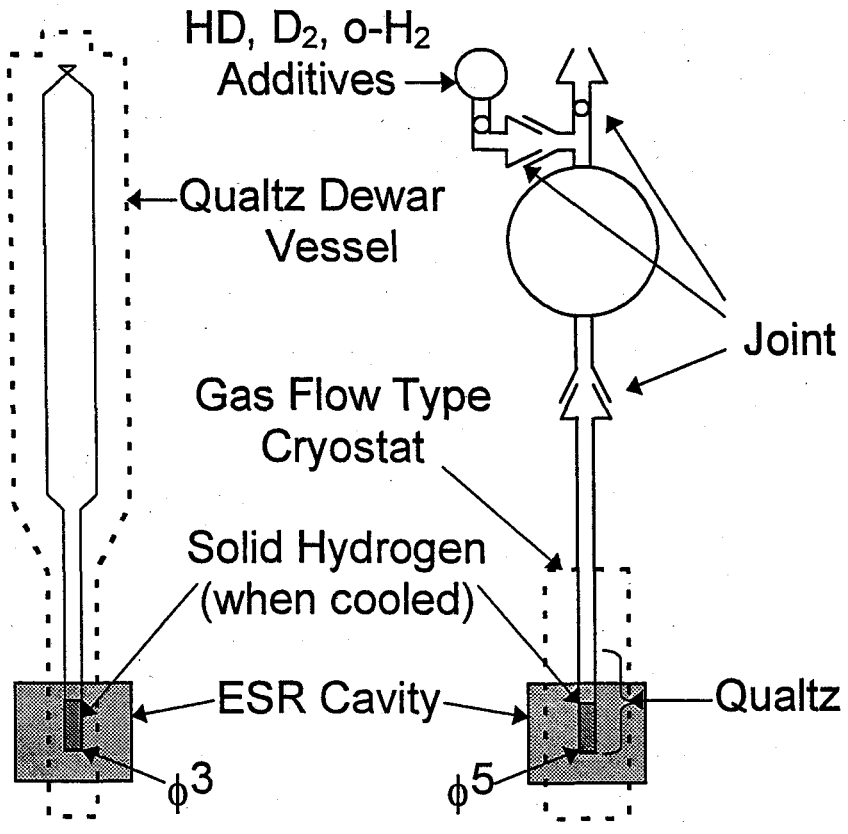

Fig. 2-4 Schematic diagram of the sample cells. The left cell is used for the quartz Dewar vessel cryostat. The right cell is used for the gas flow type cryostat. Details of these cryostats are shown in Figs. 2-5 and 7.

2. 1. 2. Cryostat

The gaseous p-H_2 sample prepared is solidified in a cryostat before X(γ)-ray irradiation and ESR measurement. In this study, two types of cryostat systems, gas flow type cryogenic temperature controller and quartz Dewar vessel, are used. Details of these cryostat systems are introduced below.

Gas flow type cryogenic temperature control system

The gas flow type cryogenic temperature control system (Scientific Instrument Inc. Model 9650-6) at JAERI was mainly used for the ESR measurement in the temperature range between 2.7~6.6 K. The schematic diagram of the system is illustrated in Fig. 2-5. Cold helium gas guided from a helium vessel is blown through the thin gap between the sample cell and helium guide, surrounded by the double layered pipe which shields thermal conduction by vacuuming. These three parts, which are located inside of the ESR cavity, are made of high-purity quartz glass to minimize the generation of paramagnetic impurities and to avoid the decrease in Q-value of the ESR cavity. This system is so complicated and tightly connected to the ESR system that it cannot be moved with keeping sample temperature around 4 K. Thus, the p-H_2 sample solidified just above the ESR cavity is irradiated with compact X-ray irradiation system, which can be settled at the position very close to the cryostat, and then shifted down to the center of the ESR cavity for ESR measurement. Details of the X-ray irradiation and ESR measurement are mentioned in Chapter 2.1.3 and 2.1.4, respectively.

The advantage of this temperature control system is wide variation of attainable temperature between 2.7~400 K with easy operation. The temperature is controlled by adjusting the flow rate of the cold helium gas together with pumping and heating by the rotary pump and heater, respectively. Especially, current on the heater is automatically adjusted by the negative feedback from temperature of the cold helium gas monitored by

Ga-As diode thermometers (A) and (B) which makes deviation of the temperature within ± 0.1 K.

The temperature of the p-H_2 solid in the system is precisely calibrated by immersing Au-0.07%Fe vs. Cr thermocouple in the p-H_2 solid. Fig. 2-6 shows the temperature of the p-H_2 solid and that of the helium gas monitored by the thermometers (A) and (B) in Fig. 2-5 as a function of the flow rate of the helium gas. The temperature of the p-H_2 solid is accurately calibrated by monitoring the temperature with the thermometers and flow rate, even when the thermocouple immersed in the p-H_2 sample is removed on the ESR measurement.

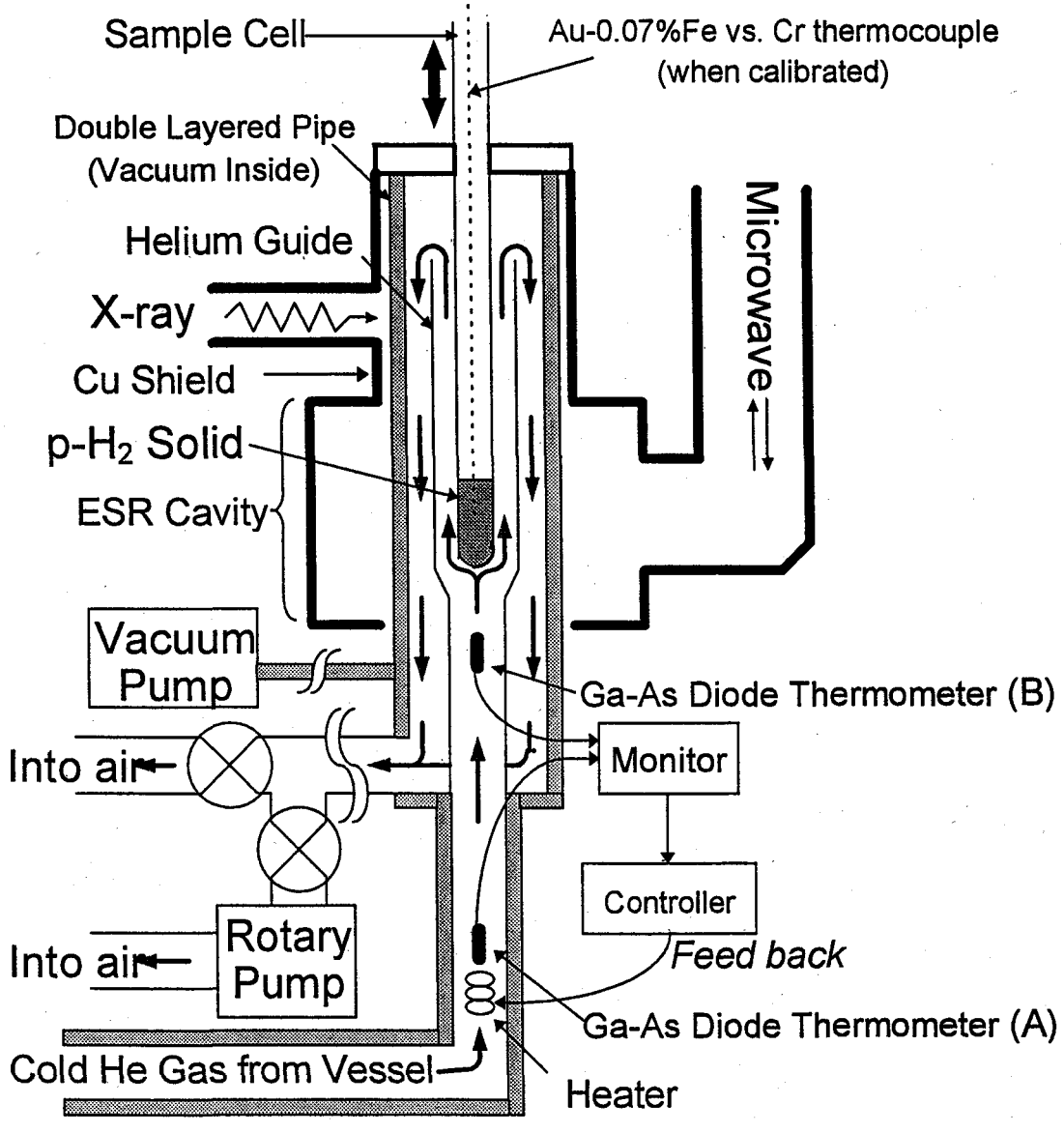

Fig. 2-5 Schematic diagram of the cryogenic temperature control system for ESR measurement.

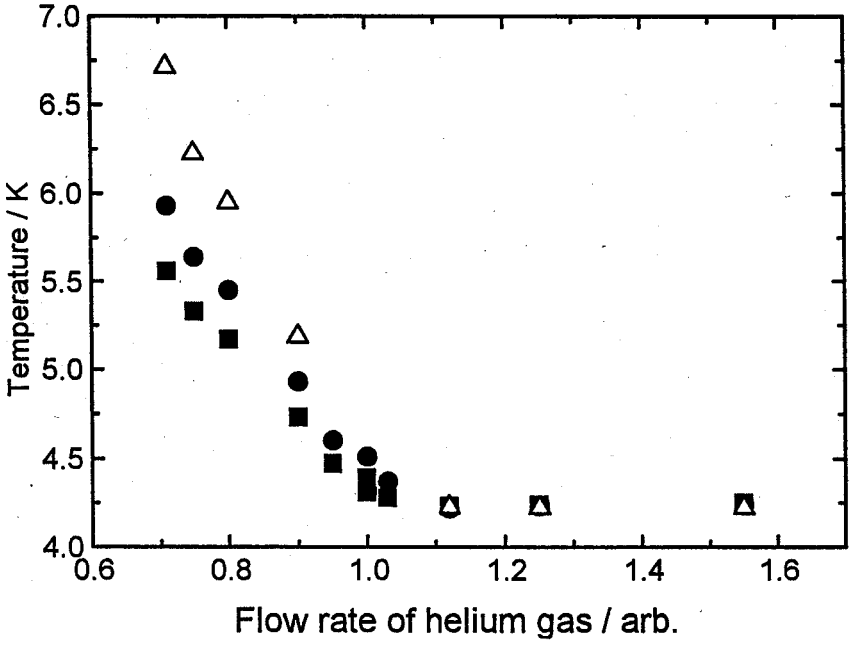

Fig. 2-6 Temperatures of the helium gas monitored by Thermometers (A) (closed squares) and (B) (closed circles) in Fig. 2-5 and of the p-H_2 solid monitored by the Au-0.07%Fe vs. Cr thermocouple immersed.

Quartz Dewar vessel system

The quartz Dewar vessel system is used for all measurements at Nagoya University and some ones at JAERI when temperature between 1.3~2.7 K is required. This system has the following two advantages. First, the p-H_2 solid settled in the quartz Dewar vessel is mobile with keeping temperature at 4.2 K, although the gas flow type system is immobile. Thus, this system is useful at Nagoya University, where C_0-60 source for radiolysis and ESR system for measurement are located at separate laboratories. Second, temperature of the sample in the quartz Dewar vessel can be cooled down to 1.3 K by connection with the pressure control system at JAERI which is lower than lowest achievable temperature of the gas flow type system of 2.7 K.

The cross sections of the Dewar vessel system are illustrated in Fig. 2-7 [2]. It consists

of outer (h) and inner (i) vessels which are liquid nitrogen and helium containers, respectively. The outer vessel has an opened gate not at the top but at the bottom (n). The cold nitrogen gas evaporated from the nitrogen container (j) passes through the thin gap between the inner and the outer vessels and goes out through the bottom gate. The gas flow rate is controlled by immersing copper wire partially in the liquid nitrogen (g). A few pieces of zeolite pellets (q) are sunk for preventing bumping of the liquid nitrogen.

The advantage of this cryostat is no ESR noise due to the bubbling of liquid nitrogen. The inner vessel of a conventional cryostat for liquid helium is usually immersed in liquid nitrogen. Since the dielectric constants of liquid and gaseous helium at 4.2 K are almost the same, the bubbling of the liquid helium in an ESR cavity does not cause the ESR noise while nitrogen bubbling induces a serious fluctuations due to large difference in the dielectric constants.

Temperature in the range between 1.3~2.7 K is controlled by pumping helium gas at adequate pressure, which is precisely controlled by the pressure control system shown in Fig. 2-8. The needle valve connected is operated with automatic controller which keeps pressure of the gaseous helium within ±0.1 % over 9 hours.

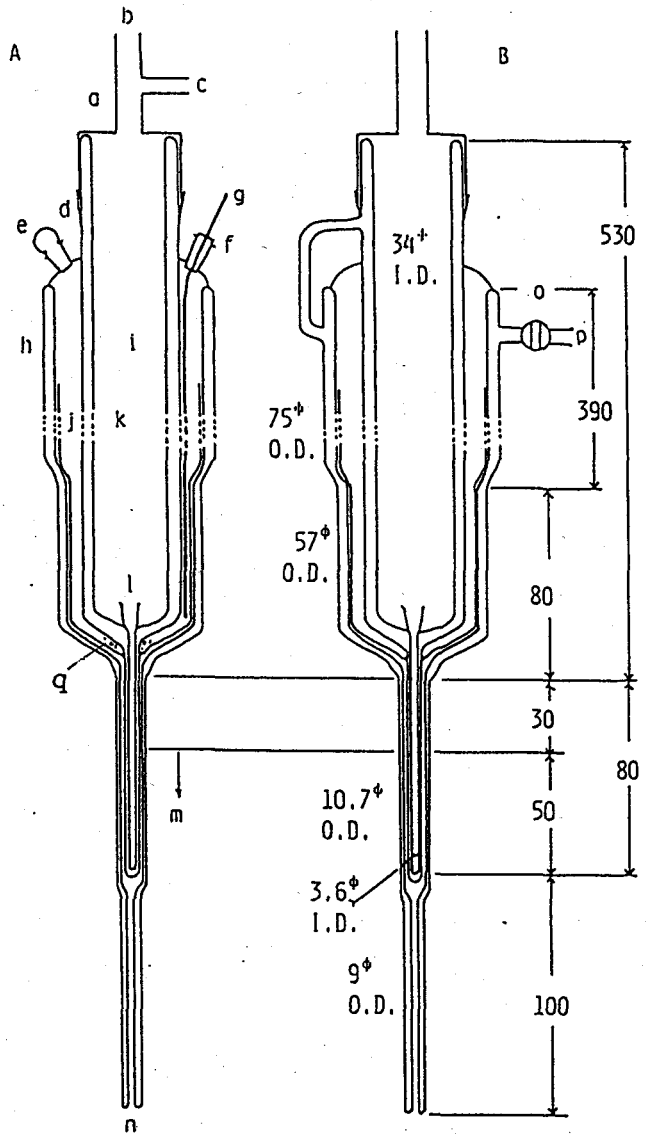

Fig. 2-7 Cross sections of the Dewar vessel type cryostat for ESR measurements [2]. Cross section B is perpendicular to the cross section A. (a) Stainless cap, (b) He inlet, (c) He outlet, (d) rubber band, (e) N_2 inlet, (f) rubber stopper, (g) heat conductor, (h) outer Dewar vessel, (i) inner Dewar vessel, (j) N_2 container, (k) He container, (l) funnel for preventing the precipitation of solidified air in the tip portion, (m) unshielded tip portion, (n) N_2 outlet, (o) stop cock, (p) to vacuum, (q) zeolite pellets.

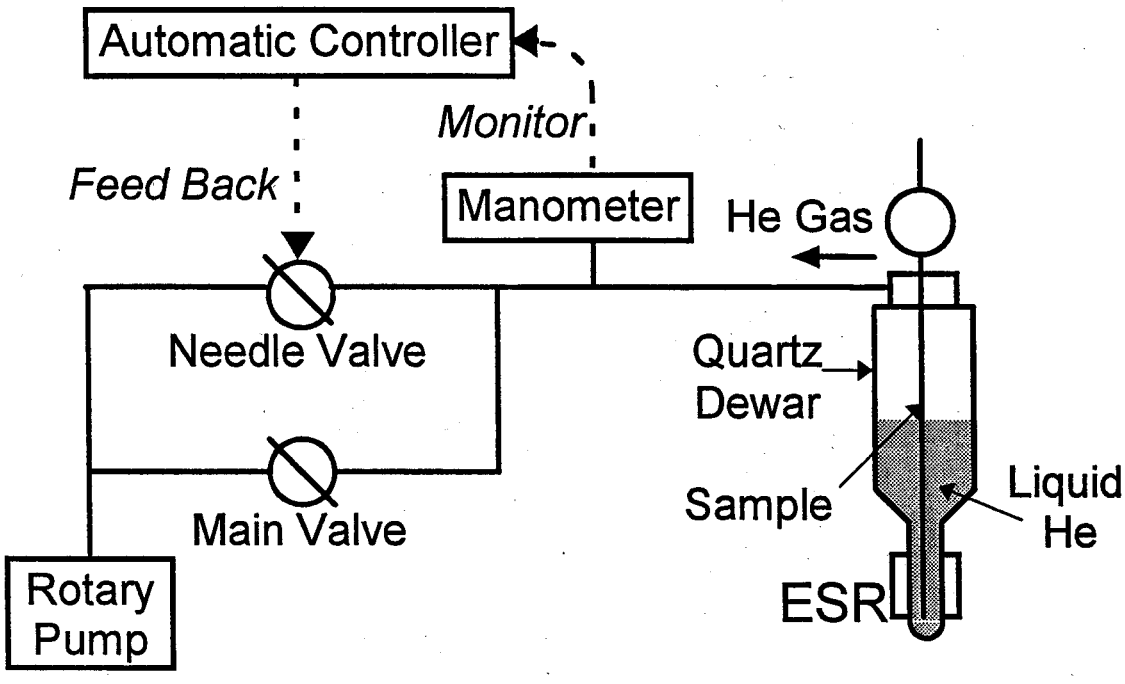

Fig. 2-8 Block diagram of the pressure control system.

2. 1. 3. Radiolysis

X-rays and γ-rays are used on the radiolysis of the p-H_2 solid to produce enough amounts of radical species for ESR measurement. Details of these irradiation systems are written below.

X-ray irradiation system

The X-ray irradiation system (Mac-Science Model XM590) at JAERI is mainly used for studying effects of temperature on behaviors of the radical species. Schematic view of the X-ray generator is shown in Fig.2-9. The X-rays are generated by electron beams (50 keV, 48 mA) exposing on a molybdate target and then introduced to the p-H_2 solid for 2.5 hours at 4.5 K. The path of the X-rays to the cryostat is shielded by a thick copper

pipe for safety. The X-ray irradiation system generates less amounts of radicals in the p-H_2 sample and high amounts of radicals in the quartz cell, which interferes ESR measurement of the p-H_2 sample, compared with γ-ray irradiation system. However, the X-ray tube is so compact and portable that the X-rays can irradiate the sample already solidified in the immobile cryostat systems, the gas flow type temperature control system (cf. Fig. 2-5) and quartz Dewar vessel connected with pressure control system (cf. Fig.2-8), which can control the temperature of the sample.

γ-ray irradiation system

The γ-ray irradiation system at Nagoya University is mainly used for studying effects of impurities on the properties behaviors of the radical species at 4.2 K. An ESR spectrum of the γ-ray irradiated p-H_2 solid has much better S/N ratio than that of the X-ray irradiated p-H_2 solid, because the γ-rays produce higher amounts of radicals in the solid p-H_2 sample with lower amounts of undesirable radicals in the quartz cell. These advantages enable us to study the detailed properties of the radicals in the p-H_2 solid at 4.2 K.

The p-H_2 sample dipped in the quartz Dewar vessel filled with helium liquid is irradiated with γ-rays in Co-60 irradiation facility at Nagoya University for 30 min to a total dose of 0.4~0.7 kGy. After the irradiation, the Dewar vessel is carried and set to the ESR spectrometer in our laboratory at Nagoya University within 30 min. The bottom tip of the Dewar vessel, where the p-H_2 solid is located, have been wrapped with an aluminum foil until settled into the ESR spectrometer for eliminating light.

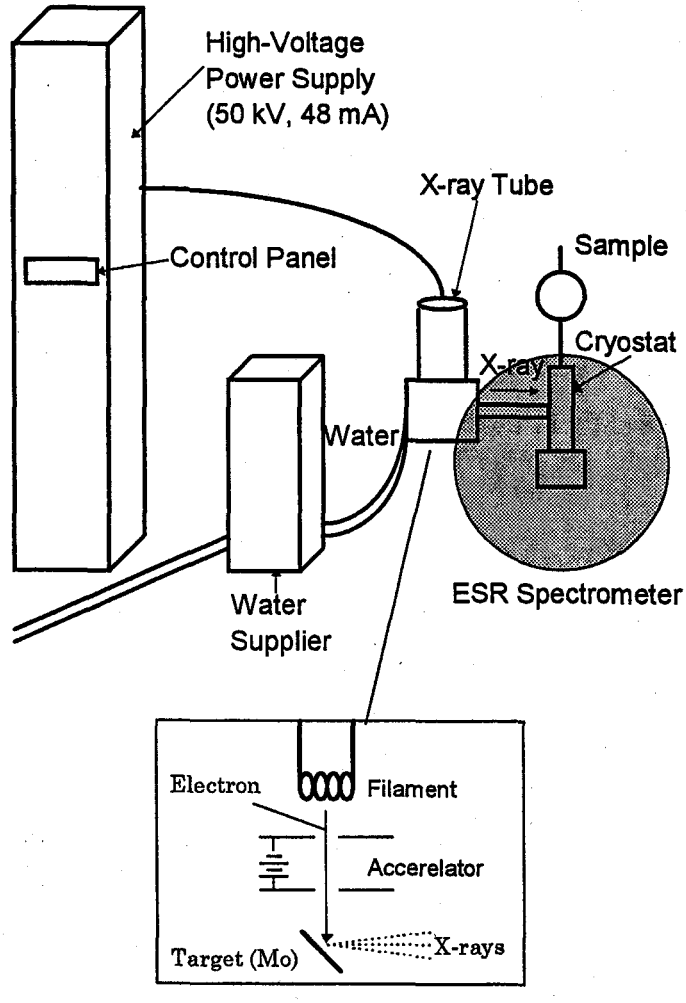

Fig. 2-9 Schematic view of the X-ray generator. The inset below shows the rough sketch of the X-ray tube.

2. 1. 4. ESR System

The standard reflection type X-Band (~9 GHz) ESR spectrometer of JEOL JES-TE200 at JAERI and JEOL RE1X at Nagoya University are used for the measurements of X and γ-ray irradiated p-H_2 solid, respectively. The Block diagram of the spectrometer is shown in Fig. 2-10. Microwave is produced by the Gunn-diode (JES-TE200) or Klystron (RE1X) oscillator and guided to the rectangular resonant cavity of TE_{011} mode. Q-value of the cavity is about 8,000. Magnetic field up to 13,000 G is generated by high-homogeneous electromagnet with 100 kHz modulation by attached modulation coils. The reflected microwave is guided to a detector crystal. The signal is amplified and phase-detected to obtain an ESR spectrum. The spectrum is digitized and monitored on the computer which is connected to the ESR spectrometer.

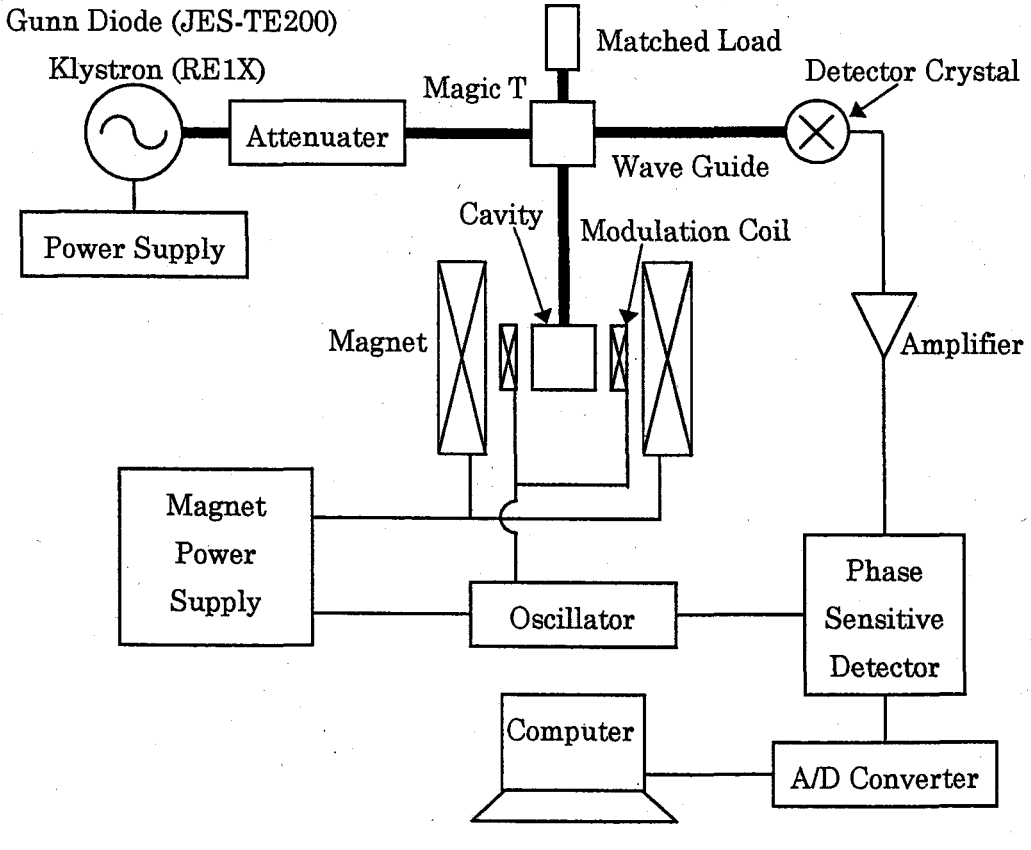

Fig. 2-10 Block diagram of JEOL JES-TE200 (RE1X) ESR spectrometer.

2. 2. ESR spectrum of new quartet signal

2. 2. 1. Radiation damage in H_2

Radiation damage in H_2 gas has been studied theoretically and experimentally. Secondary electrons produced by irradiation ionize and excite the H_2 molecules. Table 2-1 shows calculated radiation damage events in H_2 gas bombard with one 100 keV electron. Main products in this step are H_2^+, e^-, and H. It was reported that almost all H_2^+ cations react with surrounding H_2 molecules to produce H_3^+ cation:

$$H_2^+ + H_2 \rightarrow H_3^+ + H + 2.25\ eV. \qquad (2\text{-}1)$$

except for recombination process [3]. Therefore, final products before recombination processes in the H_2 gas are H_3^+, e^-, and H.

Processes	Products	Number of events	Ion pairs
Ionization	$H_2^+ + e^-$	2 377	0.87
	$H^+ + e^- + H$	341	0.12
	$2(H^+ + e^-)$	14	0.01
		2 732	1.00
Excitation	$H_2^* \rightarrow H_2 + h\nu$	1788	1.16
	$H_2^* \rightarrow 2H$	740	
	$H_2^* \rightarrow H^* + H$	614	
	$H_2^* \rightarrow 2H^*$	28	
Atom production (sum from above)		3 105	1.14

Table 2-1 Calculated radiation damage events in H_2 gas bombarded with one 100 keV electron that loses all its energy

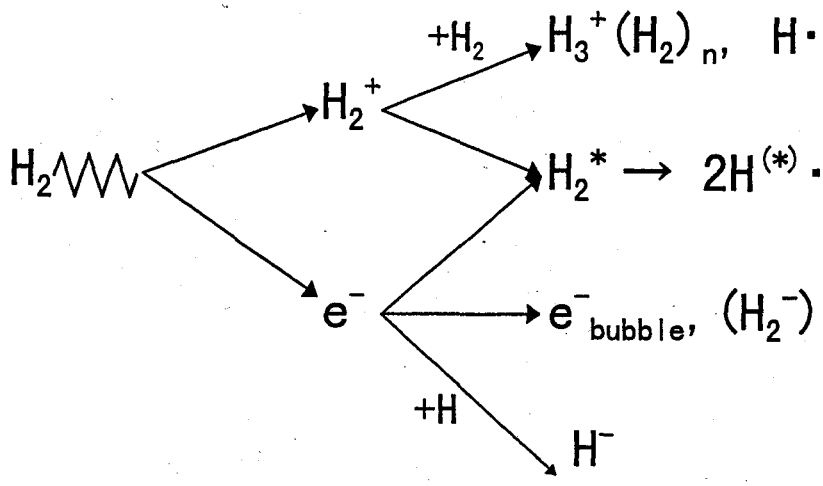

Fig. 2-11 Formations of radical and ionic species by X- or γ-ray radiolysis in H_2 solid. H_2* and H* show these species at excited states.

The radiation damage in H_2 solid have not been well understood in contrast to that in H_2 gas. However, similar products have been expected which are shown in Fig. 2-11. The H_3^+ cation strongly attracts surrounding H_2 molecules to produce $H_3^+(H_2)_n$ cluster and e^- is trapped in one site of the hydrogen solid with repulsing surrounding H_2 molecules making an electron bubble, e_{bub} [3~5]. When e^- encounters with the H atoms, H^- anion is produced due to the following electron transfer reaction,

$$e^- + H \rightarrow H^- + 0.75\ eV. \qquad (2\text{-}2)$$

Thus, final products before recombination processes in the H_2 solid have been inferred to be $H_3^+ (H_2)_n$, e_{bub}, H, and H^-. The latter two species are possible to observe using ESR spectroscopy and some works have been done [6,7].

2. 2. 2. ESR spectrum of new quartet signal

Figs. 2-12 (a) and (a') show the ESR spectrum of γ-ray irradiated n-H_2 solid with

applied microwave power of 10 nW and 100 μW, respectively . Only signals of H atoms are observed in accord with previous report [6,7] except for those of color centers in irradiated quartz cell around 3280 G. The absence of the signal of e_{bub} should be ascribed to the low yields or, perhaps, absence of the species. Next, the high-resolution ESR experiment using p-H_2 solid (cf. Chapter 1) is done to the further study of radiation damage. Fig. 2-12 (b) and (b') shows the ESR spectrum of γ-ray irradiated p-H_2 solid. No big difference is seen in (b). However, new weak but clear signals at around 3264 and 3277 G depicted by allows in (b') are observed in addition to normal H-atom signals for the first time [8].

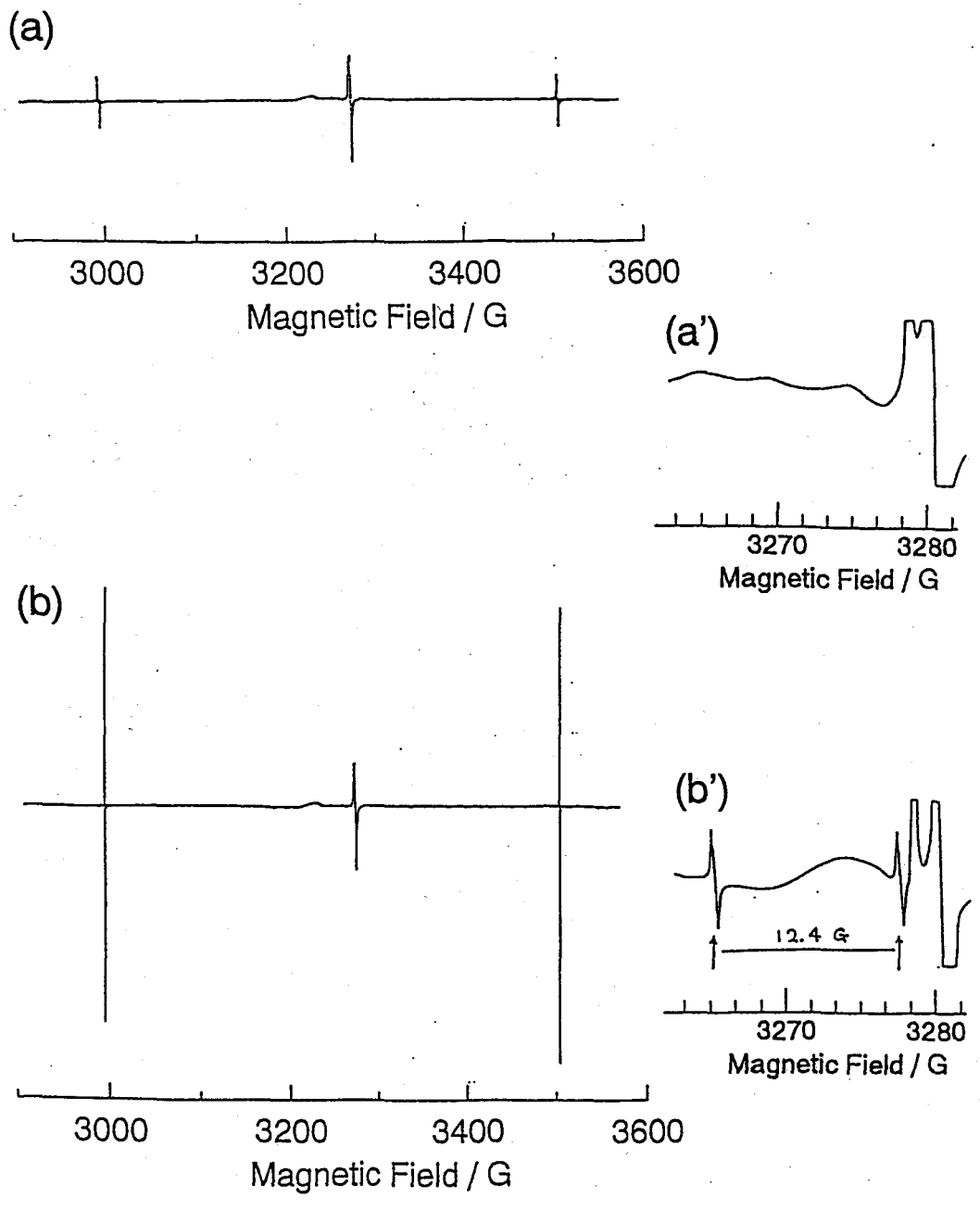

Fig. 2-12 ESR spectra of γ-ray irradiated solid n-H_2 (a), (a') and p-H_2 (b), (b') with applied microwave frequency of 9200 MHz at 4.2 K. Very sharp signals around 3000 and 3500 G in (a) and (b) are assigned as H atoms. Sharp signal around 3280 G and broad signal around 3220 and 3270 G are assigned as color centers in irradiated quartz cell. Spectra (a) and (b) were measured with microwave power of 10 nW to avoid saturation of signal intensity of the H atoms, whereas (a') and (b') were observed with that of 100 μW.

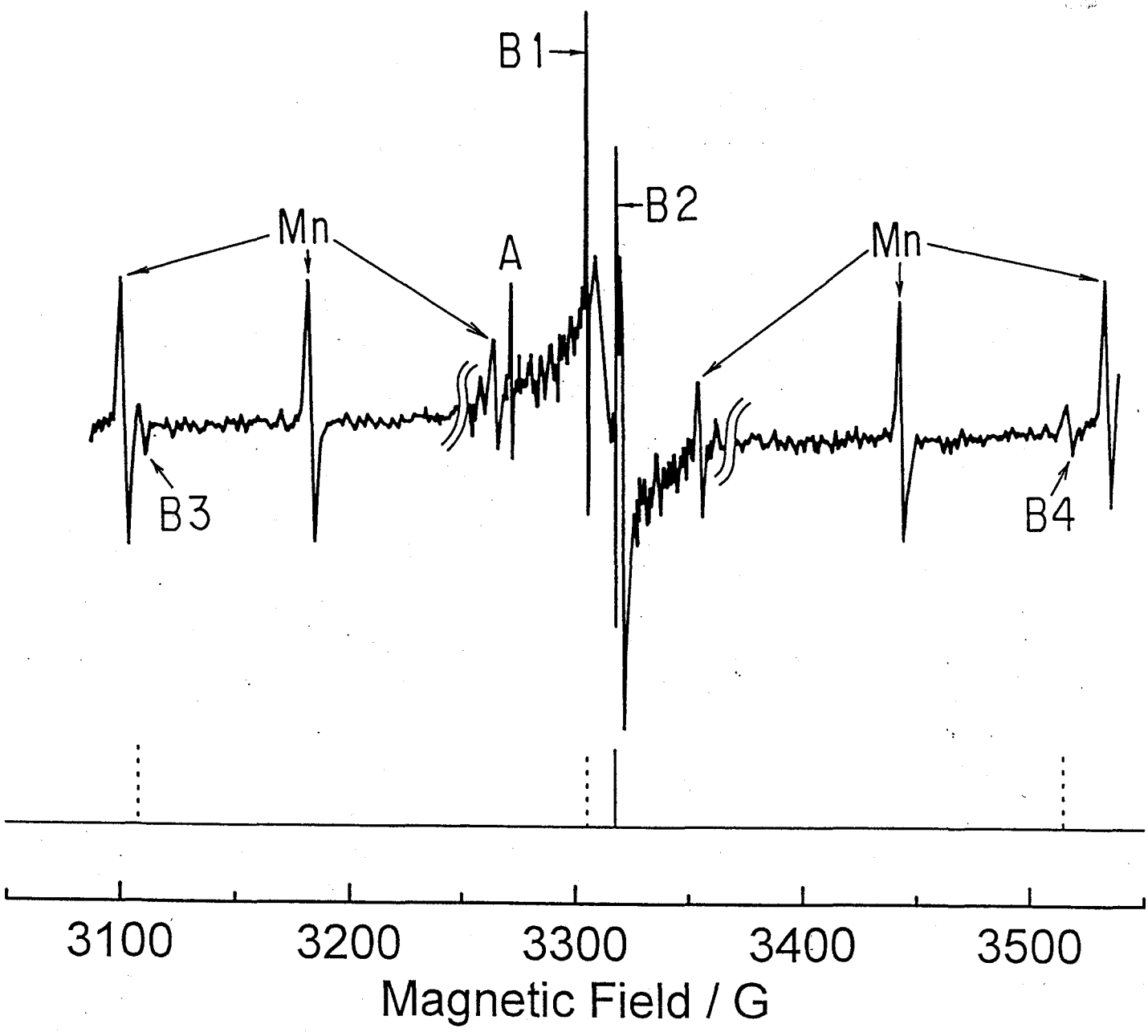

Fig. 2-13 ESR spectrum of γ-ray irradiated solid p-H_2 at 4.2 K. Applied microwave frequency and power are 9290 MHz and 100 μW, respectively. Peaks depicted by Mn are those of manganese as an ESR marker. A broad peak overlapped on B1 and B2 and a sharp singlet at 3340 G are peaks of color centers of the irradiated quartz cell. The stick diagram scaled below is the calculated signal positions and intensities (depicted by line length) of the specie with $I = 0$ (solid line) and 1(dotted line), $g = 2.0023$, and $A' = 203$ G.

Fig. 2-13 shows ESR spectrum of the γ-ray irradiated p-H_2 solid over a wide range of magnetic field with applied microwave power of 100 μW [9~11]. We observed not only signals depicted by B1 and B2 corresponding to the doublet signals in Fig. 2-12 (b'), but also small signals depicted by B3 and B4 and small signal depicted by A1, which have not been observed in n-H_2.

Only the B1~B4 signals are analyzed in this study, because intensity of the quartet signals are reproducible, whereas that of A1 signal is not yet clear. Resonance magnetic fields, linewidths, and intensity of the B1~B4 signals are shown in Table 2-2. A hint to identify the newly observed resonance signals is obtained by the fact that the *g*-factor of the B2 signal is exactly coincides to that of the free electron value and other three signals B1, B3, and B4 may be attributed to the hyperfine-splitting triplet, because the separated gaps are nearly equal. An ESR spectrum of the species which has $S \geqq 1$ and/or orbital angular quantum number $L \geqq 1$ has broad linewidths and shifted *g*-factor from 2.0023 due to the crystal field and orbital angular moment [12,13] so that these possibilities are denied. Therefore, the most plausible model to be considered is two new type unpaired electron systems whose two nuclear spins of 1/2 couple parallel or antiparallel forming I = 1 or 0, respectively. The I = 1 system will show the triplet hyperfine structure while single ESR signal is expected for I = 0 system. The most natural model to show these features is that an electron couples with a H_2 molecule forming a newly proposed ion H_2^- with ortho (I =1) or para (I = 0) coupling. The detailed analysis on this point will be given in chapter 3.

Hamiltonian of the species is described with the Zeeman energy, $g\mu_B \boldsymbol{S}\boldsymbol{H}_0$, and Fermi contact interaction energy, $\tilde{A}\boldsymbol{I}\boldsymbol{S}$,

$$\mathrm{H} = g\,\mu_B \boldsymbol{S}\,\boldsymbol{H}_0 + \tilde{A}\,\boldsymbol{I}\,\boldsymbol{S}. \qquad (2\text{-}3)$$

where μ_B is Bohr magneton, $\boldsymbol{H}_o$ is external magnetic field, and $\tilde{A}$ is Fermi contact term.

Signal	B1	B2	B3	B4
Resonance field /G	3305.5	3317.9	3108	3515
ESR Linewidth / G	0.21	0.13	1.9	1.9
Intensity / arb.	1.0 ± 0.1	1.0 ± 0.1	1.1 ± 0.2	1.1 ± 0.2

Table 2-2. Resonance magnetic field, when microwave frequency of 9290 MHz is applied, ESR linewidth, and intensity of the B1~B4 signals.

When $g\mu_B \boldsymbol{S}\boldsymbol{H}_0 >> \tilde{A}\boldsymbol{I}\boldsymbol{S}$ and $\boldsymbol{H}_0 // z$, the following equation can be derived from Eq. (2-3),

$$\begin{aligned} H &= g\,\mu_B S_z H_0 + A_x I_x S_x + A_y I_y S_y + A_z I_z S_z \\ &= g\,\mu_B S_z H_0 + A_x I_x S_x + \{(A_x + A_y)/4\}(I^+S^- + I^-S^+) + (A_x - A_y)/4\}(I^+S^+ + I^-S^-)\} \end{aligned} \tag{2-4}$$

where off-diagonal elements of $\tilde{A}$ are eliminated. When $A \equiv A_x = A_y = A_z$ are assumed, the energy levels, $E(\pm 1/2, m)$, at $S_z = \pm 1/2$, $I_z = m$, are described as [12,13]

$$E(\pm 1/2, m) = \pm\frac{g\mu_B H_0}{2} \pm \frac{mA}{2} \pm \frac{I(I+1) - m^2}{4g\mu_B H_0} A^2 - \frac{m}{4g\mu_B H_0} A^2 . \tag{2-5}$$

Fig. 2-14 shows the energy levels of the species with S = 1/2 and I = 0(a), 1(b). The allows show the allowed ESR transitions, which occur at the following resonance condition:

$$h\nu = g\mu_B H_0 + Am + \frac{A^2}{2g\mu_B H_0}\{I(I+1) - m^2\} \tag{2-6}$$

This equation is found to be

$$H_0 = \frac{h\nu - Am - \dfrac{A^2}{2g\mu_B H_0}\{I(I+1) - m^2\}}{g\mu_B} \qquad (2\text{-}7)$$

Thus, the resonance magnetic fields of Tr.1~Tr.4 transitions, $H_{Tr.1}$~$H_{Tr.4}$, are given by

$$H_{Tr.1} = \frac{h\nu}{g\mu_B} \qquad (2\text{-}8)$$

$$H_{Tr.2} = \frac{h\nu - A - A^2 / 2h\nu}{g\mu_B} \qquad (2\text{-}9)$$

$$H_{Tr.3} = \frac{h\nu - A^2 / h\nu}{g\mu_B} \qquad (2\text{-}10)$$

$$H_{Tr.4} = \frac{h\nu + A - A^2 / 2h\nu}{g\mu_B}. \qquad (2\text{-}11)$$

The simulated ESR spectrum derived from the Tr.1~Tr.4 transitions with $A' \equiv A / \mu_B$ = 203 G is shown in the stick diagram at the bottom of Fig. 2-13. The solid line in the stick diagram shows the simulated ESR signal of the species with $I = 0$ ($H_{Tr.1}$), while the dotted lines show the signals with $I = 1$ ($H_{Tr.2\text{-}4}$). The resonance magnetic fields of the simulated spectrum accurately correspond to those of B1~B4 signals within the errors of ± 0.05 G, which is well within experimental errors. The ratio of the species with $I = 0$ to that with $I = 1$ is 1 : 3, because ESR intensities among B1~B4 signals are the same (cf. Table 2-2). As the summary, it was found that the species which assigns the quartet signals in Fig. 2-13 has $S = 1 / 2$ with no orbital angular moment, $I = 0$, 1(with intensity ratio of 1 : 3), g =

2.0023, and $A' = 203$ G.

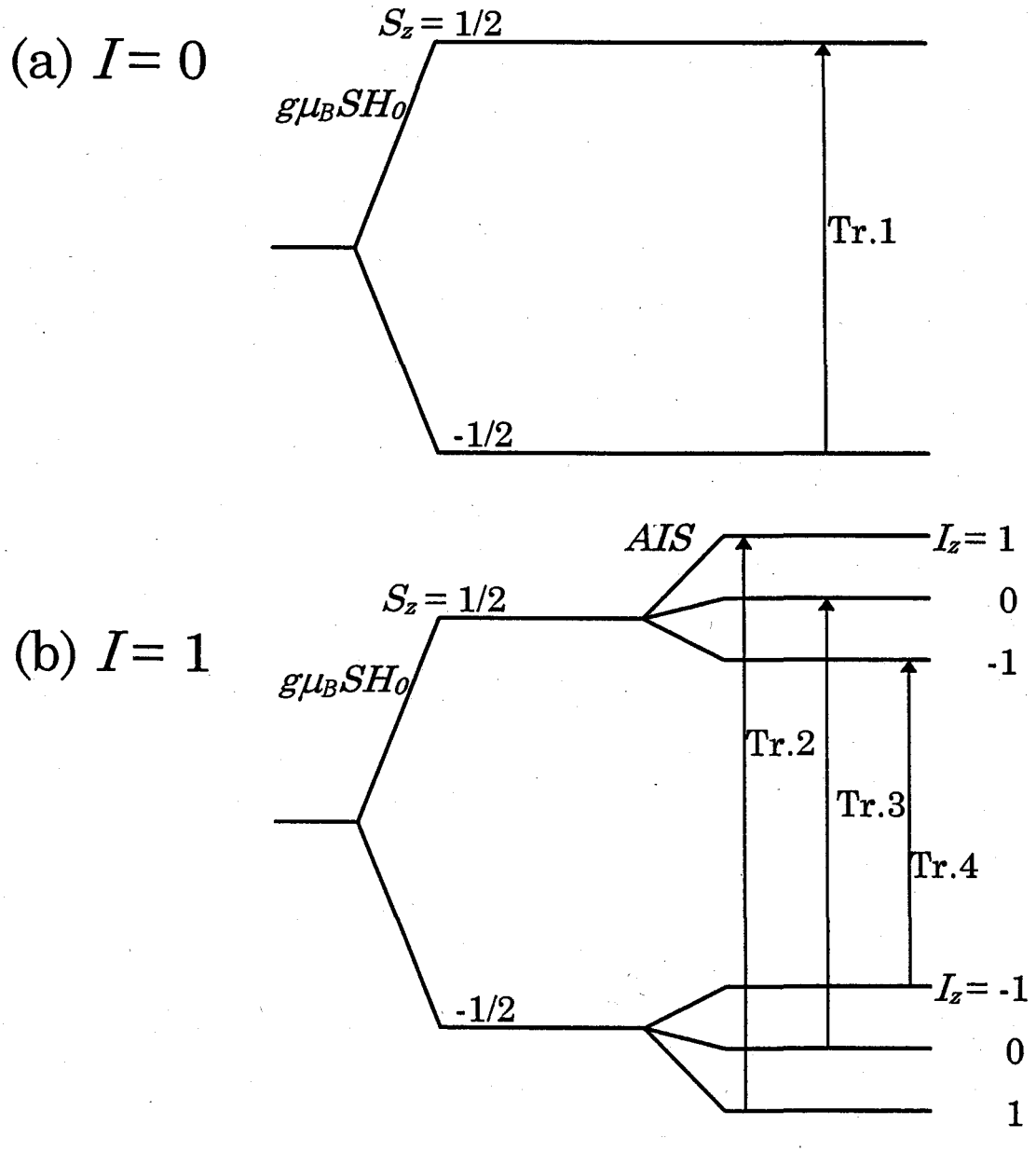

Fig. 2-14 Energy levels of the species with $S = 1/2$ and $I = 0$(a), 1(b). Arrows depicted by Tr.1-4 show allowed ESR transitions.

References

[1] T. Miyazaki, T. Hiraku, K. Fueki and Y. Tsuchihashi, J. Phys. Chem. 95 (1991) 26.

[2] T. Ichikawa, H. Yoshida, H. Yamada, S. Tokairin and Y. Ikegami, J. Magn. Reson. 64 (1985) 518.

[3] P. C. Souers, Hydrogen Properties for Fusion Energy (University of California Press, Berkeley, 1986).

[4] P. C. Souers, E. M. Fearon, R. L. Stark, R. T. Tsugawa, J. D. Poll and J. L. Hunt, Can. J. Phys. 59 (1981) 1408.

[5] R. L. Brooks, S. K. Bose, J. L. Hunt, Jack R. MacDonald and J. D. Poll, Phys. Rev. B 32 (1985) 2478.

[6] A. Ya. Katunin, I. I. Lukashevich, S. T. Orozmamatov, V. V. Sklyarevskii, V. V. Suraev, V. V. Filippov, N. I. Filippov and V. A. Shevtsov, Pis'ma Zh. Eksp. Teor. Fiz. 34 (1981) 375, [JETP Lett. 34 (1981) 357.

[7] T. Miyazaki, H. Morikita, K. Fueki and T. Hiraku, Chem. Phys. Lett. 182 (1991) 35.

[8] T. Miyazaki, K. Yamamoto and Y. Aratono, Chem. Phys. Lett. 232 (1995) 229.

[9] T. Kumada, T. Inagaki, T. Nagasawa, Y. Aratono and T. Miyazaki, Chem. Phys. Lett. 251 (1996) 219.

[10] T. Kumada, T. Inagaki, N. Kitagawa, Y. Aratono and T. Miyazaki, J. Phys. Chem. 101 (1997) 1198.

[11] T. Kumada, Y. Aratono and T. Miyazaki, J. Low. Temp. Phys. 111 (1998) 509.

[12] A. Abragam, The principle of Nuclear Magnetism (Oxford Press, 1961).

[13] C. P. Slichter, Principles of Magnetic Resonance (Harper and Row, 1963).

Chapter 3

Assignment of the ESR spectrum and the stability of H_2^-

3. 1. Assignment of the quartet signals

The ESR spectrum of the newly observed quartet signals is discussed. It is concluded that the observed signals come from a new molecular ion H_2^- and other many possibilities are dropped off as are seed in the following subsections.

3. 1. 1. Impurity radicals

A few amounts of contaminants such as nitrogen, oxygen, hydrocarbon, and water should exist in the p-H_2 sample. However the species which assigns the quartet signals is neither these impurity ions nor their relative radicals because of the following reasons. First, the nuclear magnetic quantum number of nitrogen atom is not 0 but 1 [1]. Thus, the species which includes nitrogen atom can not assign the B2 signal, even though it can assign the B1~B3 signals. Second, the wave function of unpaired electron in hydrocarbon radicals is mainly located on the carbon atom. This strongly reduces hyperfine interaction between the electron and nuclear spins of the hydrogen atoms. For example the isotropic hyperfine couplings of the neutral species of CH_3 and positively charged species of CH_4^+ are 23 and 54 G, respectively [1], which are much smaller than 203 G. Third, it has been found that ESR intensity of the quartet signals in γ-ray irradiated solid p-H_2-O_2 (0.048 and 1.1 mol %) mixtures is the same as that in irradiated pure p-H_2 sample [2] and that the ESR intensity in p-H_2-H_2O (1.02 mol %) mixture is smaller (not shown). These results indicate that these impurity ions and their relative radicals cannot assign the quartet signals.

The p-H_2 sample also contains HD molecules at a natural abundance of 0.03 mol %.

Thus, it is expected that the quartet signals may be assigned as the species which contains D atoms. We studied the effects of HD and D_2 molecules added to the pure p-H_2 sample on the ESR intensity of the quartet signals. However, the ESR intensity does not increase but decreases with the increase in the concentrations of the HD and D_2 impurities (cf. Fig. 4-2). Therefore, it is proved that the species which assigns quartet signals does not contain D atoms.

3. 1. 2. Hydrogen ions [3]

The hyperfine splitting between the B3 and B4 signals (407 G) is comparable to that of H atoms (508 G), suggesting that the quartet signals are assigned as the species which consists of merely some H atoms. Since the species of the quartet signals has $S = 1/2$ and $I = 0$, 1 (cf. Chapter 2), the radical should be composed of one unpaired electron together with two protons whose nuclear magnetic moments ($I = 1/2$) couple in antiparallel ($I = 0$) or in parallel ($I = 1$). Therefore, only two candidates, H_2^+ cation and H_2^- anion, remain [3].

H_2^+ cation

The H_2^+ cation has been extensively studied in gas phase, especially by Carrington and co-workers [4], but has never been reported in condensed phases [5]. Fig. 3-1 shows various species observed in an arc discharge in hydrogen. The H_2^+ cation appears only at pressure below 1 Pa and is replaced at higher pressures by the H_3^+ cation [6] due to the following reaction:

$$H_2^+ + H_2 \rightarrow H_3^+ + H + 2.25 \text{ eV}, \qquad (3\text{-}1)$$

The H_2^+ cation is stable only in a high vacuum. Even in outer space, it seems that the H_3^+ cation have the upper hand [7]. Therefore, it has been considered that, in condensed phases, the H_2^+ cation cannot exist in the p-H_2 solid.

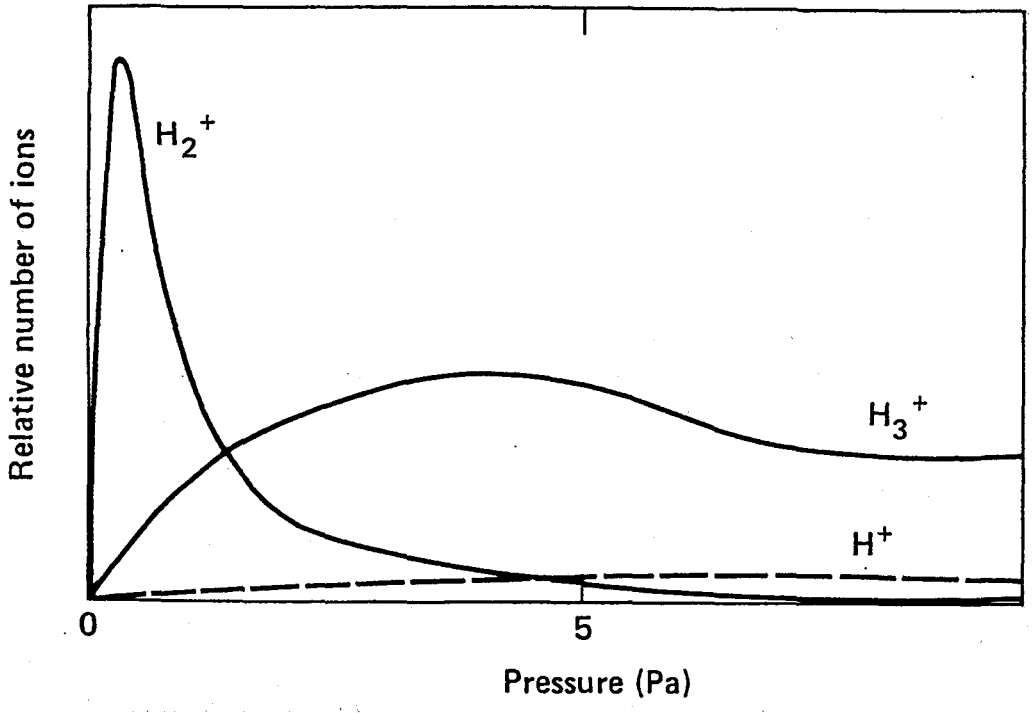

Fig. 3-1. The reaction of H_2^+ to H_3^+ in an arc discharge in H_2 gas. It should be noted that H^+ is generated by the reaction: $H_2^+ + H_2 \rightarrow H + H + H^+$.

H_2^- anion

The final candidate for the observed ESR signals is the H_2^- anion, which is sketched in Fig. 3-2. It is concluded that the H_2^- anion can assign the observed quartet signals, because the observed hyperfine coupling of 203 G is reasonable for the H_2^- anion model. Details are discussed below.

The hyperfine coupling of the H atom, whose unpaired electron is located at 1s orbital, is 508 G. When the unpaired electron is located at two equivalent 1s orbitals in the neighboring H atoms separated by the distance larger than their diameter (~2 Å) with the jump rate faster than microwave frequency, the hyperfine coupling becomes 254 G (= 508 / 2 G), because overlapping between wavefunction of the electron and that of each proton becomes a half due to the jumping. As shown in Fig. 3-3, with the decrease in the distance

between these two H atoms, the equivalent 1s orbitals in these H atoms split into 1s bonding ($1\sigma_g$) and antibonding ($1\sigma_u$) orbitals due to their mixing. The hyperfine coupling of the electron in $1\sigma_g$ orbital becomes larger than 254 G. For example, the hyperfine coupling of the H_2^+ cation, whose unpaired electron is located at the $1\sigma_g$ orbital, was observed to be no less than 290 G using microwave absorption spectroscopy [4] and calculated to be 334 G [8]. On the other hand, the unpaired electron in the H_2^- anion, located at outer $1\sigma_u$ orbital, repulsively interacts with the other two electrons located at the inner $1\sigma_g$ orbital. It is expected that the repulsive interaction spreads the $1\sigma_u$ orbital and makes the hyperfine coupling of the H_2^- anion smaller than 254 G. Thus, it can be concluded that isotropic hyperfine coupling constant of 203 G observed is quite reasonable for that of the H_2^- anion and it is very difficult to discover any alternative.

A center which has H_2^- anion character has recently been detected in LiF crystals after exposure to X-rays [9]. This was formed from the initially trapped H atom impurities on annealing. There is remarkably large hyperfine coupling constant to sets of Li^+ and F^- nuclei comparable with those for F centers in LiF, and the center seems to have considerable F-center-like properties. The hyperfine coupling of 260 G to the two equivalent protons is almost exactly half of that for H atoms in this matrix (254 G) which

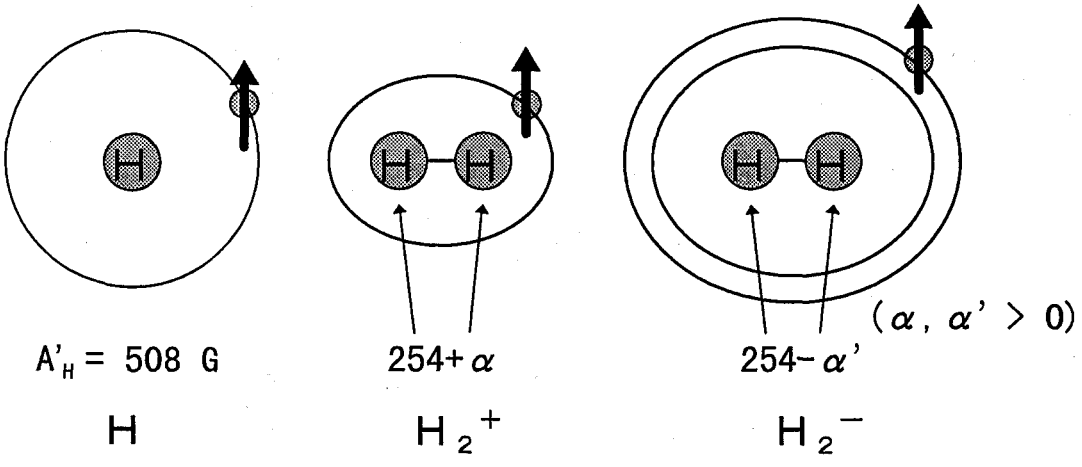

Fig. 3-2 Models of H, H_2^+, and H_2^-.

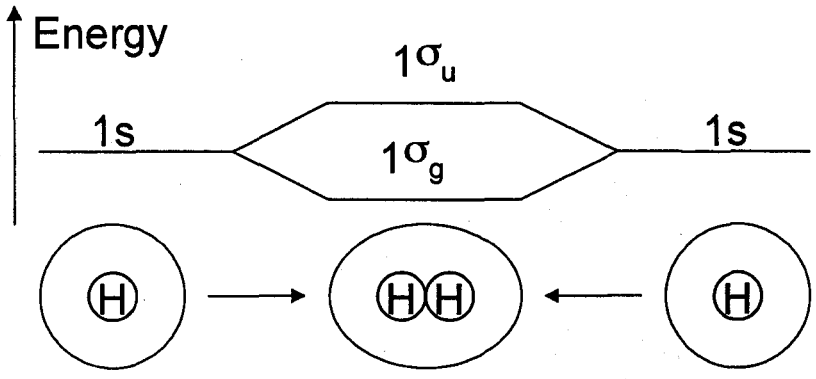

Fig. 3-3 Energy level of 1s orbital in an isolated H atom and that of $1\sigma_g$ and $1\sigma_u$ in a H_2 molecule.

is surprisingly large for a negative ion. Although this center can be somewhat different from expectation for H_2^- anions in p-H_2 solid, the result supports the assignment of the H_2^- anions model in the p-H_2 solid.

3. 2. Theoretical calculation of the stability of H_2^- anion in solid hydrogen [10]

There are two problems that do not support the presence of the H_2^- anion, although the observed hyperfine coupling constant strongly suggests the formation of the H_2^- anion. One is the electrorepulsive property of the H_2 molecule. As is mentioned above, the H_2^- anion may have two electrons in a bonding $1\sigma_g$ orbital and one electron in an antibonding $1\sigma_u$ orbital, so that it is expected to be stable. However, because of strong repulsive interactions among these electrons, the H_2 molecule is highly electrorepulsive and the H_2^- anion in the gas phase releases its excess electron within 10^{-14} sec [11, 12]. The other is mobility of the H_2^- anion. The H_2^- anion embedded in the H_2 solid as a substitutional-type impurity may give its excess electron to one of nearby H_2 molecules very quickly due to the following electron transfer reaction

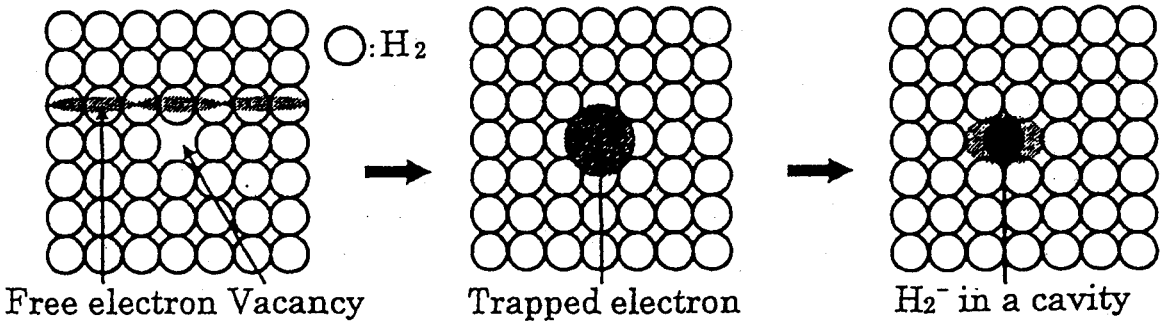

Fig. 3-4 Schematic representation of the process of H_2^- formation and stabilization in a H_2 solid. A free electron generated by ionizing radiation is first trapped in a vacancy. One of the adjacent H_2 molecules pick up the electron to convert to H_2^-.

$$H_2^- + H_2 \rightarrow H_2 + H_2^- \qquad (3\text{-}2)$$

because of light mass of the electron and of good symmetry between the reactants and products. The hopping rate of the excess electron and therefore the decay rate of the H_2^- anions are expected to be very fast even when the electron is occasionally trapped on a H_2 molecule. However the H_2^- anions are observed in p-H_2 solid with a half-lifetime of about 5 hours at 4 K. In this paragraph, the formation and stability of the H_2^- anion in p-H_2 solid is explained using the following cavity model.

Fig. 3-4 shows the model on the formation and stabilization of the H_2^- anion in a p-H_2 solid. The p-H_2 solid generally contains many vacancies and cavities, which can trap free electrons to generate trapped electrons. The zero-point energy of the trapped electrons, E_t, is derived from [13]

$$\sqrt{V_0 - E_t} = \sqrt{U_p(r_c) + E_t}\cot\left[\sqrt{\frac{2m\{U_p(r_c) + E_t\}}{\hbar^2}}r_c\right] \qquad (3\text{-}3)$$

where V_0 is the minimum energy of free electrons in a medium, R_c is the radius of the

vacancy or cavity and is 2.18 Å [14], and $U_p(r_c)$ is the polarization potential arising from dipole interactions between the electron and medium, and is approximately given by

$$U_p(r_c) = \frac{e^2(D_{op} - 1)}{2D_{op}r_c} \tag{3-4}$$

Here D_{op} is the optical dielectric constant of the medium and is 1.34 for the H_2 solid. The value of V_0 for H_2 liquid has been estimated by a photoelectron emission study to be larger than 2 eV [15]. Assuming $V_0 = 2$ eV for the H_2 solid, the zero-point energy of a localized electron in a vacancy of the H_2 solid is estimated to be 1.82 eV. Thus, conversion of free electrons into trapped electrons, e_t^-, is a spontaneous exothermic reaction.

The observed anionic species is, however, not e_t^- but H_2^- anion. The H_2^- anion can be generated from e_t^- by transferring a neighboring H_2 molecule from the wall of the vacancy to the center of the resultant cavity. Although the H_2^- anion in vacuum automatically dissociates into a H_2 molecule and a free electron, the H_2^- anion in the H_2 solid can be stabilized in the cavity due to very strong repulsive interaction between the excess electron in the anion and surrounding H_2 molecules. The heat of H_2^- formation, E_f, from e_t^- is defined as the difference of total energies between the $H_2 + e_t^-$ state and the trapped H_2^- anion state, $H_{2,t}^-$, as

$$E_f = E_{H2,t-} - (E_{H2} + 1.82 \text{ eV}) \tag{3-5}$$

The total energy of $H_{2,t}^-$ depends on the potential curve. Assuming one H_2^- anion to be trapped in a spherical cavity with a volume corresponding to two H_2 molecules, the potential energy for $H_{2,t}^-$ is estimated by a first-order perturbation method, as

$$U_{H2,t-}(R) = U_{H2-}(R) - \int_0^{r_c} \varphi(R,r)U_p(r_c)\varphi(R,r)d^3r + \int_0^{r_c} \varphi(R,r)V_0\varphi(R,r)d^3r$$

$$= U_{H2^-}(R) - [U_p(r_c) + V_0]\rho(R, r_c) + V_0 \qquad (3\text{-}6)$$

Here R is the bond length of the H_2^- anion, $r_c = 2.75$ Å ($= (2.16^3 \times 2)^{1/3}$) is the radius of the cavity, $U_{H2^-}(R)$ is the potential energy of the H_2^- anion in vacuum, $\varphi(R, r)$ is the wave function of the excess electron in the H_2^- anion, and $\rho(R, r_c)$ is the density of the negative charge in the cavity.

The energies and the wave functions of the H_2^- anion have been calculated quantum-mechanically using several types of basis sets [16-23]. One of the fundamental difficulties for the calculation is that the result strongly depends on the basis set. Since H_2 molecule has negative electron affinity, the most stable state for the H_2^- anion is obviously a ground-state neutral H_2 molecule with a ground-sate free electron. For preventing the dissociation of a H_2^- anion into the H_2 molecule and free electron, it is necessary to eliminate a free electron-type basis set and to use only an atomic orbital-type basis set. This very artificial confinement of electrons around two protons inevitably causes a strong dependence of the calculated result on the basis set. The purpose of the present study is, however, not to calculate the accurate energy of H_2^- but to know whether H_2^- can possibly be trapped in the H_2 solid. Fig. 3-5 shows the potential curves of H_2 and H_2^- as calculated with the doublet substituted coupled cluster (CCD) method with the 6-311++G(3d, 3p) basis set [24]. The calculated potential energy of the most stable H_2^- anion is lower than that of H_2 molecule + free electron by about 2 eV.

Fig. 3-6 compares the potential curves for $H_{2,t}^-$ and $H_2 + e_t^-$. The potential curve for the $H_2 + e_t^-$ state was obtained simpy by adding 1.82 eV to the potential energy of H_2. It is evident from the figure that $H_{2,t}^-$ is potentially more stable than $H_2 + e_t^-$. The heat of $H_{2,t}^-$ formation is then positive and the conversion of e_t^- to $H_{2,t}^-$ becomes a spontaneous exothermic process. The simple quantum-mechanical calculation shows that H_2^- is generated and trapped in H_2 solid by the exothermic reaction between the trapped electron and H_2. The actual heat of $H_{2,t}^-$ formation is probably much higher than

calculated one, since the wave function used is not accurate enough for expressing the observed $H_{2,t}^-$ state.

Our model also answers the question why the excess electron of the H_2^- anion does not migrate freely in the H_2 solid. The excess electron can migrate freely if it is located in the homogeneous (defect free) region of the H_2 solid. However, migration of the excess electron needs the migration of the cavity, since H_2^- is stabilized in the cavity.

Radiation-chemical reactions taking place by γ-ray irradiation of the H_2 solid are summarized as follows:

$$\left.\begin{aligned} &H_2 + \gamma \rightarrow H_2^+ + e^-, \\ &H_2^+ + H_2 \rightarrow H_3^+ + H, \\ &e^- + H_3^+ \rightarrow H_2 + H, \\ &e^- + H \rightarrow H^-, \\ &e^- + \otimes \rightarrow e_t^-, \\ &e_t^- + H_2 \rightarrow H_{2,t}^- \end{aligned}\right\} \quad (3\text{-}7)$$

where ⊗ denotes a vacancy.

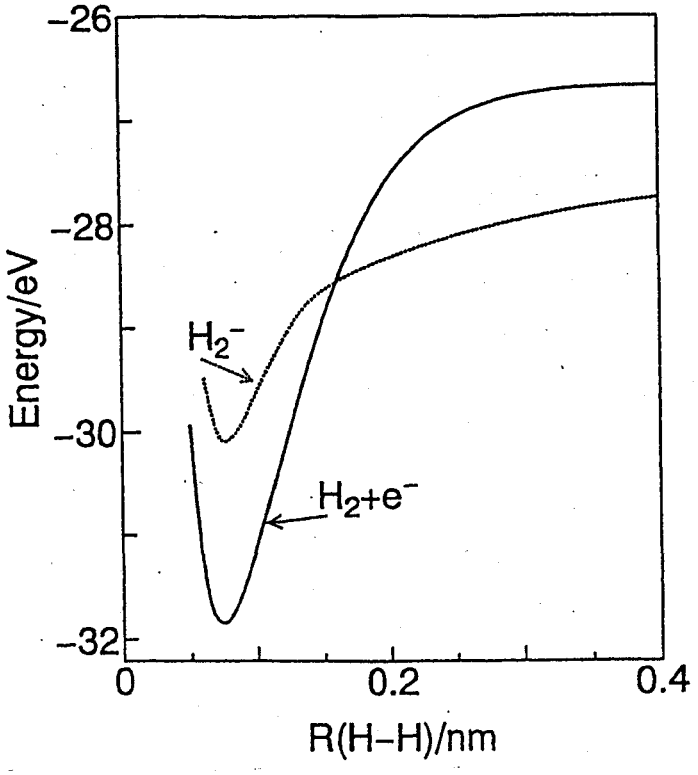

Fig. 3-5 Potential curves for free H_2^- and free H_2 + free electron with zero kinetic energy.

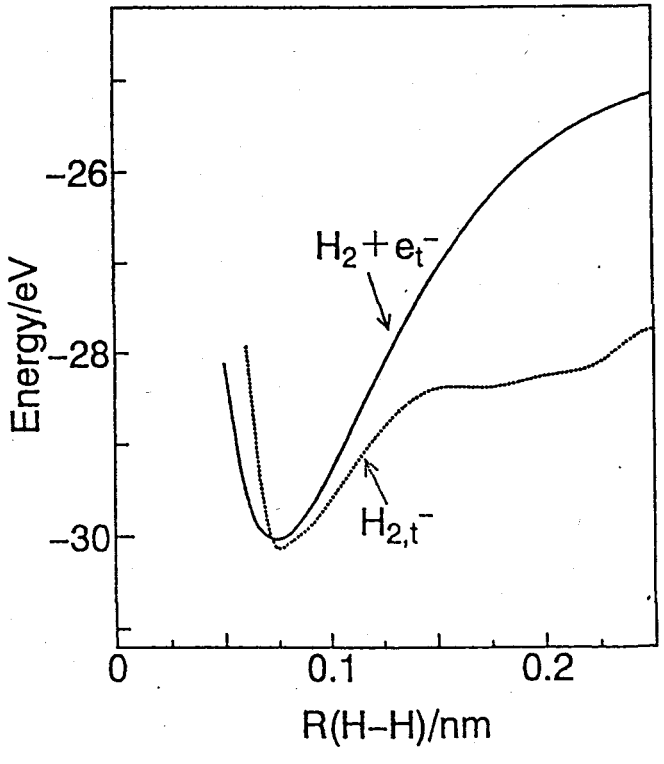

Fig. 3-6 Comparison of the potential curves of H_2 + e_t^- (trapped electron) in a vacancy with a radius of 2.18 Å and $H_{2,t}^-$ (trapped H_2^-) in a cavity with a radius of 2.75 Å.

3. 3. Experimental study of the stability of H_2^- anions in p-H_2 solid

Stability of the H_2^- anions is experimentally studied. Fig. 3-7 shows the ESR intensity of the H_2^- anions, $I_{ESR}(T)$, in X-ray irradiated p-H_2 solid in the temperature range between 2.8~6.5 K. Generally, as depicted by the solid curve in the figure, ESR sensitivity of paramagnetic species varies inversely as temperature [25, 26]. The ESR intensity of the H_2^- anion also varies inversely as temperature below 5 K; however, it remarkably decreases with the increase in temperature above 5 K. Moreover, it should be noted that this decreased intensity reversibly increases with the decrease in temperature. Fig. 3-8 shows the relative amounts of the H_2^- anions, $I_{amount}(T)$, obtained due to the correction of the ESR intensity by the sensitively as follows,

$$I_{amount}(T) = I_{ESR}(T) \times T. \qquad (3\text{-}8)$$

The anormally above 5 K cannot be explained by the variation of the sensitivity, indicating that the amounts of the H_2^- anions themselves reversibly decrease about 5 K.

The anionic species in the exited state complementarily produced above 5 K has not been observed experimentally, although it should exist. However, it is confirmed that the excited state is not the delocalized state of the excess electron in the H_2^- anion but the some localized state of the H_2^- anion. As shown in Fig. 3-9, the reversible decrease in the ESR intensity above 5 K is observed both in o-$H_2^-$and in p-H_2^-. If the electrons in a H_2^- anion delocalize above 6 K and randomly trapped into another p-H_2 molecules to form H_2^- anion below 5 K, the ratio of o-H_2^- anions to p-H_2^- anions should not be 3 : 1 but be about 1 : 99, because the concentration of o-H_2 molecules in the p-H_2 solid used in the experiment is about 1 mol % (Chapter 2). It is expected that the exited state is assigned as H_2^- anions at vibronic excited states. As discussed above, the excess electron generated by X(γ)-ray radiolysis is trapped in one H_2 molecule together with the cavity to form H_2^- anion, because total energy in the localized state is lower than that in delocalized state.

This aspect is similar to distortion of solids around localized unpaired spin by Jahn-Teller effect [27,28]. When the localized electron together with surrounding distortions is exited, the electron together with surroudings exchanges with other equivalent states, showing vibronic state. The H_2^- anions at the exited state may show the vibronic state. When the electron transfers around the cavity with the hopping rate faster than the applied microwave frequency (~9 GHz), its ESR spectrum has singlet signal at g = 2.0023. Although the singlet signal is not observed above 6 K, this absence would be ascribed to the low resolution of the spectrum.

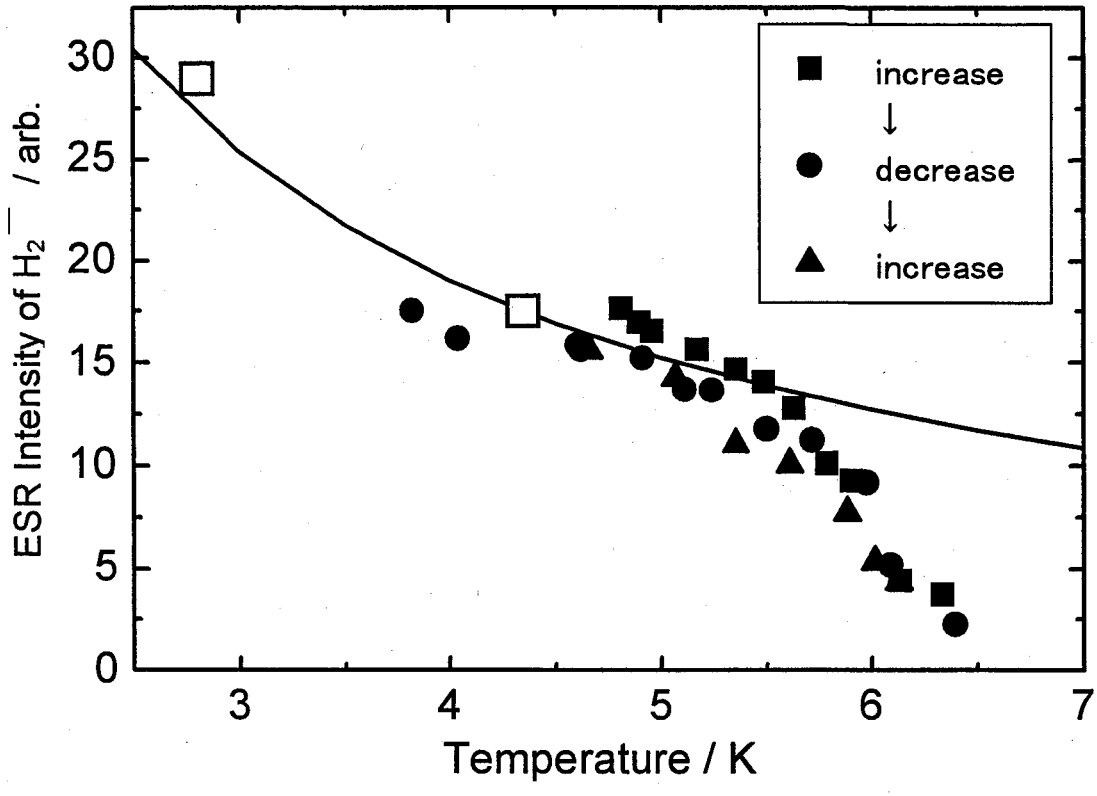

Fig. 3-7 ESR intensity of the H_2^- anions as a function of temperature. The temperature was continuously increased from 4.8 to ~7 K (closed squares), decreased to 3.8 K (closed circles), and then increased up to ~7 K (closed triangles). All the data depicted by closed symbols are obtained within ~40 min, which is much shorter than lifetime of the H_2^- anions of ~5 hours (cf. Fig. 4-1). Data depicted by open squares also shows the intensity by decreasing temperature from 4.3 K to 2.7 K, which is normalized to the data depicted by closed symbols at 4.3 K. Solid line shows ESR sensitivity of paramagnetic species which is inversely proportional to the temperature.

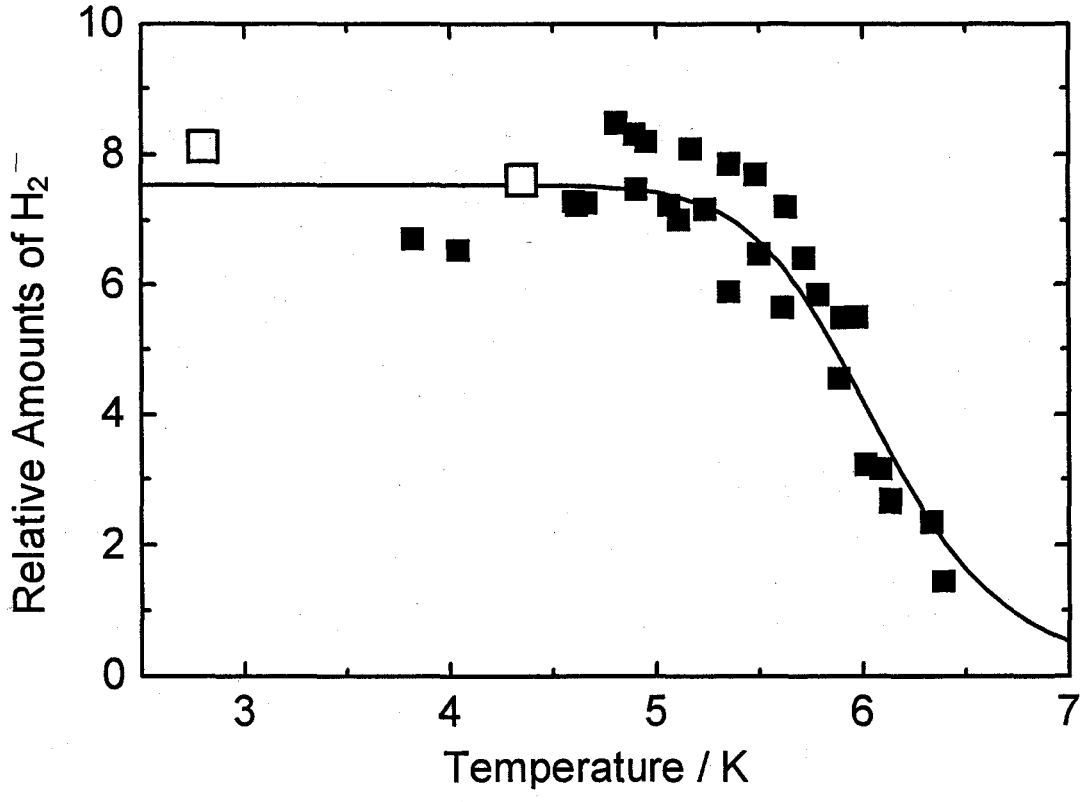

Fig. 3-8 Relative amounts of H_2^- anions which are obtained from the data in Fig. 3-5 and Eq. (3-8). The solid curve is theoretical fitting of Eq. (3-9) with $n = (3 \pm 2) \times 10^9$ and $E_{ex} = 118 \pm 40$ K.

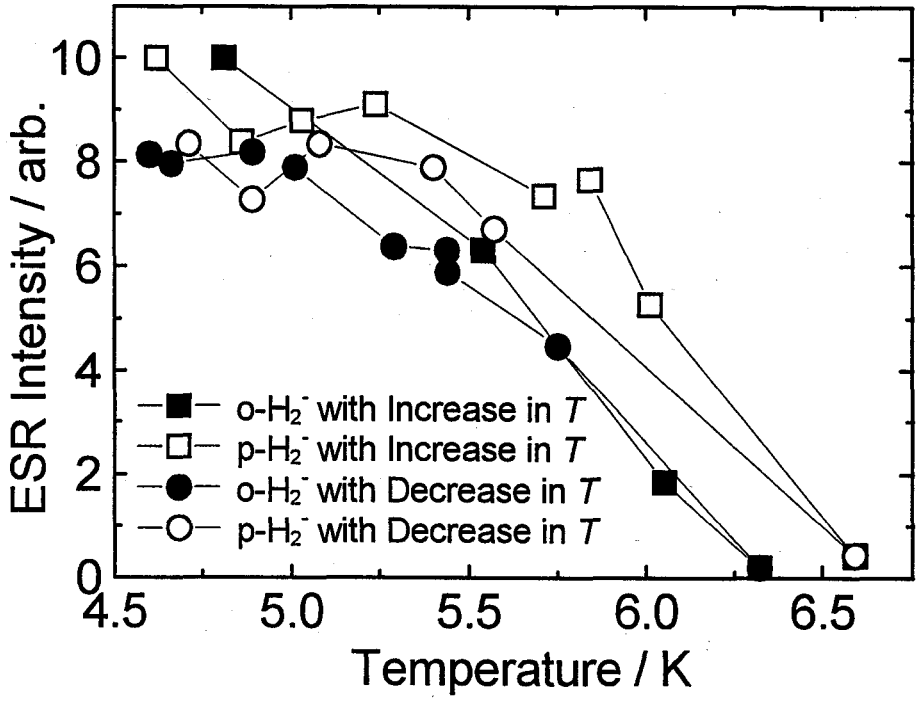

Fig. 3-9 ESR intensity of o-H_2^- (B1) (closed symbols) and p-H_2^- (B2) (open symbols) as a function of temperature. The temperature was continuously increased from 4.6 to ~7 K (squares) and then decreased to 4.5 K (circles). All of the data were obtained within 30 min, which is much shorter than lifetime of the H_2^- anions of ~5 hours at 4.5 K (cf. Fig. 4-1).

References

[1] Y. Tabata, Y. Ito and S. Tagawa, Handbook of Radiation Chemistry (CRC Press, 1991).

[2] T. Kumada, T. Inagaki, T. Nagasawa, Y. Aratono and T. Miyazaki, Chem. Phys. Lett. 251 (1996) 219.

[3] M. C. R. Symons, Chem. Phys. Lett. 247 (1995) 607.

[4] A. Carrington, I. R. McMab and C. A. Montgomerie, J. Phys. B 22 (1989) 3551.

[5] T. Oka, Rev. Mod. Phys. 45 (1992) 1141.

[6] H. D. Smith, Phys. Rev. 25 (1925) 452.

[7] T. de Jong, Astron. Astrophys. 20 (1972) 263.

[8] M. J. Stephen and J. P. Auffray, J. Chem. Phys. 31 (1959) 1329.

[9] A.. V. Egranov, A. I. Nepomnyachitkh, V. V. Otroshok and B. P. Chernyago, Phys. Stat. Sol. (b) 155 (1989) 155.

[10] T. Ichikawa, H. Tachikawa, J. Kumagai, T. Kumada, and T. Miyazaki, J. Phys. Chem. A 101 (1997) 7315.

[11] N. S. Buchelkinov, Usp. Fiz. Nauk. 65 (1958) 351.

[12] G. L. Schulz, Rev. Mod. Phys. 45 (1973) 423.

[13] T. Ichikawa and H. Yoshida, J. Chem. Phys. 73 (1980) 1540.

[14] The value of 2.18 Å is derived by subtracting the radius of H_2 molecule (1.6 Å) from the lattice constant of p-H_2 solid (3.78 Å [5]).

[15] B. Halpern, H. Lekner and S. A. Rice, Phys. Rev. 156 (1967) 351.

[16] H. A. Van der Hart and J. Mulder, Chem. Phys. Lett. 61 (1979) 111.

[17] C. W. McCurdy, Phys. Rev. A25 (1982)2529.

[18] J. Senokowich, P. Rosmus, W. Domcke and H. J. Werner, Chem. Phys. Lett. 11 (1984) 211.

[19] N. H. Sabelli and E. A. Gislason, J. Chem. Phys. 82 (1985) 4577.

[20] E. Derose, E. A. Gislason and N. H. Sabelli, H. Chem. Phys. 82 (1985) 4577.

[21] A. C. Roach and P. J. Kuntz, J. Chem. Phys. 84 (1986) 822.

[22] E. F. Derose, E. A. Gislason, N. H. Sabelli and K. M. Sluis, J. Chem. Phys. 88 (1988) 4878.

[23] A. S. Shalabi, Mol. Phys. 85 (1995) 1033.

[24] Ab initio MO calculation program, Gaussian 92, Revision F. 3.

[25] A. Abragam, The principle of Nuclear Magnetism (Oxford Press, 1961).

[26] C. P. Slichter, Principles of Magnetic Resonance (Harper and Row, 1963).

[27] H. A. Jahn and E. Teller, Phys. Rev. 49 (1936) 834.

[28] F. S. Ham, Phys. Rev. A 138 (1965) 1727.

Chapter 4

Long-Time Decay and its Temperature Dependence [1]

As shown in Fig 4-1, the H_2^- anions exponentially decay in the X(γ)-ray irradiated p-H_2 solid with a half-life-time of ≤ 5 hours. The long-time decay process is irreversible, as opposed to spontaneous and reversible decrease in the amounts of H_2^- anions above 5 K (cf. Fig. 3-7). It is expected that the irreversible long-time decay occurs due to reaction with some reactant impurity in the solid. In this chapter, the decay behaviors of the H_2^- anions and their temperature dependence are examined.

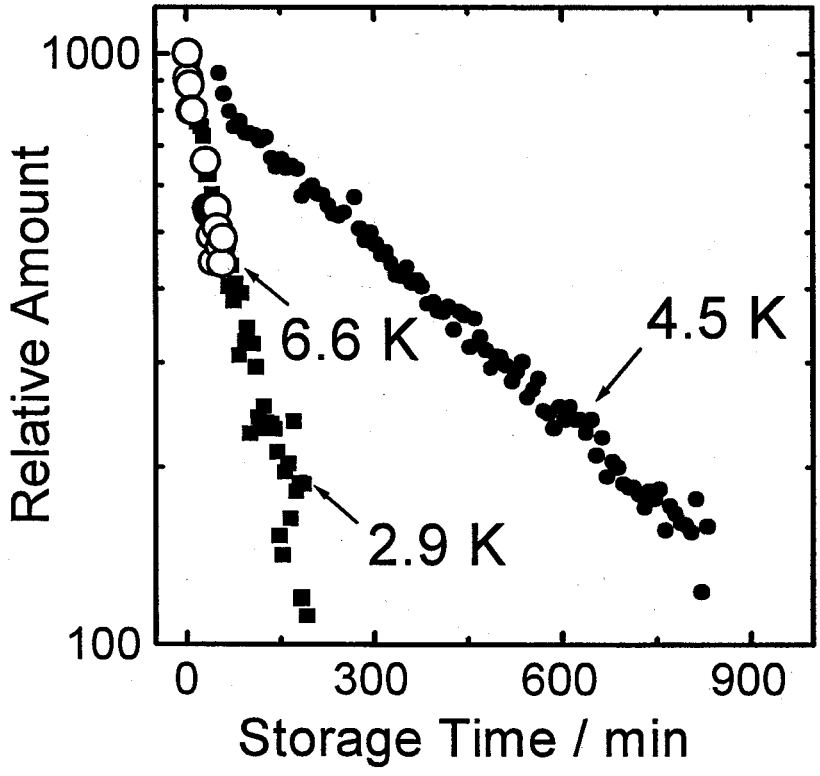

Fig. 4-1. Decay behaviors of H_2^- anions in X-ray irradiated solid p-H_2 at 2.9, 4.5, and 6.6 K. The ordinate has been made logarithmic. All amounts at $t = 0$ are normalized to 1000.

4. 1. Assignment of the reactant impurity

When the H_2^- anion and some reactant impurity diffuse and encounter in the solid, the H_2^- anion can react with the reactant impurity with little activation energy, because of low stability of the H_2^- anion (cf. Chapter 3). Thus, the rate constant for the decay of the H_2^- anions should be controlled by that for the diffusion of these species. Since the H_2^- anion decay exponentially, the decay rate constant at temperature T, $k(T)$, can be described by the homogeneous decay kinetics as [2],

$$\frac{d[H_2^-(t)]}{dt} = -k(T)[R][H_2^-(t)], \qquad (4\text{-}1)$$

where $[H_2^-(t)]$ and $[R]$ are the concentrations of the H_2^- anion and reactant impurity at time t, respectively. If $[R]$ is much larger than $[H_2^-(t)]$ and keeps unchanged in the time scale of ~ 10 hours, the following equation can be derived from Eq. (4-1),

$$[H_2^-(t)] = [H_2^-(0)] \exp(-D(T)\, t). \qquad (4\text{-}2)$$

Here, $D(T)$ denotes the decay rate constant of the H_2^- anions at temperature T with

$$D(T) = k(T)[R]. \qquad (4\text{-}3)$$

As shown in Eq, (4-3), the decay rate constant of the H_2^- anions is proportional to the concentration of the reactant species, R, in the p-H_2 sample. Therefore, we assigned the reactant species by measuring effects of concentration of contaminant species on the decay rate constant of the H_2^- anions.

4. 1. 1. Effects of ionic and radical species on the decay behavior

Ionic and radical species such as H_3^+ cations and H atoms simultaneously produced in irradiated p-H_2 solid are the most plausible candidates for the reactant impurity, because the cations and H atoms strongly attract electrons with affinities of 8.70 and 0.75 eV, respectively [3]. Table 4-1 shows the initial yields of the H_2^- anions and H atoms and decay rate constants of the H_2^- anions at 4.2 K in the p-H_2 solid irradiated with X-rays for 17, 50, and 150 min and with γ-rays for 30 min (0.4 kGy). The decay rate constants are approximately the same within their experimental errors, although the initial yields of the H_2^- anions, which should be proportional to those of cations, and of the H atoms vary among these four samples. If the H_2^- anions react with the cations or with the H atoms via: $H_2^- + H \rightarrow H_2 + H^-$, the decay rate constant of the H_2^- anions should be proportional to the initial yields of the cations (H_2^- anions) or H atoms, respectively. However, it does not depend on these initial yields, indicating that the H_2^- anions decay due to the reaction neither with the cations nor with the H atoms.

Radiolysis	X-ray 17 min	X-ray 50 min	X-ray 150 min	γ-ray 30 min
Initial yields of H_2^- (mol %)	4.8×10^{-12}	2.4×10^{-11}	4.0×10^{-11}	1×10^{-10}
Initial yields of H (mol %)	2.8×10^{-8}	8.5×10^{-8}	2.6×10^{-7}	3×10^{-6}
Decay rate constant of H_2^- (s^{-1})	$(6\pm3)\times10^{-5}$	$(3.4\pm0.7)\times10^{-5}$	$(3.8\pm0.2)\times10^{-5}$	$(3.2\pm0.5)\times10^{-5}$

Table 4-1. Initial yields of H_2^- anions and H atoms and decay rate constant of H_2^- anions in X-ray (60 kV, 45 mA) or γ-ray (Co-60, 0.3 kGy) irradiated pure p-H_2 at 4.2 K.

4. 1. 2. Effects of hydrogen molecular impurity on the decay behavior

Hydrogen molecular impurities in the pure p-H_2 sample are also the plausible candidates for the reactant. Although these molecular impurities are less reactive, concentrations of these impurities such as o-H_2 (1-4 mol %) and HD (0.03 mol %) are much larger than those of the H atoms and ionic species (< 10^{-6} mol %). Fig. 4-2 shows decay behaviors of the H_2^- anions in γ-ray irradiated pure p-H_2, and p-H_2-o-H_2, p-H_2-HD, and p-H_2-D_2 mixture solids at 4.2 K. The H_2^- anions in the p-H_2-HD(D_2) mixtures decay faster than those in pure p-H_2, while the H_2^- anions in the p-H_2-o-H_2 mixtures decay slower. This result shows that the existence of HD and D_2 molecules accelerate the decay

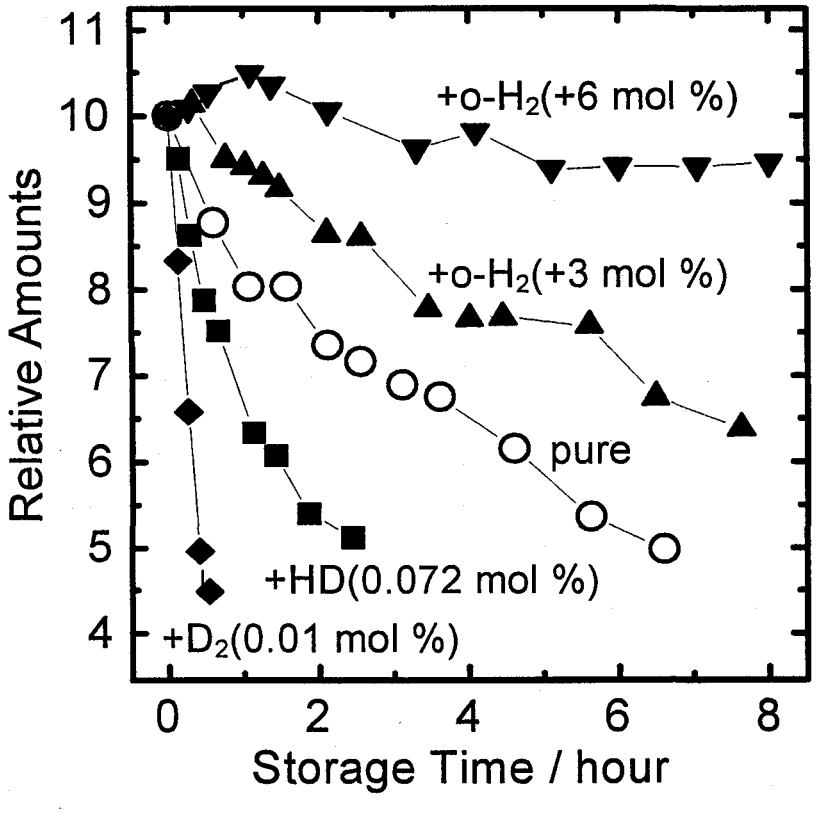

Fig. 4-2 Decay behaviors of H_2^- anions in γ-ray irradiated pure p-H_2, and p-H_2-o-H_2, p-H_2-HD, and p-H_2-D_2 mixture solids at 4.2 K. Concentrations of o-H_2 molecules in p-H_2-o-H_2 mixtures shown in the parentheses do not include those originally contained in pure p-H_2. All amounts at t = 0 are normalized to 10.

of the H_2^- anions, whereas the o-H_2 molecules disturb.

Fig. 4-3 shows the decay rate constant of the H_2^- anions as a function of the concentrations of HD and D_2 molecules in the p-H_2 solid. It has been found that the decay rate constant is proportional to the concentration of the HD molecules and the solid fitting line approximately pass through the origin. It should be noted that the decay rate constant at the concentration of HD at 0.03 mol % in Fig. 4-3 shows that measured in the pure p-H_2 solid. Therefore, this proportionality indicates that the H_2^- anions decay due to the reaction with HD molecules even in the pure p-H_2 solid.

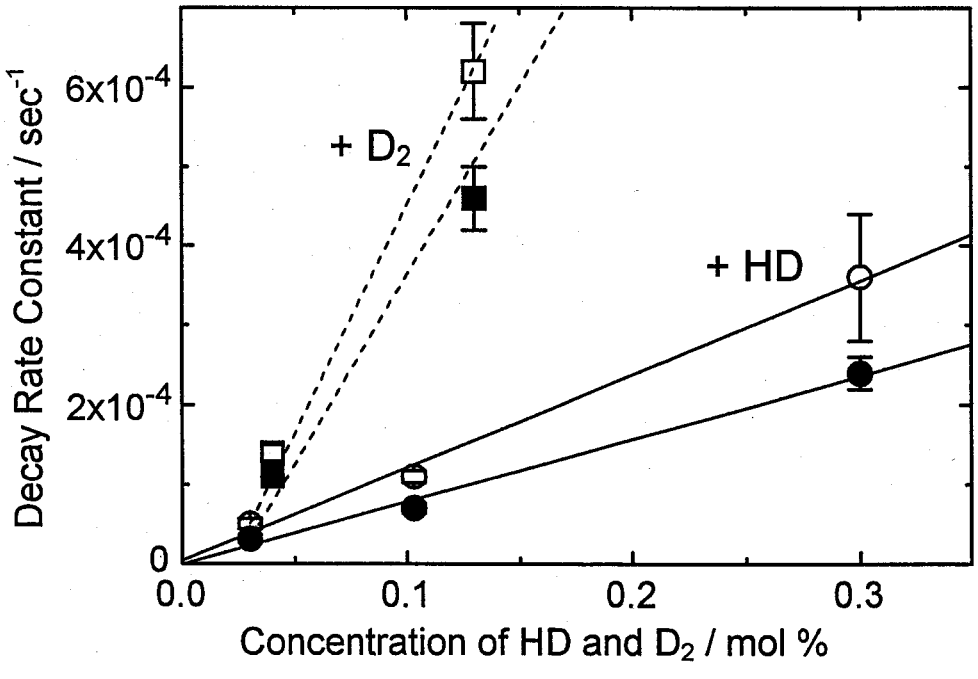

Fig. 4-3 Decay rate constant of the H_2^- anions in γ-ray irradiated solid p-H_2 containing additional HD and/or D_2 molecules at 4.2 K. Open and closed circles, fitted by solid lines, depict the decay rate constants of p-H_2^- and o-H_2^- anions as a function of concentration of HD, respectively. Open and closed squares, fitted by broken lines, depict the decay rate constants of p-H_2^- and o-H_2^- anions as a function of concentration of D_2 together with that of HD at natural abundance of 0.03 mol %.

4. 2. Decay Mechanism with HD(D_2)

As discussed above, the H_2^- anion decay via the reaction with the HD(D_2) molecule in the p-H_2 solid. Although it seems that the HD(D_2) molecules cannot react with the H_2^- anions, the attractive interaction of the H_2^- anions with the HD(D_2) molecules at J= 0 is somewhat stronger than that with H_2 molecules at J= 0 and makes H_2^--HD(D_2) complexes in the solid, which cannot be observed because of broadening of their ESR spectrum. In this paragraph, the decay mechanism of the H_2^- anions with the HD(D_2) molecules is discussed.

4. 2. 1. Attractive interaction of the H_2^- anion with HD(D_2) molecule in p-H_2 solid

The H_2, HD, and D_2 molecules interact with the H_2^- anion mainly due to charge-induced dipole and charge-quadruple interactions. The Hamiltonian of a point charge q and a neutral diatomic molecule is of the form [4]:

$$H = H_0 + H_s \tag{4-4}$$

where H_0 is the Hamiltonian of the unperturbed molecule and H_s describes the interaction and is given by,

$$H_s = -\frac{1}{2}\frac{\alpha q^2}{R^4} + (-\frac{\gamma q^2}{3R^4} + \frac{qQ}{R^3})P_2(\cos\theta). \tag{4-5}$$

In Eq. (4-5), R is the separation between the center of mass of the molecule and the point charge, θ denotes the orientation of the molecule with respect to $\boldsymbol{R}$, and P_2(cos θ) is the Legendre polynomial. α and γ are the mean polarizability and its anisotropy, that is, α = (1/3)($\alpha_{//}$ + 2$\alpha_{\perp}$) and γ = $\alpha_{//}$ - $\alpha_{\perp}$, where $\alpha_{//}$ and $\alpha_{\perp}$ are the polarizabilities of the molecule along and perpendicular to its axis, respectively. the quantity Q denotes the quadrupole

moment in a molecule-fixed frame.

The first term in Eq. (4-5) refers to the interaction energy of the point charge with the isotropic induced dipole created on the molecule by its electric field $E = q / R^2$. Its order of magnitude is $6.6 \times 10^4 / R^4$ K, where R is in Å. The interaction energy of the point charge with the dipole due to the anisotropic part of the polarizability of the molecule is given by the second term, and is of order of magnitude $(1.7 \times 10^4 / R^4)\, P_2(\cos\theta)$ K. The third term represents the interaction energy of the molecular quadrupole with the gradient of the field of the point charge, its order of magnitude is $(2.2 \times 10^4 / R^3)\, P_2(\cos\theta)$ K. It is clear that for larger separation R the quadrupole term always dominates over the polarizability term.

The matrix element of the Legendre polynomial, $\langle J,m|P_2(\cos\theta)|J',m\rangle$ is only different from zero if $J' = J, J \pm 2$, that is, even and odd J states do not mix. In particular we have

$$\left\langle J,m\left|P_2\right|J,m\right\rangle = \frac{J(J+1)-3m^2}{(2J-1)(2J+3)} \tag{4-6}$$

$$\left\langle J,m\left|P_2\right|J+2,m\right\rangle = \left\langle J+2,m\left|P_2\right|J,m\right\rangle = \left[\frac{9(J-m+2)(J-m+1)(J+m+2)(J+m+1)}{4(2J+3)^2(2J+1)(2J+5)}\right]^{1/2} \tag{4-7}$$

Taking the first, ΔE_1, and second, ΔE_2, order perturbation term into consideration, we obtain the energy shift, ΔE, of the ground state due to the mixing with other rotational states,

$$\Delta E = \Delta E_1 + \Delta E_2 = -\frac{\alpha q^2}{2a_0}\left(\frac{a_0}{R}\right)^4 - \sum_J \frac{\left\{\frac{qQ}{a_0}\left(\frac{a_0}{R}\right)^3 - \frac{q^2\gamma}{3a_0}\left(\frac{a_0}{R}\right)^4\right\}^2 \left\langle J,0\left|P_2(\cos\theta)^2\right|0,0\right\rangle^2}{E_J^{(0)} - E_0^{(0)}} \tag{4-8}$$

$E_J^{(0)}$ is the unperturbed rotational energy of the hydrogen molecules described as,

$$E_J^{(0)} = J(J+1)\frac{\hbar^2}{2I_{moment}} \tag{4-9}$$

where I_{moment} is the moment of inertia. Although $|\Delta E_1|$ of the H_2, HD, and D_2 molecules are the same, $|\Delta E_2|$ of HD(D_2) at $J = 0$ is higher than that of H_2, because the moment of inertia of the HD(D_2) molecule is larger than that of the H_2 molecule. For HD molecule, it should be considered that the charge-permanent dipole and -other induced multiple moments interaction in addition to Eq. (4-8), because the centers of mass and charge relative to a point charge for HD molecule is different [4]. Fig. 4-4 shows the energy shifts of the H_2, HD, and D_2 molecules at $J = 0$ induced by a negative charge [4]. The shifted energy of HD and D_2 being lower than that of H_2 causes the attraction force between the H_2^- anion and HD(D_2) molecule in the p-H_2 solid.

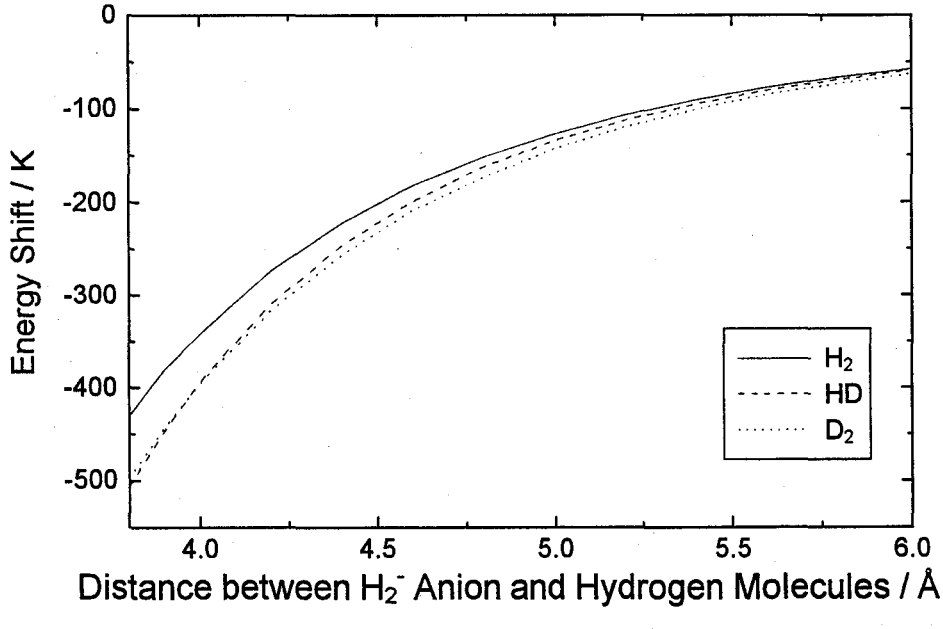

Fig. 4-4 Energy shift of H_2, HD, and D_2 molecules at $J = 0$ induced by a negative charge in H_2^- anion as a function of distance between the H_2^- anion and hydrogen molecules [4].

4. 2. 2. Product of the reaction

It is expected that the H_2^- anions react with their neighboring HD molecules in the p-H_2 solid to become another anionic species, which has not been observed. In this paragraph, the product of the reaction is discussed.

Inability to form HD^- anions in p-H_2 solid

First, it is considered that the H_2^- anion reacts with the HD molecule to produce HD^- anion as follows:

$$H_2^- + HD \rightarrow H_2 + HD^-. \qquad (4\text{-}10)$$

However, ESR spectrum of the HD^- anion could be observed neither in the pure p-H_2 nor in the p-H_2-HD mixture. The H_2^- anion does not decay via the electron transfer reaction because of endothermic process. Addition of an excess electron to H_2 or D_2 molecules weaken the bond between the two nuclei, which reduces the zero-point vibrational energy. The reduction of the zero-point energy is much higher for lighter particles, so that Eq. (4-10) becomes endothermic [5].

Formation of electron bubbles in p-H_2-HD(D_2) [6]

Fig. 4-5 shows ESR spectra of γ-irradiated solid (a) p-H_2-D_2 (11 mol %), (b) p-H_2-HD (11 mol %), and (c) pure p-H_2 at 4.2 K with microwave frequency and power of 9290 MHz and 5 nW. A narrow and sharp singlet signal at $g = 2.002$ is observed in (a) and (b), but not in (c). The broad signal around 3319 G is due to color centers in the irradiated quartz cell. ESR linewidth of the singlet signal is 0.26 G (a) and 0.4 G (b), which is comparable to that of H atoms (0.21 G) and of p-H_2^- anions in pure p-H_2 (0.13 G (cf. Table 2-2)). Fig. 4-6 shows microwave power saturation behaviors of the ESR intensities of the narrow singlet signal in p-H_2-D_2 (11 mol %), H atoms, and H_2^- anions in pure p-H_2 at 4.2 K. The ESR intensity of the singlet signal saturates at very low microwave power

as compared with that of the H atoms and H_2^- anions.

This narrow singlet signal in Fig. 4-5 (a) and (b) is assigned to the electron bubbles due to the following reasons. First, this signal is narrow singlet one with *g*-factor of 2.002 which is almost the same with that of free electron (g_e = 2.0023) within experimental errors. This characteristics clearly shows that the species which assign the singlet signal has S = 1/2, L = 0, A = 0 [7]. Second, the ESR power saturation behavior in Fig. 4-6 shows that the spin-spin and spin-lattice relaxation rates of the singlet signal are smaller than not only that of H_2^- anions but also that of neutral species of H atoms [6]. Generally, these rate decrease with the increase in the interaction between electric spins in the radicals and surrounding lattice and spins in solids [8,9]. Radius of the electron bubbles in H_2 solid is reported to be 4.7 Å [3] which is remarkably larger than that of H atoms trapped in substitutional site of H_2 solid (3.78 Å). Thus, it is expected that the electron bubbles has very slow relaxation rate which saturates its ESR intensity so easily. As

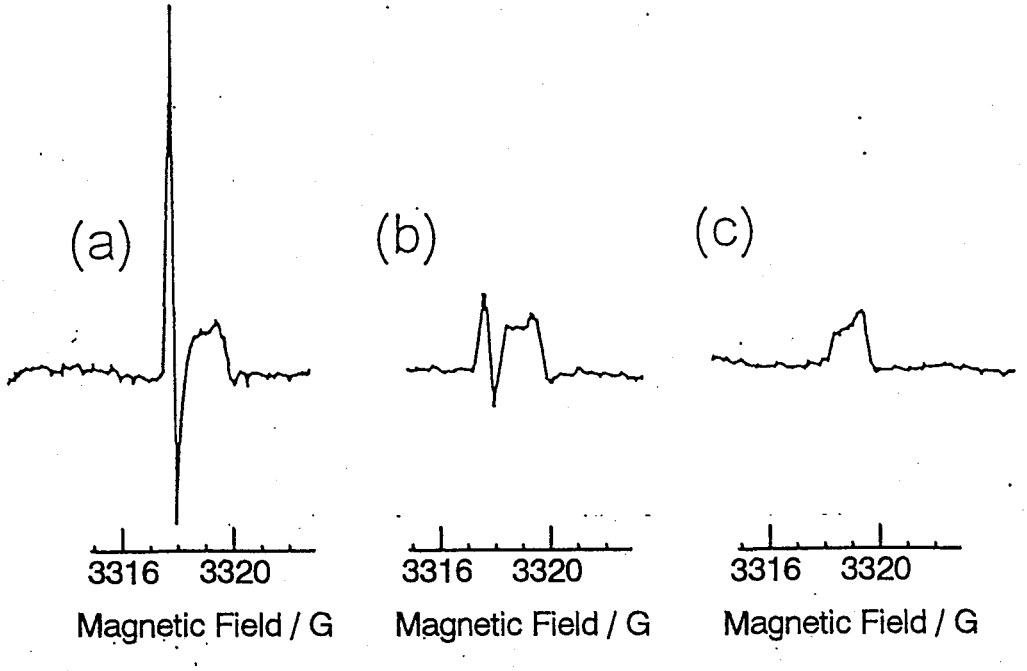

Fig. 4-5 ESR spectrum of γ-ray irradiated (a) p-H_2-D_2(11 %), (b) p-H_2-HD(11 %), and (c) pure p-H_2 at 4.2 K. Microwave frequency and power are 9290 MHz and 5 nW, *g*-factor of the singlet signal is 2.002. The broad peak around 3319 G is due to color centers of an irradiated quartz cell.

discussed above, characteristics of the singlet signal, *g*-factor, ESR linewidth, and microwave power saturation behavior, are consistent with those of electron bubbles. Therefore, the singlet signal is assigned as electron-bubbles.

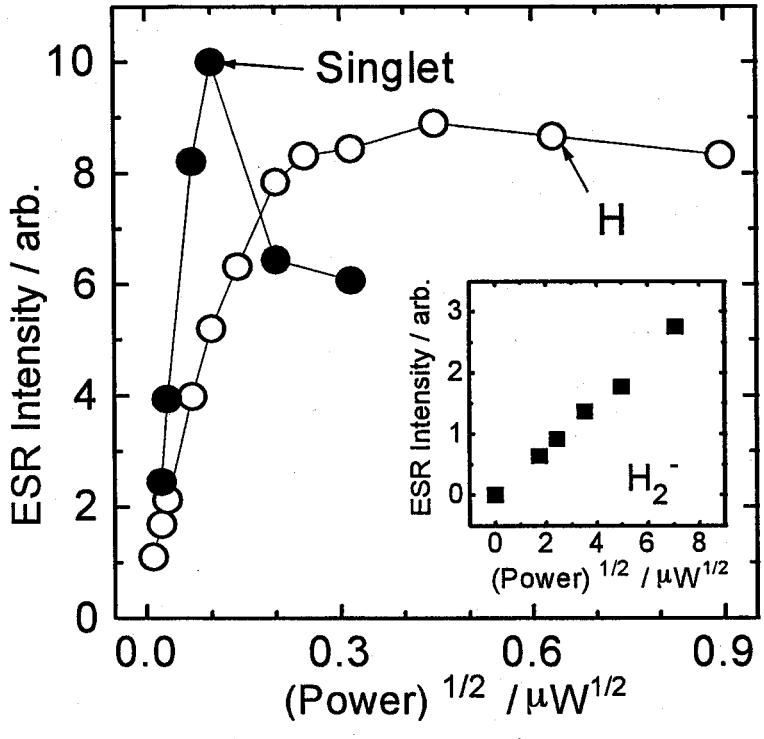

Fig. 4-6 Microwave power saturation behavior of the singlet signal (closed circles) in Fig. 4-5 (a), H atoms (open circles), and H_2^- anions (closed triangles) in pure p-H_2 at 4.2 K. The ESR intensities among three signals were not correlated for each other. Microwave power of 5 nW yields the microwave magnetic field of 0.27 mG.

Fig. 4-7 shows initial yields of the electron bubbles and H_2^- anions as a function of concentrations of D_2 molecules in solid p-H_2-D_2 mixtures at 4.2 K. The initial yields of the electron bubbles increase with the increase in the concentration of D_2 molecules, whereas those of the H_2^- anions decrease. It should be noted that scale of the initial yields of electron bubbles on the ordinate is much larger than that of H_2^- anions by a factor of thousands. Thus, total yields of anionic species observed continuously increase with the increase in the concentration of D_2 molecules. This result shows that D_2 molecules in p-H_2 solid make many trapping sites for excess electrons to form electron bubbles. Similarly, it is expected that HD molecules in p-H_2 solid also make these trapping sites. It is considered that these trapping sites are formed due to interaction between negative

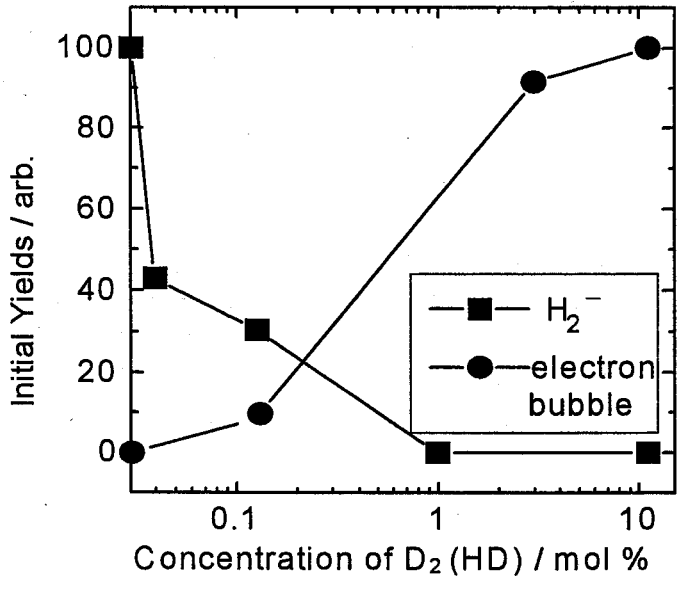

Fig. 4-7 Initial yields of the H_2^- anions and electron bubbles in γ-ray irradiated solid p-H_2-D_2 (0-11 mol %) mixtures at 4.2 K. Concentration of D_2 molecules together with HD at a natural abundance of 0.03 mol % is scaled on the absicca. Initial yields of H_2^- anions in pure p-H_2 and those of the electron bubbles in p-H_2-D_2 (11 mol %) mixture are normalized to 100, although the former is much smaller than the latter by a factor of thousands.

charges and $HD(D_2)$ molecules which is stronger than that between the negative charges and H_2 molecules (cf. Fig. 4-4). In addition, the size of the $HD(D_2)$ molecules is smaller than that of H_2 molecules in H_2 solids, because of lower zero-point vibration of the $HD(D_2)$ molecules [10]. The smaller zero-point vibration probably makes the trapping sites which catches electrons to form bubbles. On the other hand, the initial yields of H_2^- anions decrease with the increase in the concentration of $HD(D_2)$ molecules. This result strongly suggests that the H_2^- anions react with the $HD(D_2)$ molecules to form electron bubbles nearby these $HD(D_2)$ molecules as follows:

$$H_2^- + HD(D_2) \rightarrow H_2 + HD(D_2) + e^-_{bubble}. \qquad (4\text{-}11)$$

Absence of the singlet signal of the electron bubbles in pure p-H_2 solid (cf. Fig. 4-5 (c)) is due to lower ESR resolution of the electron bubbles, because power of incident microwave power on the measurement of the electron bubbles must be turned down to avoid its saturation. Stability of the H_2^- anions is about 5 K (cf. Chapter 3), whereas the intermolecular interaction energy between H_2^- anion and $HD(D_2)$ molecule at $J = 0$ is lower than that between H_2^- and H_2 by a factor of 80 K at $r = a_0$ [4]. The electrons in the H_2^- anions is probably released by the energy perturbation due to $HD(D_2)$ molecules to form electron bubbles nearby the $HD(D_2)$ molecules.

Effects of Ne atoms on the decay behavior are also studied. Fig. 4-8 shows decay behaviors of the H_2^- anions in pure p-H_2 and p-H_2-Ne mixtures at 4.2 K. Ne atoms accelerate the decay of the H_2^- anions. Moreover, as shown in Fig. 4-9, new sharp singlet signal at $g = 2.0023$ are observed. ESR intensity of the new singlet signal saturates at very low microwave powers compared with that of H_2^- anions (cf. Fig. 4-10). Since characteristics of the singlet signal, narrow linewidth, ESR g-factor, and power saturation behavior (cf. Fig. 4-9), are very similar to those observed in Fig. 4-5 (a)(b), the singlet signal is also assigned as electron bubbles. These results indicate that, similarly to HD and D_2 molecules, H_2^- anions react with Ne atoms to produce electron bubbles via the

following reaction,

$$H_2^- + Ne \rightarrow H_2 + Ne + e^-_{bubble}. \quad (4\text{-}12)$$

This result strongly supports the decay mechanism of the H_2^- anions in p-H_2 solid depicted by Eq. (4-11).

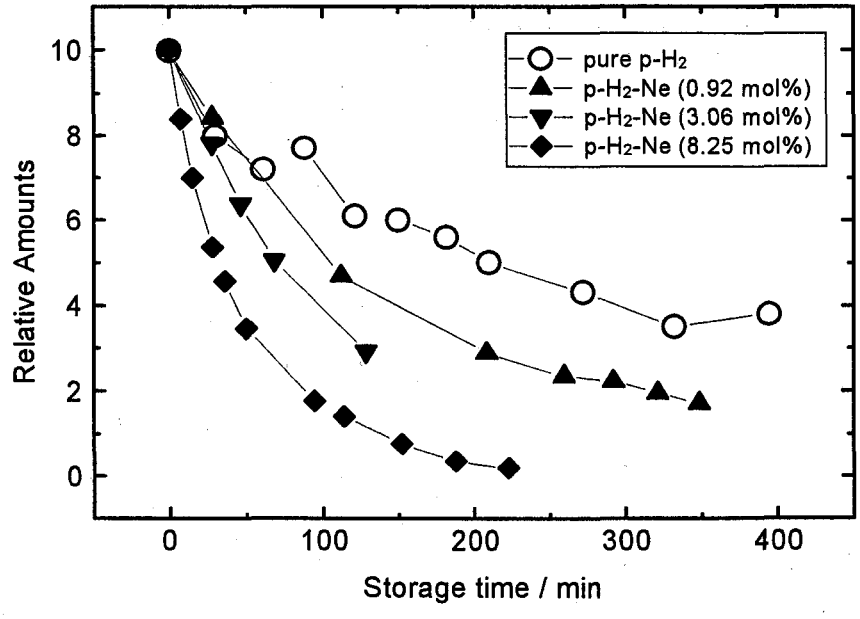

Fig. 4-8 Decay behaviors of H_2^- anions in γ-ray irradiated solid pure p-H_2 and p-H_2-Ne mixtures at 4.2 K. All amounts at t = 0 are normalized to 10. It should be noted that only few amounts of the Ne atoms could be dissolved in the p-H_2 solid.

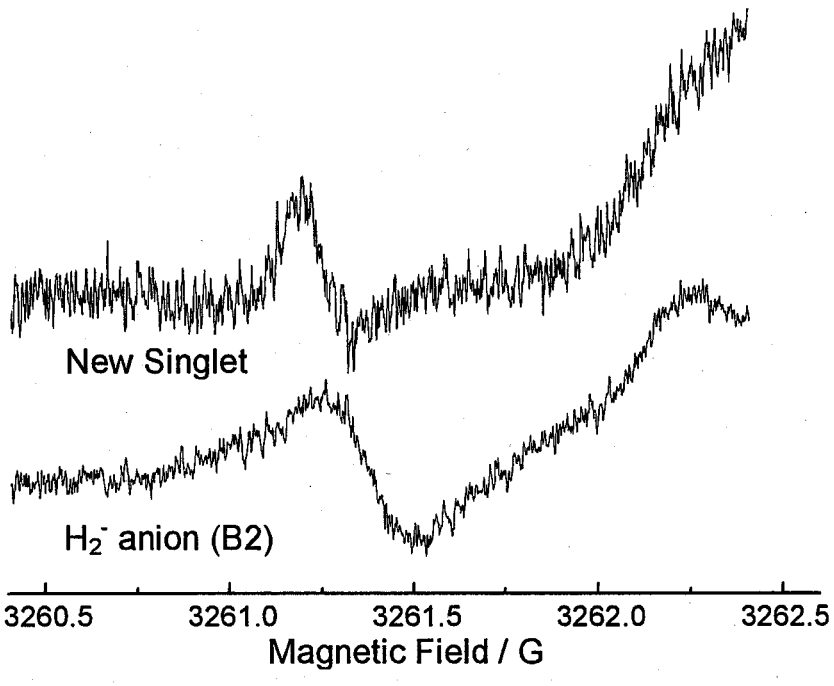

Fig. 4-9 ESR spectrum of the new singlet signal and H_2^- anions (B2 signal) in X-ray irradiated solid p-H_2-Ne (1.2 mol %) mixture with microwave power of 2.06 nW and 25 μW, respectively. These two signals do not overlap, because power saturation behaviors of these two signals are completely different for each other (cf. Fig. 4-7). Steep increase above 3260 G is due to the signal of irradiated ESR quartz cell.

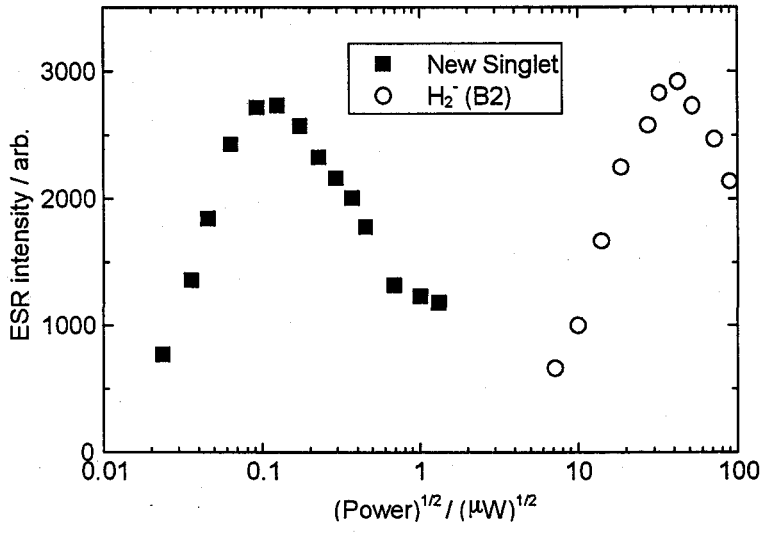

Fig. 4-10 ESR power saturation behaviors of the new singlet signal (cf. Fig. 4-6) and H_2^- anions (B2) in X-ray irradiated p-H_2-Ne (1.02 mol %) solid. The ordinate scales of these two intensities are not correlated for each other.

4. 2. 3. Diffusing species

In this paragraph, we discuss which species, the H_2^- anions or HD molecules, mainly diffuse in the p-H_2 solid. It is concluded that the diffusing species is assigned as HD molecules due to the following reasons. It is expected that the H_2^- anions cannot diffuse in the p-H_2 solid, because of their very heavy effective mass. The effective mass of the H_2^- anion should be much heavier than mass of the H_2^- anion itself, because, as discussed above, the H_2^- anion should attracts surrounding molecules to form H_2^- cluster in the p-H_2 solid. It has been reported that effective masses of positive and negative charges trapped in superfluid helium are much larger than mass of one helium atom by a factor of 40 – 200 by forming icebergs and bubbles, respectively [11]. Since the p-H_2 solid is also quantum media, similar results are expected. On the other hand, Sullivan et al. [12,13] have been reported that the HD molecules diffuse in solid p-H_2 via quantum tunneling and thermally activated diffusion mechanism below and above 9 K, respectively. As discussed below, the decay rate constant of the H_2^- anions show various temperature dependence which suggests the quantum tunneling diffusion of the reactants. Moreover, it has been reported that the diffusion rate constant of the HD molecules decrease with the increase in the concentration of o-H_2 molecules, which is consistent with our result shown in Fig. 4-2. Thus, it is concluded that the decay of the H_2^- anions is due to the diffusion of HD molecules to H_2^- anions.

4. 3. Para-ortho Conversion and Resonance Diffusion of H_2^-

Fig. 4-11 shows decay behaviors of ortho-H_2^- (B1 in Fig. 2-13) and para-H_2^- (B2) anions in γ-ray irradiated p-H_2 solid at 4.2 K. These data reproducibly show that the p-H_2^- anions decay a little faster than the o-H_2^- anions. Fig. 4-12 shows the ratios of the amounts of the o-H_2^- ($I_{o\text{-}H2^-}$) and p-H_2^- ($I_{p\text{-}H2^-}$) anions to the total amounts of the H_2^- (I_{H2^-}) anions, which are calculated as

$$\frac{I_{o\text{-}H2^-}}{I_{H2^-}} = \frac{I_{B1} + I_{B3} + I_{B4}}{I_{B1} + I_{B2} + I_{B3} + I_{B4}} = \frac{3I_{B1}}{3I_{B1} + I_{B2}}, \quad (4\text{-}13)$$

$$\frac{I_{p\text{-}H2^-}}{I_{H2^-}} = \frac{I_{B2}}{I_{B1} + I_{B2} + I_{B3} + I_{B4}} = \frac{I_{B2}}{3I_{B1} + I_{B2}}, \quad (4\text{-}14)$$

respectively, where I_{Bi} (i = 1-4) shows the ESR intensity of Bi signal. While the ratio of the o-H_2^- anions gradually increases, that of the p-H_2^- anions decreases. In this paragraph, we discuss the small difference in the decay behaviors.

4. 3. 1. Parity conservation law in H_2 molecule and H_2^- anion and their ortho-para conversion

First, we discuss the quantum states of the H_2 molecules and H_2^- anions. Since a proton is a Fermion, the parity of the wave function of species, Ψ, must be antisymmetric on exchanging each proton in a homonuclear diatomic molecule such as a H_2 molecule and a H_2^- anion. This restricts the combination of the wave functions of the internuclear vibration, $\varphi_{vib.}$, molecular rotation, $\varphi_{rot.}$, nuclear spin, $\varphi_{nuclear\ spin}$, and electron, φ_e, because Ψ is described as

$$\Psi = \varphi_{vib.} \times \varphi_{rot.} \times \varphi_{nuclear\ spin} \times \varphi_e. \quad (4\text{-}15)$$

The parities of the wave functions of the H_2 molecules and H_2^- anions are summarized in Table 4-2. According to the restricted combinations, rotational quantum number of the o-H_2 molecule at a ground state is not 0 but 1, whereas that of the p-H_2 molecule is 0. This makes energy of the o-H_2 molecules higher than that of the p-H_2 molecules by 170.5 K at low temperature [14]. Although the ortho-para conversion of the H_2 molecules is forbidden, the o-H_2 molecules very slowly convert into the p-H_2 molecules due to magnetic perturbations [15]. On the other hand, the rotational quantum numbers of the

p-H_2^- and o-H_2^- anions at a ground state are 1 and 0, respectively, because the wave function of the electrons in the H_2^- anions is based on the antisymmetric wave function of $^2\Sigma^+_u$, whereas that in the H_2 molecule is based on the symmetric wave function of $^2\Sigma^+_g$ [16]. This antisymmetry changes the combination between the rotational and nuclear spin quantum states and makes energy of the p-H_2^- anions higher than that of the o-H_2^- molecules. Thus, p-H_2^- anion can convert into the o-H_2^- anion. Therefore, it is concluded that the small difference in the decay behaviors of B1 and B2 signals in Fig. 4-11 indicate the conversion form p-H_2^- to o-H_2^-.

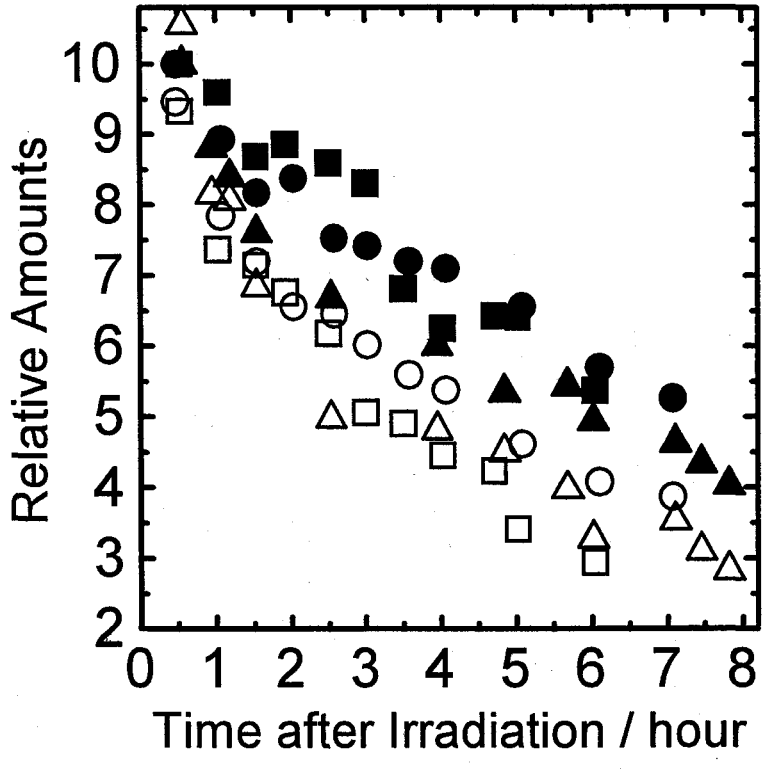

Fig. 4-11 Decay behaviors of H_2^- anions in γ-ray irradiated p-H_2 solid at 4.2 K. Closed symbols shows relative amounts of o-H_2^- anions. Open symbols shows those of p-H_2^- anions. Circles, squares, and triangles are the results in three samples separately prepared under the same condition. All mounts of B1 signal at $t = 0$ are normalized to 10.

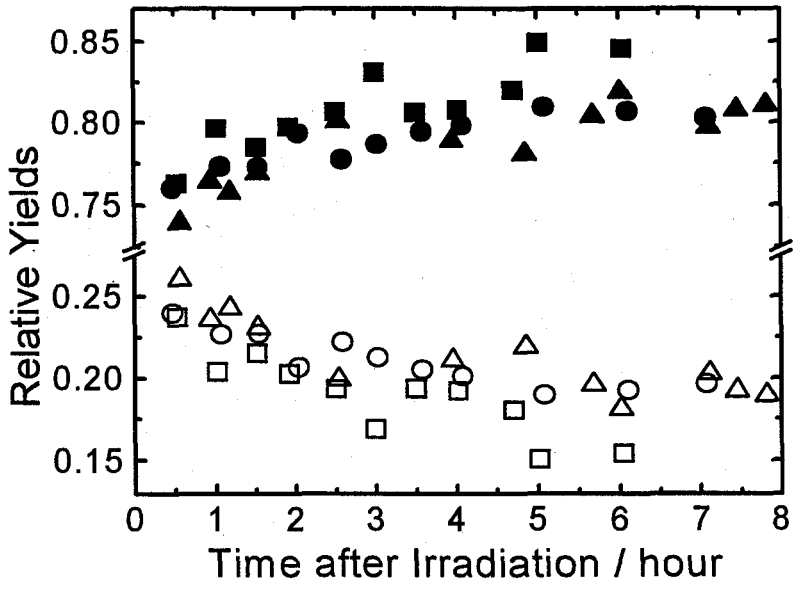

Fig. 4-12 Ratios of the amounts of p-H_2^- (●, ■, ▲) and o-H_2^- (○, □, △) to the total amounts of H_2^- anions (see text).

	Vibration	Rotation	Electron	Nuclear Spin
p-H_2	sym.	sym.($J = 0$)	sym.	anti.
o-H_2	sym.	anti.($J = 1$)	sym.	sym.
p-H_2^-	sym.	anti.($J = 1$)	anti.	anti.
o-H_2^-	sym.	sym.($J = 0$)	anti.	sym.

Table 4-2 Parities of wave functions in H_2 molecules and H_2^- anions at ground state. "sym." and "anti." represent symmetry and antisymmetry of these wave functions, respectively.

4. 4. Temperature Dependence of the Decay Rate Constant

Fig. 4-1 shows the decay behavior of the H_2^- anions in X-irradiated solid p-H_2 at 2.9, 4.5, and 6.6 K. The H_2^- anions at 4.5 K decay slower than those at 2.9 K, although the H_2^- anions at 6.6 K decay faster than those at 4.5 K. Since particles in insulators generally diffuse via thermally activated process, their diffusion rate constants increase exponentially with temperature. Thus, this anomalous temperature dependence shown in Fig. 4-1 suggests that the HD molecules diffuse in the p-H_2 solid not via the thermally activated process but via quantum mechanical tunneling at lower temperatures. In this paragraph, effects of temperature on the decay of the H_2^- anions are precisely examined to study the quantum tunneling diffusion of the HD molecules.

Fig. 4-13 shows the decay rate constant of the H_2^- anions as a function of temperature in the range between 1.3–6.6 K. The decay rate constant proportionally increases with the increase in temperature below 3 K and decreases with the increase between 3–5 K, although it exponentially increases with the increase above 5 K. The decay rate constant of the H_2^- anion shown in Fig. 4-13 was tentatively fitted by the equations as follows:

$$D_{lowT} = D_I(T/\Theta_D), \qquad (T < 3\ \mathrm{K}) \qquad (4\text{-}16)$$

$$D_{highT} = D_{II}(\Theta_D/T)^{\alpha} + D_T \exp(-E_a/kT). \qquad (T \geq 3\ \mathrm{K}) \qquad (4\text{-}17)$$

The solid curves show the fitting ones with the parameters $D_I = 6.7\times10^{-3}$ s^{-1}, $D_{II} = (3.8 \pm 0.9)^{-11}$ s^{-1}, $\alpha = 4.47 \pm 0.07$, $D_T = 300 \pm 190$ s^{-1}, $E_a = 93 \pm 4$ K, when $\Theta_D = 100$ K [17] was assumed. The second term in Eq. 4-17 shows the decay rate constant due to the thermally activated diffusion of the HD molecules. E_a showing thermal activation energy for the diffusion of 93 ± 4 K is comparable to that for diffusion of HD (91 ± 8 [18], 91 ± 10 [12], 112 K [13]), o-H_2 (96 K [19]), H atoms (103 ± 5 K [20]), and positive and negative charges (about 100 K) [21] in solid H_2. It has been considered that these diffusions occur due to thermally activated vacancy with formation energy of ~ 100 K. Therefore, it is concluded that the exponential increase in the decay rate constant with

temperature above 5 K is also due to the diffusion of HD via the thermally activated process. On the other hand, the linear increase below 3 K and decrease between 3–5 K cannot be explained the thermally activation process, suggesting the quantum tunneling mechanism. Moreover, the decrease in the decay rate constant of the H_2^- anions with the increase in concentration of o-H_2 molecules at 4.2 K also suggests the quantum tunneling, because the tunneling probability generally decreases with the increase in the energy level misalignment of solids due to impurity (cf. Chapter 5).

It has been reported that the decay rate constant of isolated H atoms in H_2 solid linearly increase with the increase in temperature below 4 K, which are explained by one-phonon assisted quantum tunneling diffusion of the H atoms. In addition, the decrease in the rate constant with the increase in temperature in p-H_2 solid has been reported on the pairing process of o-H_2 molecules and on the diffusion of HD molecules. These results have been explained by two-phonon assisted quantum tunneling mechanism. The anomalous temperature dependence of the decay rate constant of the H_2^- anions below 5 K is compared with that predicted by these quantum tunneling mechanisms in the next chapter.

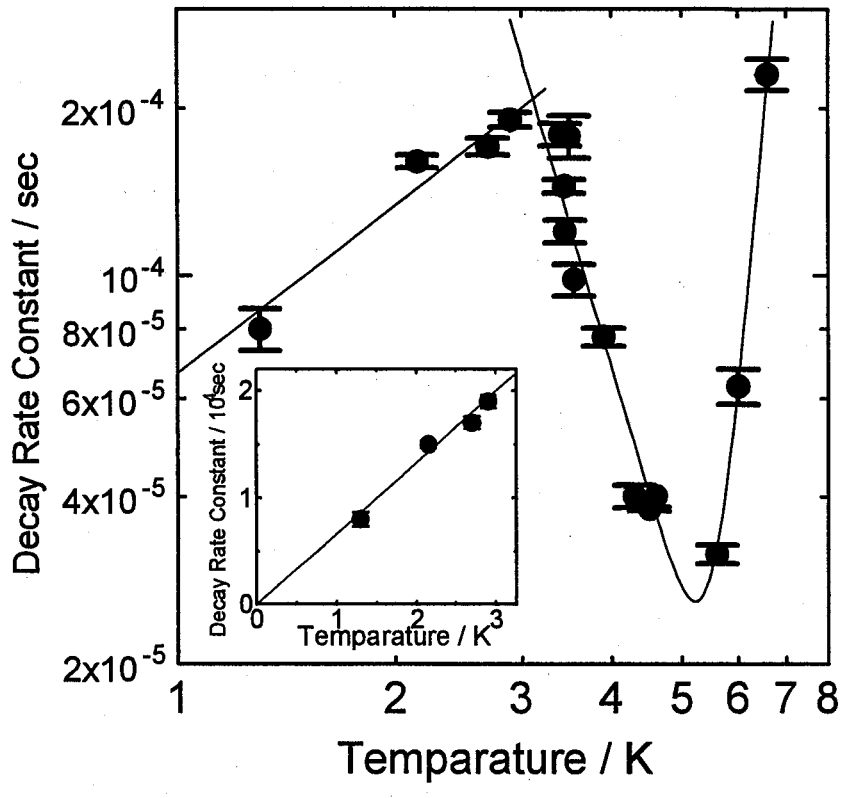

Fig. 4-13 Decay rate constant of H_2^- anions in X-rays-irradiated solid p-H_2 in the temperature range between 1.3~6.6 K. The both temperature and pressure scales have been made logarithmic. The error-bars depict standard deviations. The solid line and curve are obtained by fitting to the function: $D(T) = 6.7\times 10^{-5} \times T\ s^{-1}$ *and* $D(T) = D_1 (\Theta_D / T)^{\alpha} + D_2 \exp(-E_a / kT)$ with parameters, $D_1 = 9.7\times10^{-12}\ s^{-1}$, $\Theta_D = 100$ K, $\alpha = 4.9$, $D_2 = 250\ s^{-1}$, and $E_a / k = 92$ K, respectively.

References

[1] T. Kumada, N. Kitagawa, S. Mori, J. Kumagai, Y. Aratono, and T. Miyazaki, submitted to J. Low Temp. Phys.

[2] W. J. Moore, Physical Chemistry (Prentice-Hall, Englewood Cliffs, 1972).

[3] P. C. Souers, Hydrogen Properties for Fusion Energy (University of California Press, Berkeley, 1986), and references therein.

[4] J. D. Poll and J. L. Hunt, Can. J. Phys. 63 (1985) 84; J. J. Miller, J. D. Poll, and J. L. Hunt, Can. J. Phys. 69 (1991) 606.

[5] T. Kumada, T. Inagaki, N. Kitagawa, Y. Aratono, and T. Miyazaki, J. Phys. Chem. 101 (1997) 1198; T. Miyazaki, T. Kumada, N. Kitagawa, K. Komaguchi, and Y. Aratono, J. Low Temp. Phys.111 (1998) 453; T. Kumada, Y. Aratono, and T. Miyazaki, J. Low Temp. Phys.111 (1998) 453.

[6] T. Kumada, S. Mori, J. Kumagai, Y. Aratono, and T. Miyazaki, submitted to Chem. Phys. Lett.

[7] C. P. Slichter, Principles of Magnetic Resonance (Harper and Row, 1963).

[8] L. Kevan and M. K. Bowman, Modern Pulsed and Continuous-Wave Electron Spin Resonance (John Wiley & Sons, New-York, 1989).

[9] S. A. Dikanov and Y. D. Tsvetkov, Electron Spin Echo Envelope Modulation Spectroscopy (CRC, Boca Raton, 1992).

[10] T. Ichikawa, H. Tachikawa, T. Kumada, J. Kumagai, and T. Miyazaki, submitted to J. Phys. Chem. A.

[11] A. J. Dahm and T. M. Sanders, Phys. Rev. Lett. 15 (1965) 949.

[12] M. Rall, D. Zhou, Erika G. Kisvarsanyi, and N. S. Sullivan, Phys. Rev. B 45 (1992) 2800.

[13] D. Zhou, C. M. Edwards, and N. S. Sullivan, Phys. Rev. Lett. 62 (1989) 1528.

[14] V. Kranendonk, Solid Hydrogen (Plenum, New-York, 1983).

[15] K. Motizuki and T. Nagamiya, J. Phys. Soc. Jpn. 11 (1956) 93; K. Motizuki and T. Nagamiya, J. Phys. Soc. Jpn. 11 (1956) 654.

[16] E. F. DeRose, E. A. Gislason, N. H. Sabelli, K. M. Sluis, J. Chem. Phys. 88 (1988) 4878.

[17] M. L. Klein and J. A. Venables, Rare Gas Solid (Academic Press, London, 1976).

[18] C. Ebner and C. C. Sung, Phys. Rev. A 5 (1972) 2625.

[19] V. Shevtsov, A. Scherbakov, P. Malmi, E. Ylinen, and M. Punkkinen, J. Low Temp. Phys. 104 (1996) 211.

[20] Ya. Katunin, I. I. Lukashevich, S. T. Orozmamatov, V. V. Sklyarevskii, V. V. Suraev, V. V. Filippov, N. I. Filippov, and V. A. Shevtsov, Pis'ma Zh. Eksp. Teor. Fiz. 34 (1981) 375 [JETP Lett. 34 (1981) 357].

[21] L. P. Mezhov-Deglin, A. A. Levchenko, and A. B. Trusov, J. Low Temp. Phys. 111 (1998) 545.

Chapter 5

Two-Stage Quantum Tunneling of HD near H_2^- [1]

When one impurity particle approaches to the other one in solids, like the pairing process of the H_2^- anion and HD molecule, we must consider the quantum tunneling of the impurity particle in the region whose potential energy levels between neighboring trapping sites are misaligned due to the interaction. Fig. 5-1 shows the energy levels of the neighboring trapping sites in a solid. When the energy level misalignment, $\delta\varepsilon$, becomes larger than the amplitude (bandwidth) of the tunneling transition, Δ_0, the quantum tunneling is suppressed (cf. Fig. 5-1 (c)). The tunneling occurs only when $\delta\varepsilon$ is compensated by the energy level fluctuation due to thermal phonons (phonon assisted tunneling) (cf. Fig. 5-1 (d)), although they usually disturb band motion at $\delta\varepsilon = 0$ (cf. Fig. 5-1 (b)) [2,3]. Because of these tunneling mechanisms are closely connected with thermal phonons, the tunneling probability shows various temperature dependence. In this chapter, the anomalous temperature dependence on the decay rate constant of the H_2^- anions shown in Fig. 4-13 is analyzed using the phonon assisted quantum tunneling models.

5. 1. Rate constant for Two- and One-Phonon Quantum Tunneling

The microscopic equation describing the quantum tunneling in a solid can be obtained using the results in Refs. [2,3]. These authors have been constructed the kinetic equation for the density matrix of particles interacting with the phonon subsystem and after eliminating the nondiagonal elements, found the equation for the particle distribution function at site $\boldsymbol{r}$, $f_{\boldsymbol{r}}$, in the lattice-site representation

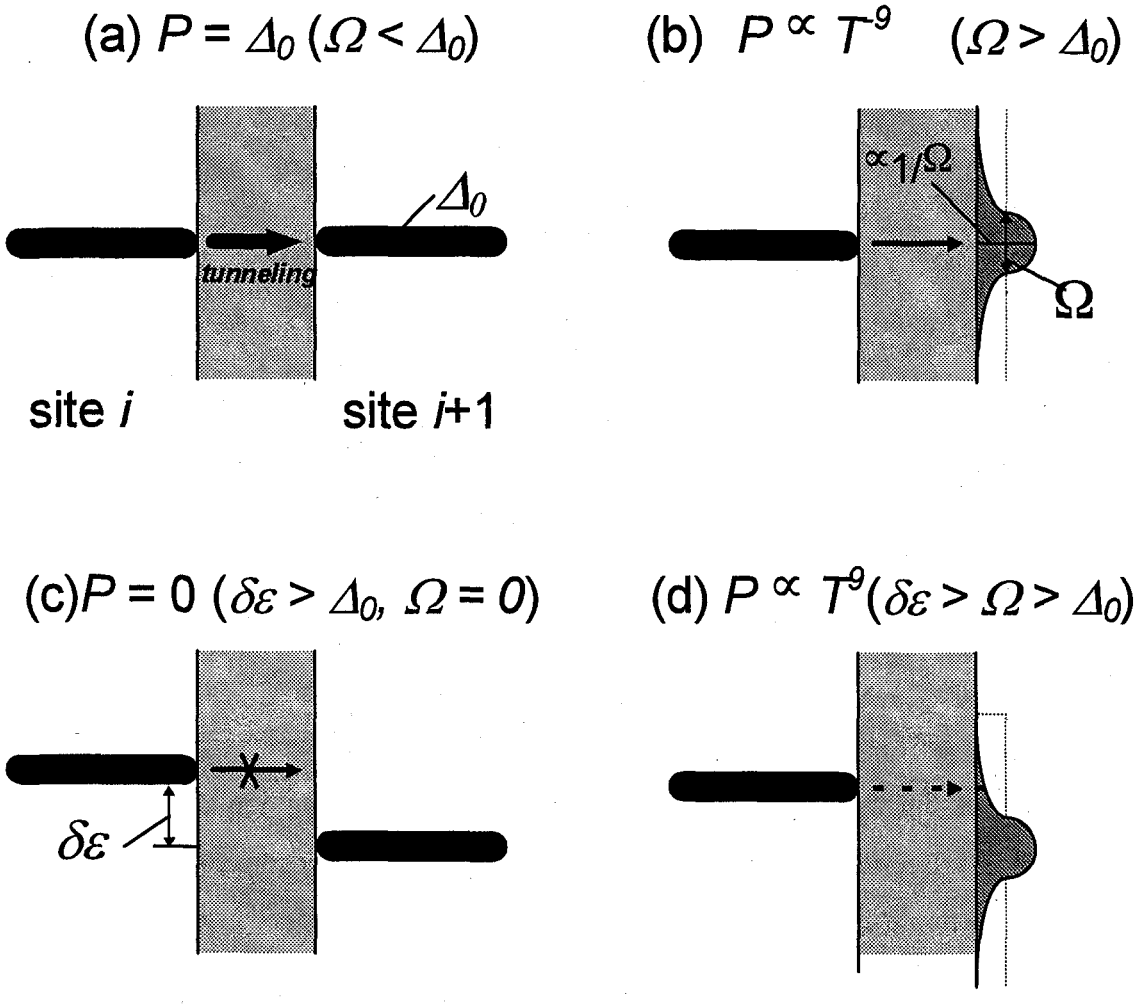

Fig. 5-1 Energy levels of an impurity particle at neighboring sites, i and $i + 1$: (a) energy levels are aligned and tunneling occurs with the probability Δ_0, when energy level fluctuation due to phonons, Ω, is less than Δ_0: (b) energy levels are fluctuated and the tunneling probability becomes smaller ($\propto 1/\Omega$) with the increase in the number of thermal phonons at $\Delta_0 > \Omega$: (c) energy levels are misaligned due to $\delta\varepsilon$ and the tunneling probability suppressed at $\delta\varepsilon > \Delta_0$ and $\Omega = 0$: (d) with the increase in the number of the thermal phonons, the tunneling probability suppressed by $\delta\varepsilon$ increases by compensating $\delta\varepsilon$ for the fluctuation ($\propto \Omega$) at $\delta\varepsilon > \Omega > \Delta_0$.

$$\frac{\partial f_r}{\partial t} + \sum_g \left\{ f_r W_{r,r+g} - f_{r+g} W_{r+g,r} \right\} = 0 \qquad (5\text{-}1)$$

Here

$$W_{r,r+g} = \frac{{\Delta_0}^2 \Omega}{{\delta\varepsilon_{r,r+g}}^2 + \Omega^2} \qquad (5\text{-}2)$$

is the probability for the quantum tunneling from site $\boldsymbol{r}$ to its nearest site $\boldsymbol{r} + \boldsymbol{g}$, where $|\boldsymbol{r}|$ is the distance between interacting two impurity particles, $\delta\varepsilon_{r,r+g}$ is the relative level misalignment between these neighboring sites, and Ω represents the mean-square relative vibration of levels due to thermal phonons.

5. 1. 1. Two-phonon quantum tunneling

When the tunneling occurs via two-phonon interaction, the following expression for Ω is described as

$$\Omega \equiv \Omega_{II} = B_{II}\, \Theta_D\, (T / \Theta_D)^9. \qquad (5\text{-}3)$$

where B_{II} is a dimensionless factor of the order of 10^6.

First, we consider the quantum tunneling at $\delta\varepsilon << \Omega_{II}$ (Fig. 5-1(b)), the following equation is derived from Eq. (5-2):

$$W_{r,r+g} = \frac{{\Delta_0}^2}{\Omega} \qquad (5\text{-}4)$$

and, by substituting Eq. (5-3) into Eq. (5-4), one obtains

$$W_{r,r+g} = \frac{\Delta_0}{B_{II}\Theta_D}\left(\frac{\Theta_D}{T}\right)^9 \qquad (5\text{-}5)$$

This probability drastically decreases with the increase in T, showing that the coherent motion (cf. Fig. 5-1 (a)) is scattered by thermal phonons (cf. Fig. 5-1 (b)). It has been reported by NMR spin-relaxation time measurement that the diffusion rate constant of HD molecules in p-H_2 solids decreases with the increase in temperature below 11 K, and that this decrease has been explained by the two-phonon scattering quantum tunneling depicted by Eq. (5-5) [4-6]. This tunneling probability, however, is not reflected to the decay rate constant of the H_2^- anions, because of the following reason. When the HD molecules diffuse in the direction toward the H_2^- anions trapped in the p-H_2 solid, $\delta\varepsilon_{r,r+g} > 10^{-3}$ K and $\Omega \leq 10^{-4}$ K below 5 K are obtained. However, Eq. (5-5) is valid only when $\delta\varepsilon_{r,r+g} << \Omega$. Therefore, Eq. (5-5) cannot explain the decrease in the decay rate constant of the H_2^- anions between 3~5 K.

Second, we consider the quantum tunneling at $\delta\varepsilon_{r,r+g} >> \Omega_{II}$ which is, on the contrary, important to study pairing process between H_2^- and HD. As depicted by broken line in Fig. 5-2, the diffusion in the direction toward the H_2^- anions occurs via the tunneling with compensating the energy level misalignment (cf. Fig. 5-1(d)), which mainly controls the pairing rate. With the decrease in the distance between the impurity particles, $\delta\varepsilon_{r,r+g}$ remarkably increases (cf. Chapter 4) and then $W_{r,r+g}$ decreases by a factor of several orders. At $\delta\varepsilon >> \Omega_{II}$, the following equation is derived from Eq. (5-2):

$$W_{r,r+g} = \frac{{\Delta_0}^2\Omega}{{\delta\varepsilon_{r,r+g}}^2} \qquad (5\text{-}6)$$

By substituting Eq. (5-3) into Eq. (5-6), one obtains,

$$W_{r,r+g} = B_{II}\Theta_D \frac{\Delta_0^{\,2}}{\delta\varepsilon_{r,r+g}^{\,2}}\left(\frac{T}{\Theta_D}\right)^9 . \qquad (5\text{-}7)$$

This probability increases with the increase in T and with the decrease in $|\delta\varepsilon|$. The decay rate constant of the H_2^- anion should reflect the tunneling probability depicted by Eq. 5-7, although the drastic increase in the decay rate constant with temperature has not been observed below 5 K.

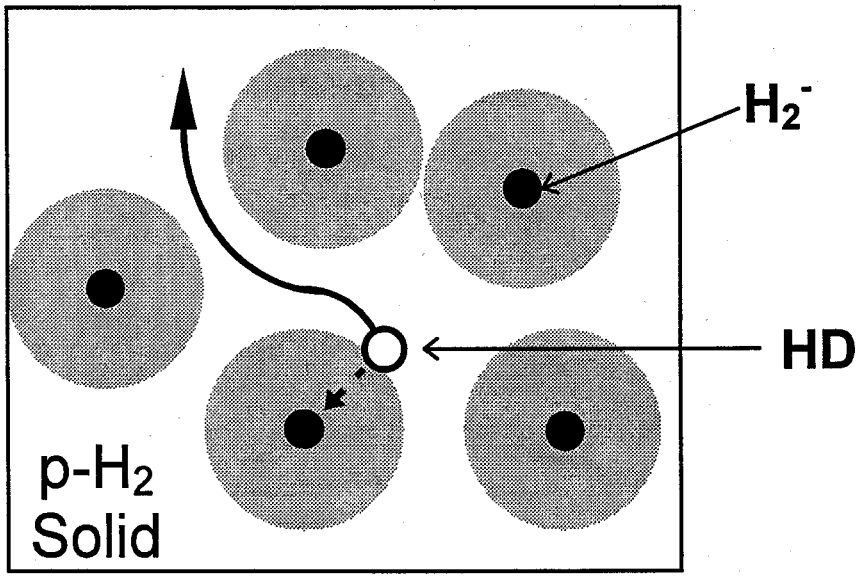

Fig. 5-2 Schematic view of the quantum tunneling diffusion of a HD molecule (open circle) in parallel (broken line) and in perpendicular (solid curve) to the direction toward one of H_2^- anions trapped in a p-H_2 solid (closed circle). Gray circles show the regions whose potential levels to the center are strongly misaligned due to the H_2^- anions. The HD molecules must pass through the misaligned potential region, where the tunneling probability is strongly suppressed, for pairing.

5. 1. 2. One-phonon quantum tunneling

When one particle migrate from site $\boldsymbol{r}$ to $\boldsymbol{r+g}$ via one-phonon assisted quantum tunneling, the following $\delta\varepsilon_{r,r+g}$ dependent expression for Ω is obtained,

$$\Omega \equiv \Omega_I = B_I \left(\frac{\delta\varepsilon_{r,r+g}}{\Theta_D} \right)^4 T \tag{5-8}$$

where B_I is a dimensionless factor of the order of unity. This one-phonon process can be dominant only when $\delta\varepsilon_{r,r+g} >> \Omega$. Thus, the following equation is obtained by substituting Eq. (5-8) into Eq. (5-6) as:

$$W_{r,r+g} = \frac{B_I \Delta_0^{\,2} \delta\varepsilon_{r,r+g}^{\,2}}{\Theta_D^{\,4}} T. \tag{5-9}$$

This process becomes dominant only at the smaller in r (larger in $\delta\varepsilon$) and lower in T, because $W_{r,r+g}$ in Eq. (5-9) strongly depends on $\delta\varepsilon_{r,r+g}$ and is less dependent on T compared with that in Eq. (5-7) ($\propto T^9$) and with that via the thermally activated process ($\propto \exp(-E_a / T)$). The linear increase in the rate constant has been reported on the recombination of the H atoms in a n-H_2 solid below 4 K [7], which has been explained by this one-phonon assisted quantum tunneling diffusion mechanism [2,3]. It is expected that the linear increase in the decay rate constant of the H_2^- anions below 3 K also shows the one-phonon assisted quantum tunneling diffusion of the H_2^- anions in the region where the H_2^- anions are close to the HD molecules.

As discussed above, the temperature dependence of the decay rate constant for the H_2^- anions below 3 K and above 5 K has been explained by the one-phonon quantum tunneling and thermally activated diffusion processes, respectively. However, that between 3~5 K ,showing the decrease with the increase in T, has not been assigned yet. Another mechanism which also controls the pairing (decay) rate is discussed in the next

paragraph.

5. 2. Biased Diffusion

The pairing time of the two impurity particles, which is inversely proportional to the decay rate constant of the isolated impurity particles, depends not only on the diffusion rate constant but also on the length of characteristic trajectory (number of jumps). Diffusion, by definition, is a random process. Since diffusion rate weakly depends on its direction in classical theory, its anisotropy is treated as a perturbation. However, this approximation is no longer valid, when particles diffuse via quantum tunneling. Since the tunneling probability crucially depends on $\delta\varepsilon_{r,r+g}$, the quantum tunneling diffusion at $\delta\varepsilon_{r,r+g} >> \Omega$ is no longer the random process and, then, the characteristic trajectory reflecting the preferred bias should be considered [8~10].

Especially, the probability of the two-phonon assisted tunneling of the HD molecules for the H_2^- anions becomes much smaller than that against the H_2^- anions, which is originated from the lower in $\delta\varepsilon$ at longer in r. This anisotropy yields "kinetic barrier" which interferes mutual approach to the H_2^- anions. Since the tunneling probability increases with temperature, the interference effects also increases with temperature. It is expected that the decrease in the decay rate constant of the H_2^- anions between 3~5 K is due to the biased two-phonon quantum tunneling diffusion.

The decrease in the pairing rate with the increase in temperature has also been reported on the o-H_2-o-H_2 pairing process in a p-H_2 solid below 0.3 K [11~13]. The decrease in the pairing rate has been explained by the biased two-phonon assisted quantum tunneling diffusion using the three-dimensional computer simulations [8~10].

The decrease in the decay rate constant of the H_2^- anions between 3~5 K was not explained quantitatively using such computer simulations, because this simulation needs very complicated calculations. However, the liner increase below 3 K, decrease between 3~5 K, and exponential increase above 5 K have been qualitatively analyzed using the one-phonon quantum tunneling, two-phonon quantum tunneling together with its

preferable bias, and thermally activated diffusion models, respectively.

References

[1] T. Kumada, N. Kitagawa, S. Mori, J. Kumagai, Y. Aratono, and T. Miyazaki, submitted to J. Low Temp. Phys.

[2] Yu. Kagan and L. A. Maksimov, Zh. Eksp. Teor. Fiz. 84 (1983) 792 [JETP 57 (1983) 459]; Yu. M. Kagan and N. V. Prokof'ev, Quantum Tunneling in Condensed Media, (North-Holland, Amsterdam, 1992).

[3] A. F. Andreev, Sov. Phys. Usp. 19 (1976) 137.

[4] M. Rall, D. Zhou, Erika G. Kisvarsanyi, and N. S. Sullivan, Phys. Rev. B 45 (1992) 2800.

[5] D. Zhou, C. M. Edwards, and N. S. Sullivan, Phys. Rev. Lett. 62 (1989) 1528.

[6] E. F. DeRose, E. A. Gislason, N. H. Sabelli, K. M. Sluis, J. Chem. Phys. 88 (1988) 4878.

[7] A. Ya. Katunin, I. I. Lukashevich, S. T. Orozmamatov, V. V. Sklyarevskii, V. V. Suraev, V. V. Filippov, N. I. Filippov, and V. A. Shevtsov, Pis'ma Zh. Eksp. Teor. Fiz. 34 (1981) 375 [JETP Lett. 34 (1981) 357].

[8] A. E. Meyerovich, Phys. Rev. B 42 (1990) 6068.

[9] M. Tammaro, M. P. Nightingale, and A. E. Meyerovich, Phys. Rev. B 47 (1993) 2573.

[10] A. E. Meyerovich, M. P. Nightingale, and M. Tammaro, *Physica B* 194-196 (1994) 925.

[11] H. Meyer, Can. J. Phys. 65 (1987) 1453.

[12] S. Washburn, R. Schweizer, and H. Meyer, J. Low Temp. Phys. 40 (1980) 187.

[13] X. Li, D. Clarkson, and H. Meyer, J. Low Temp. Phys. 78 (1990) 335.

Chapter 6

Conclusion

Experimental study of H_2^- anions trapped in p-H_2 solids was reported in this thesis. Experimental techniques, results, and discussions are summed as follows.

Studies of ESR spectra of radical species trapped in a p-H_2 solid have very high-resolutions. Since p-H_2 molecules have no nuclear spin moment, ESR linewidths of the radical species trapped are not broadened by the inhomogeneous internal magnetic fields due to superhyperfine interaction with its surrounding p-H_2 molecules. This technique of high-resolution ESR spectroscopy was employed for the precise study of the hydrogen ions in hydrogen solids.

New ESR quartet signals with very narrow linewidth and small intensity were observed for the first time in a X(γ)-ray irradiated p-H_2 solid. It turned out that the radical species which assigns the quartet signals has the electric spin quantum number of 1 / 2, ESR *g*-factor of 2.0023, and hyperfine coupling constant of 203 G. It is concluded that the newly observed quartet signals come from a new molecular ion H_2^- and other many possibilities are dropped off.

Stability of the H_2^- anion in the p-H_2 solid was discussed. The H_2^- anion observed in the p-H_2 solid has very long lifetime, although it suddenly dissociates into a H_2 molecule and a free electron within 10^{-14} sec in gas phase. Since H_2 molecules are highly electron repulsive, different from the free electron in gas phase, a excess electron trapped in the p-H_2 solid repulsively interact with its surroundings. It is expected that the excess electron in the p-H_2 solid is attached to one of the surrounding H_2 molecules, forming the H_2^- anion, to minimize the repulsive interaction. The energies of the H_2^- anion and H_2 molecule + excess electron trapped in the p-H_2 solid were compared theoretically and

concluded that the H_2^- anion is rather stable.

The stability of the H_2^- anion in the p-H_2 solid was evaluated by experiment. As discussed above, the H_2^- anions are stabilized by the assists of surrounding crystal fields. The thermal phonons would disturb the assists and dissociate excess electrons from the H_2^- anions. It was found that the ESR signals of the H_2^- anions suddenly and reversibly disappear above 6 K. This phenomenon indicates that the excess electrons in the H_2^- anions are excited to be vibronic states. Moreover, the H_2^- anions irreversibly disappear at higher temperatures above ~ 7 K. This result shows that the electrons in the H_2^- anions are dissociated and delocalized. Therefore, it is concluded that the stability of the H_2^- anions in the p-H_2 solid is about 6 K.

Long-time decay of the H_2^- anions was studied. The H_2^- anions decay within 5 hours at 4.2 K. It was expected that the H_2^- anions react with electron attractive species of cations or H atoms; however, the decay does not become faster at higher concentration of these species in the p-H_2 solid. On the other hand, the decay rate constant linearly increase with the increase in the concentration of HD (D_2) molecules added. Moreover, as opposed to the H_2^- anions, larger amounts of electron bubbles are observed in the p-H_2 solid containing higher concentration of HD (D_2) molecules. These results indicate that the H_2^- anions react with the HD molecules originally contained in the p-H_2 solid at natural abundance to form the electron bubbles. Electrons induce a little larger quadruple moment in the heavier species of HD molecules at ground state than that in p-H_2 molecules. The small difference in the interaction energy with the HD molecule makes the H_2^- anion unstable and dissociates into H_2 molecule + electron in bubble.

The decay rate constant of the H_2^- anions in the p-H_2 solid show various temperature dependence in the temperature range between 1.3 ~ 6.6 K. The decay rate constant increases exponentially with the increase in temperature above 5 K. This result is consistent with thermally activated theory and the activation energy of about 100 K obtained by fitting is comparable to that of other impurity particles trapped in H_2 solids.

However, the decay rate constant increases not exponentially but linearly with the increase in temperature below 3 K and decreases with the increase between 3 ~ 5 K. The former phenomenon shows one-phonon assisted quantum tunneling diffusion of the HD molecules which assists the pairing of the reactant species of H_2^- anions and HD molecules in the p-H_2 solid. On the other hand, The latter phenomenon shows two-phonon assisted quantum tunneling diffusion of HD molecules in the direction against the pairing. Since the rate for the two-phonon quantum tunneling increases with the increase in temperature, the pairing is interfered more effectively at higher temperatures. The anomalous temperature dependence of the H_2^- anions ascribed to the two kinds of quantum tunneling diffusions of the HD molecules in the p-H_2 solid.

Acknowledgment

The present investigation has been carried out from 1995 to 1999 in Research Group for Atomic Tunneling Reactions at Japan Atomic Energy Research Institute.

The author wishes to express his deepest gratitude to Professor Tetsuo Miyazaki of Nagoya University and Dr. Yasuyuki Aratono of Japan Atomic Energy Research Institute for their valuable guidance and directions and for their continuous encouragement throughout his investigation.

He would like to express his profound gratitude to Professor Muneyuki Date of Japan Atomic Energy Research Institute, who introduced him to this area of research, for his critical readings, valuable guidance, and directions on the work of doctoral dissertation.

He would like to express his deep gratitude to Professor Yoshichika Onuki of Osaka University for his valuable guidance and directions.

Deep appreciation should be directed to Dr. Jun Kumagai of Nagoya University, Dr. Kenji Komaguchi of Hiroshima University, Dr. Shigeru Ohira of Japan Atomic Energy Research Institute, Mr. T. Matsumoto, Mr. H. Inagaki, T. Nagasawa, N. Kitagawa, S. Mori, T. Noda, and other members of the Miyazaki Laboratory for their active collaborations and discussions. Without their technique aids this thesis would have never be completed.

The author thanks Dr. Toshiyuki Takayanagi and Yuzuru Kurosaki of Japan Atomic Research Institute for their hot discussions.

Last but not least, the author is grateful to his wife, Tomoe Kumada and his parents, Kippei Kumada and Fujiko Kumada for their continual encouragement and all kinds of support to every thing he faced.

November 1998

Takayuki Kumada